MATHEMATICAL MODELLING OF METALLIC CORROSION PROCESSES - A CHEMICAL ENGINEERING APPROACH

A thesis submitted in partial fulfillment of the requirements of the regulations of the degree of Doctor of Philosophy of the University of London

by

John Paul Fletcher M.A.(Cantab)

Imperial College

Acknowledgements

The work described in this thesis was carried out at the Central Electricity Research Laboratories and is published by permission of the Central Electricity Generating Board. Thanks are particularly due to Dr. P. L. Surman and Dr. W. S. Kyte, of the Central Electricity Research Laboratories, Leatherhead, and to Dr. D. A. Young and Dr. D. L. Pyle of the Department of Chemical Engineering and Chemical Technology, Imperial College, for their help and guidance throughout the project, and to Mrs K. Davies for her helpful typing.

This thesis is dedicated to all the many people who have asked how I am getting on. Without them it would not have been possible.

ABSTRACT

The corrosion of mild steels in carbon dioxide at elevated temperatures has been of concern within the nuclear industry. In the past, work has been undertaken to quantify the oxidation and identify the factors upon which it is dependent. This work has shown that initially protective oxidation can be followed after a variable time by non-protective oxidation. Work has proceeded to elucidate the mechanisms responsible for this phenomenon, and has suggested mechanisms for some of the transport steps of the oxidation.

In this work models for the different transport steps are developed, and a mass balance of the oxidation constructed by which they can be quantitatively related. The equations are simplified to a point where solution is justified by the experimental information available, and where solution is practicable using a digital computer.

The computed results are analysed by the use of overall weight-gain-time equations, and by factorial experiments to isolate the parameters to which the results are sensitive. The overall model is consistent with experimental results. Although not fully quantitative, it reproduces observed detailed effects in the two layer oxide, and predicts that breakaway is likely to be caused by competition for space in the inner oxide layer.

This approach establishes the utility of an overall mass balance model in a complex problem with uncertainties of information, where simple models are inadequate to account for observation.

CONTENTS

	LIST OF TABLES	8
	LIST OF FIGURES	10
1.	INTRODUCTION	11
2.	LITERATURE	21
	2.1 Introduction	21
	2.2 Thermodynamics	23
	2.3 Weight Gain Data	30
	2.4 Physical Observations	46
	2.4.1 Carbon Formation	48
	2.4.2 Physical Properties of the Oxide	51
	2.5 The Mechanism of Oxidation	53
3.	MATHEMATICAL MODELLING	60
	3.1 Introduction	60
	3.1.1 The Mass Balance	62
	3.2 Order of Magnitude of the Processes Involved	65
	3.2.1 Estimation of the Mass Transport Required	66
	3.2.2 Estimation of the Gas Diffusion Coefficient	67
	3.2.3 Gas Diffusion outside the Oxide	71
	3.2.4 Gas Diffusion across the Oxide	73
	3.2.5 Transport of Metal across the Oxide	77
	3.3 Development of the Model	79
	3.3.1 Simplification to Two-point Model	81
	3.3.2 Justification of Further Simplification	87
	3.3.3 Incorporation of the Volume Mechanism	90
	3.3.4 The Two-point Model	93

3.4 The Models for Rate Processes 94

3.4.1 Oxidation Reactions 94

3.4.2 Carbon Formation 95

3.4.3 Gas Diffusion 96

3.5 The Assembled Model 96

3.5.1 Effectiveness Factors 97

3.5.2 Conclusion 100

4. NUMERICAL SOLUTION OF THE MODEL 101

4.1 Introduction 101

4.2 Evaluation of the Derivatives 102

4.3 Choice of Integration Algorithm 108

4.3.1 Test Performance of the Integration Routine 112

4.3.2 Performance in Integrating the Model 113

4.4 Implementation of the Model 116

5. RESULTS 120

5.1 Cases Computed 120

5.1.1 Results from each Case 123

5.2 Analysis of Weight Gain Data 124

5.2.1 Models fitted to Weight Gain Data 126

5.2.2 Results of Weight Gain Data Analysis 129

5.3 Comparison of the Models 129

5.3.1 Factorial Analysis of Parameter Variation 134

5.3.2 Further Examination of Significant Effects 141

5.4 Detailed Results 145

5.4.1 Relative Sizes of the Two Oxide Layers 146

5.4.2 CO Concentration and Carbon Formation 146

5.4.3 Inner Layer Volume 147

5.4.4 Rate Controlling Processes 152

5.5 Conclusion 153

6. CONCLUSIONS 155

6.1 Discussion and Limitations 155

6.2 The Current Situation 157

6.3 Other Variables not Considered 160

6.4 Final Conclusions 161

APPENDICES

A1 Manual for Thermodynamic Program 163

A2 Program Flowsheet for Mathematical Model 188

A3 Manual for Integration Program 195

A4 Specimen Output 213

A5 Methods used to Analyse Weight Gain Data 223

A5.1 Least Squares Linear fit 223

A5.2 The Durbin-Watson Test 223

A5.3 Minimax Method 224

A5.4 Factorial Analysis of Variance 226

LIST OF SYMBOLS 228

LIST OF REFERENCES 232

LIST OF TABLES

1.1 Coolant gas composition for Bradwell Reactor 14

1.2 Bradwell Reactor design and operating parameters 15

1.3 Steel compositions for use in Magnox Reactors 17

2.1 Free energies of reactions (2.2.1-4) at 823K 25

2.2 Variation of equilibrium with temperature for reaction (2.2.1) 25

2.3 Variation of equilibrium with temperature for reaction (2.2.2) 27

2.4 Variation of partial pressure and CO/CO_2 for reaction (2.2.2) 27

2.5 Equilibrium values for reaction (2.2.7) 28

2.6 Equilibrium data for reactions (2.2.9-10) 31

2.7 Reactor gas outlet temperatures and pressures 32

2.8 Weight gain data for mild steels in CO_2 38

2.9 Weight gain data for low alloy steels in CO_2 40

2.10 Weight gain data for iron in CO_2 42

2.11 Weight gain rate data for steels in CO_2 43

3.1 Diffusion coefficient for CO/CO_2 70

3.2 Limits of gas diffusion regimes 76

4.1 Cases of solution of Equation (4.2.1) 103

4.2 Test results for the integration algorithm 114

5.1 Values of parameters used in the model 121

5.2 Details of runs reported here 122

5.3 Output dependent variables from the model 125

5.4 Model fitting results for case 5 of Run 5624 130

LIST OF TABLES Continued

5.5 Rate constants of cases plotted in Figures (5.1-2) 133

5.6 Factorial Analysis Results for Run 6888 135

5.7 Factorial Analysis Results for Run 6970 136

5.8 Factorial Analysis Results for Run 6984 137

5.9 Factorial Analysis Results for Run 7085 138

5.10 Factorial Analysis Results for Run 6888a 139

5.11 Key to Tables (5.6-10) 140

LIST OF FIGURES

1.1	Outline diagram of a Magnox Reactor	12
2.1	Equilibrium for iron and steel oxidation in CO_2	29
2.2	Transition from protective to breakaway oxidation	35
2.3	Two layer oxide formed on steel oxidised in CO_2	47
2.4	Breakaway oxide excresence	49
2.5	Carbon distribution in magnetite	52
2.6	Suggested CO concentration-time profile	58
3.1	Schematic diagram of mass balance	64
3.2	Schematic diagram of oxide growth	64
4.1	Schematic diagram of numerical integration progress	117
5.1	Logarithmic graph of weight gain for cases from Runs 6888 and 6888a	131
5.2	Graph of weight gain for cases from Runs 6888 and 6888a	132
5.3	Graph of weight gain for cases 5, 14, 23 and 32 of Run 6888a	142
5.4	Graph of weight gain for cases 2, 3, 26 and 27 of Run 7056	143
5.5	Graph of weight gain for cases 5, 6, 29 and 30 of Run 5624	144
5.6	Graph of X1/X2 for cases 5, 6, 29 and 30 of Run 5624	148
5.7	Graph of CO for cases 5, 6, 29 and 30 of Run 5624	149
5.8	Graph of Z for cases 5, 6, 29 and 30 of Run 5624	150
5.9	Graph of Dimensionless groups for case 29 of Run 5624	151

1. Introduction.

A chemical engineering approach to the general problem of metal corrosion has been applied to a particular problem of some importance in the nuclear power industry: the corrosion of steels by carbon dioxide gas at the elevated temperatures and pressures employed in the gas cooled nuclear reactor.

The nuclear power stations at present in use for commercial power generation in the U.K. are all of the so-called 'Magnox' type. This type of reactor takes its name from the magnesium-aluminium alloy used to contain the uranium metal fuel rods in the core. A simplified diagram of a typical layout is shown in Figure (1.1). Heat is removed by a forced draught of carbon dioxide gas at a maximum temperature of 400°C and a pressure of up to 20 bar. Around the fuel is an array of graphite blocks which act as the neutron-moderator; these blocks are in contact with the coolant gas. The coolant is circulated through the shell side of a heat exchanger, where the heat is transferred to a steam-turbine cycle of conventional design. Part of the gas flow is passed through a fixed-bed drying plant, to control the gas moisture level.

Godfrey and Phennah (1968abc) have written a series of papers describing the operational chemical composition of the coolant gas of a particular Magnox station, at Bradwell. The most significant impurity is carbon monoxide, which varies considerably, but can be up to 1.5% by volume. It is formed principally by radiolytic decomposition of carbon dioxide, though it is unlikely that the graphite is completely inert. Other impurities are water, hydrogen, methane, nitrogen and

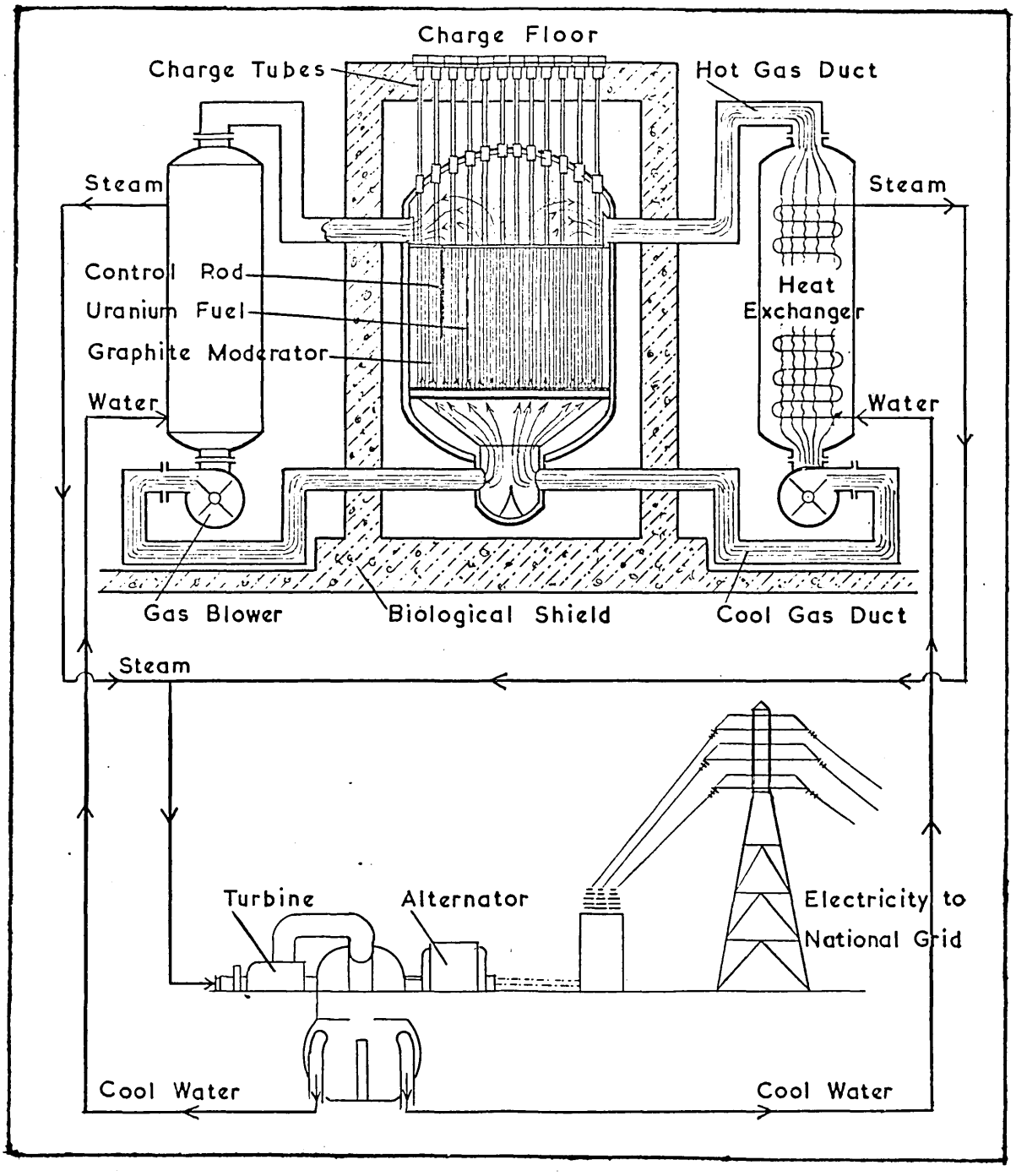

Figure 1.1 Outline diagram of a Magnox Reactor
Reference Hinton (1958)

argon. Their concentrations under standard operating conditions are given in Table (1.1), with relevant parameters of the reactor as a whole in Table (1.2). All these data are taken from Godfrey and Phennah (1968a). It is necessary to control the water content to prevent condensation in cold parts of the gas circuit, and Godfrey and Phennah (1968b) showed that such control of water was sufficient to determine also the contents of hydrogen and methane, because of chemical reactions in the gas phase and on the graphite surface. The inter-relationship between these gases was made plain by experiments in which they injected hydrogen or methane in single shots and followed the transient response of the coolant composition, while the reactor was running. One must acknowledge the reactor coolant has a complex composition, which is nevertheless independent of metal corrosion processes, though the reverse may not be true.

Because of the radiation hazards, many of the steel components of a nuclear reactor become completely inaccessible once the reactor has been started up. In-service testing and replacement are impossible; the only parts of the gas circuit which can be examined easily are the interior of the heat exchanger and adjacent pipes outside the main pressure vessel. The in-core components must therefore be made of material which can operate for the whole life of the power station. Accordingly, it is very important to establish the corrosion performance of the materials by testing under simulated reactor conditions.

Moore and Raine (1961) reviewed the corrosion properties required of the different steels needed for various duties in the Magnox reactors.

Table 1.1 Typical Coolant gas composition range of impurity concentrations for Bradwell 'Magnox' Reactor.

Impurity	Reactor 1		Reactor 2
	October 1964-July 1965	From July 1965	From 1964
CO (v/o)	0.10-1.50	0.10-1.50	0.10-1.50
H_2O (p.p.m.)	5	10-20	5
H_2 (v.p.m.)	100-150	120-150	50-100
CH_4 (v.p.m.)	30-45	60-80	10-25
O_2 (v.p.m.)	< 1	< 1	< 1
N_2 (v.p.m.)	Variable 100-1000		
A (v.p.m.)	1-10	1-10	1-10

Taken from Godfrey and Phennah (1968a).

Table 1.2 Bradwell reactor design and operating parameters.

Reactor power	537.6 MW (thermal)
Weight of moderator graphite	1240 tonnes
Graphite (PGA bulk density)	1.72 g/cc
Graphite open pore volume (effective)	0.12 cc/g
Total weight of carbon dioxide coolant	70 tons
Weight of gas under irradiation in core	2.6 tons (approx.)
Fraction of total thermal power deposited in moderator	0.056
Coolant gas pressure	132.8 lb/sq. in. absolute
Coolant gas temperature (a) Bulk inlet (b) Bulk outlet	 180°C 390°C
Mean energy deposition rate in graphite	0.023 W/g
Total coolant gas recirculation rate	5400 lb/s
Mean gas dwell time in fuel channels	0.8 s (approx.)
Rate of gas processing through driers (total - two driers)	6 lb/s

Taken from Godfrey and Phennah (1968a).

These are summarised in Table (1.3). They reported oxidation of samples of the relevant materials in the range of temperatures 350-500°C in simulated reactor atmospheres for up to 10,000 h. They had misgivings about the linearity of Arrhenius plots of the logarithm of oxidation rate against reciprocal temperature, which are necessary to obtain corrosion rates by extrapolation to the reactor operating temperatures. Such rates are difficult to measure directly because the time needed for the experiments is very long. However, in general the oxidation of steels in CO_2 could be expressed in the form:

$$W = kt^n \qquad (1.1)$$

where W is the weight gain at time t, and k is a temperature dependent constant. Initially, indeed for periods up to 10,000 h, the value of n is $\frac{1}{2}$, and the oxidation proceeds protectively at a decreasing rate. At longer times, however, the oxidation accelerates, and the value of n becomes 1, so that the oxidation is linear, and non-protective. This is known as breakaway oxidation or corrosion.

Breakaway corrosion has become a serious technical problem. Although known at higher temperatures, it has occurred unexpectedly under reactor operating conditions. This has necessitated restriction of the working temperatures to reduce corrosion so that the original reactor design lifetime, which is matched to that of the generating plant, will be maintained. Therefore, much recent attention has been given to the measurement of the oxidation under simulated reactor conditions, and attempts have been made to elucidate the oxidation mechanism, including the effect upon it of water impurity

Table 1.3 Steel Compositions for use in Magnox reactors.

Material	Analysis, % Total C	Si	Mn	S	P	Ni	Cr	Mo	Cu	V
Heat exchanger										
1. Rimming steel	0.027	< 0.5	0.38	0.032	0.021	< 0.05	0.03	< 0.05	0.12	
2. Al killed steel	0.13	Trace	0.38	0.022	0.024	0.10	0.05	< 0.05	0.07	
3. Si killed steel	0.10	0.12	0.48	0.024	0.019					
PRESSURE VESSEL STEELS										
Boiler Quality										
Steel 4	0.180	0.176	0.68	0.027	0.026	0.12	0.083	0.026		
Steel 5	0.174	0.176	1.30	0.027	0.016	0.11	0.048	0.033		
Steel 6 (grain controlled)	0.16	0.2	1.27	0.032	0.020					
Low Alloy Steels										
7. 2¼%Cr-1%Mo	0.14	0.18	0.53	0.008	0.014	0.15	2.32	0.86		
8. Mn-Cr-Mo-V	0.21	0.17	1.31	0.025	0.021	0.03	0.57	0.25	0.125	0.1
9. Ni-Mn-Mo-V	0.12	0.148	0.18			1.1	0.17	0.325		0.16
10. 1%Cr-½Mo	0.09	0.45	0.49	0.014	0.014	0.13	0.88	0.55		

Taken from Moore and Raine (1961).

in the gas.

The oxide formed on iron and mild steel oxidised at temperatures below 570°C in CO/CO_2 mixtures is magnetite (Fe_3O_4), formed by the reaction:

$$3Fe + 4CO_2 = Fe_3O_4 + 4CO \qquad (1.2)$$

Above 570°C, wustite (FeO) is formed. This has been widely reported, for example by Surman (1973), and Cameron (1958) has shown that these are indeed the thermodynamically stable phases. The protective oxide formed in the initial stages has been shown by Antill, Peakall and Warburton (1969) to contain up to about 2% by weight of carbon, either free or as carbides, but the breakaway oxide formed in the later stages contains up to 10% of carbon by weight. Cameron (1958) has shown that the reactions (1.3-4) are thermodynamically possible at temperatures between 350°C and 550°C.

$$2CO = CO_2 + C \qquad (1.3)$$

$$3Fe + 2CO = Fe_3C + CO_2 \qquad (1.4)$$

Several different suggestions have been made about the mechanism of breakaway oxidation. Thus, Moore and Raine (1961) and Price and Whittle (1967) suggested that the protective oxide is non-porous, growing by bulk solid state diffusion and is disrupted by accumulation of stress within it, so that the gas can penetrate to the metal surface and cause increased oxidation. Surman and Castle (1969), on the other hand suggested that the protective oxide is porous, so that gas can react at the metal surface to form magnetite and some carbon, and

that it is the carbon which eventually leads to disrupting stresses in a previously stress-free oxide. In addition, some iron, they suggested, is transported through the oxide as a vapour phase of surface compound, to be oxidised at the gas-oxide interface.

Further work by Gibbs (1973) has suggested that both iron vapour-phase transport, and the bulk solid state diffusion of iron, are too slow to account for the observed oxidation rates. Indeed it is now plain that the oxidation occurs partly by CO_2 reaching the metal surface through the porous oxide, and partly through grain-boundary or surface diffusion of iron outwards to the gas, where it is oxidised: the simultaneous deposition of carbon at the metal-oxide interface then creates stresses which eventually cause breakaway.

During the development of the mathematical model described in this thesis, there was a significant shift towards a consensus about the essential components of the oxidation mechanism. Indeed, it is true to say that the problem itself evolved during the course of its study, the ultimate requirements being to account for the structure of the oxide as observed in experiment, and for the changes which occur at breakaway. The model developed here is concerned with the oxide growth by oxidation and carbon formation, before the point of breakaway, and the factors which cause breakaway.

The methods which have been employed in the construction of this model are based on those of mathematical modelling as understood in a chemical engineering context. The basis of such modelling is the formulation of consistent mass and energy balances, to cover the system of interest, and the identification of the relevant variables,

parameters and boundary conditions. The most important step in the development of equations is the assessment of the required amount of detail, so that the system is neither over-complex, nor so simplified as to be meaningless.

The development and numerical solution have been carried out with due regard to the considerable uncertainties in the values of many of the parameters of the model. Attention has, therefore, been paid to the response of the model to these parameters, in order to assess the relative importance of their effects upon the oxidation rate. The use of this modelling approach is justified, despite the uncertainties, by the importance of the technical problem, and by the complexity of the system, which make it difficult by simpler calculations to allow for the interactions between different mechanisms significant during the oxidation.

2. Literature.

2.1 Introduction.

The study of the oxidation of mild steels in high pressure conditions has been undertaken mainly in response to the needs of the nuclear industry for information about how these materials behave under the conditions found in practice in a nuclear reactor. The research has had as its aim the understanding of the mechanisms involved, in order to find ways of reducing the oxidation rate, or avoiding corrosion conditions. Most of this section is devoted to a study of this work, in order to draw out the evidence needed to construct a mathematical model of the oxidation process.

The first area of interest is the thermodynamics and chemistry of the reactions, particularly some consideration of equilibrium within the iron-oxygen-carbon system. This forms an essential background to the whole problem. It is then necessary to summarise and discuss a large amount of often discordant data obtained by the many workers who have observed and characterised the oxide formed under different conditions. Much work has been done on specimens oxidised under test conditions in the laboratory. In ideal tests the conditions are designed to simulate as far as possible the conditions in the nuclear reactor. However, in practice the tests are usually performed at higher temperatures than the design values, in order to accelerate the experiment such that assessment is possible on a practical time scale. Other tests at atmospheric pressure, or with other variations from reactor conditions, have been performed mainly to test mechanistic deductions about the oxidation. All these experiments yield specimens

which have been analysed by a variety of techniques. Electron microscopes have been much used, to photograph both sections and surfaces at large magnifications. Such photographs form the basis of many arguments, but the interpretations made by different groups of workers sometimes differ. Complementary tests have been used to establish both the overall composition of the oxide, and, in some cases, the distribution of carbon within it. The main conclusion of these studies is that the onset of the breakaway phenomenon, mentioned in Section (1), is marked by a considerable change in the physical appearance of the oxide formed, although chemically it appears not to change.

The same experiments also provided data on some physical properties of the oxide, such as voidage. For test specimens it is possible to establish an overall weight gain curve, from intermittent or continuous weight records, while other experiments have established the rate of the carbon formation reactions and their dependence on gas composition. It is difficult to establish how factors other than weight gain vary with time, because determination usually involves destruction or damage to the specimen. This means that the principal data available for comparison with any model of the process will be such weight gain information.

The model must be based upon the understanding of the mechanisms involved, derived from analysis of the experiments. This analysis has proceeded during the course of the present work, and the result is a measure of consensus among different groups of workers about the mechanisms occurring during oxidation.

2.2 Thermodynamics.

Magnetite (Fe_3O_4) is formed on mild steel and iron which is oxidised in mixtures of CO and CO_2 below 570°C, though above 570°C the oxide formed is wustite (FeO)(Price and Whittle, 1967). The formation reaction of magnetite is

$$3Fe + 4CO_2 = Fe_3O_4 + 4CO \qquad (2.2.1)$$

Price and Whittle (1967) also report the formation of carbon within the oxide, and give the following reactions for this process.

$$2CO = CO_2 + C \qquad (2.2.2)$$

$$3Fe + 2CO_2 = Fe_3O_4 + 2C \qquad (2.2.3)$$

$$3Fe + 4CO = Fe_3O_4 + 4C \qquad (2.2.4)$$

They state that these are all thermodynamically feasible at 500°C, giving the free energy values quoted in Table (2.1). All of these reactions involve solid phases, and at least one gas. The phase rule predicts that reactions (2.2.1) and (2.2.2) will have one degree of freedom for the gas composition, i.e. that the pressures of CO and CO_2 are not independent at equilibrium, and that for reactions (2.2.3) and (2.2.4) there are no degrees of freedom; a fixed pressure of the gas involved will be the equilibrium value at any temperature. In fact these four reactions are not independent, and the last two can be considered as linear combinations of the first two.

Cameron (1958) has reported a great deal of thermodynamic data for the iron-carbon-oxygen system. However, his reported free energy values differ in some respects from those of Price and Whittle (1967).

These also are given in Table (2.1), together with results calculated from thermodynamic data of Kelley (1960), using the computer program described in Appendix 1. The latter two calculations are relatively consistent, the difference from Price and Whittle's results being a discrepancy of approximately 3 kcal mol^{-1} in reaction (2.2.1), also carried into (2.2.3-4).

The equilibrium (2.2.1) can be expressed as a ratio of CO to CO_2 in equilibrium with both solid phases, which will be independent of pressure, where the gases are approximately ideal. Cameron (1958) has evaluated this ratio as the equation (2.2.5), where T is the temperature Kelvin. Evaluation of this equation, together with similar results from the program of Appendix 1, are given in Table (2.2).

$$\log_{10} \frac{CO}{CO_2} = -\frac{237.1}{T} + 0.330 \qquad (2.2.5)$$

Both of these calculations show that over the temperature range of interest, from 350°C to 550°C, the ratio is sufficiently close to unity to make this a useful approximate value in the model.

The equilibrium of reaction (2.2.2) is not independent of pressure. Here Cameron (1958) calculates the equilibrium to be as in equation (2.2.6), with T in Kelvin.

$$\log_{10} \frac{CO^2}{CO_2} = -\frac{8905}{T} + 9.113 \qquad (2.2.6)$$

This has been evaluated in Table (2.3), together with results calculated by the program of Appendix 1.

This information can be used to calculate, for reaction (2.2.2), the

Table 2.1 Free Energies of Reactions (2.2.1-4) at 823K.

Equation	Price & Whittle (1967)	Cameron (1958)	Kelley (1960)	Antill et al (1969)
	kcal $mole^{-1}$	kcal $mole^{-1}$	kcal $mole^{-1}$	kcal $mole^{-1}$
(2.2.1)	2.44	- 0.603	- 0.85	-
(2.2.2)	- 6.48	- 6.43	- 6.33	-
(2.2.3)	-10.5	-13.4	-13.5	-
(2.2.4)	-23.48	-26.2	-26.2	-22 ± 10

Table 2.2 Variation of equilibrium ratio CO/CO_2 with Temperature for reaction (2.2.1).

Temperature		Cameron (1958)	Direct Calculation (Appendix 1)
°C	K	CO/CO_2	CO/CO_2
200	473	0.68	0.51
300	573	0.82	0.67
400	673	0.95	0.85
500	773	1.06	1.04
600	873	1.14	1.25

equilibrium partial pressure of CO for a given total pressure. This is given in Table (2.4) for 1 and 20 bars. The results show that the equilibrium concentration is below the practical concentrations, for the temperature range 350°C to 550°C.

Thus it has been established that in the temperature and gas composition range of interest, reactions (2.2.1-2) are both possible thermodynamically. This is, therefore, true also of reactions (2.2.3-4), which are linear combinations of (2.2.1-2). A chemical driving force is thus available, whatever may be the kinetic limitations to the rates of these reactions.

These are not the only possible reactions. Cameron (1958) gives corresponding thermodynamic data for reactions which form carbides of iron. The reaction (2.2.7) can occur, the equilibrium being given by Cameron as equation (2.2.8), T being in Kelvin. This is evaluated in Table (2.5).

$$3Fe + 2CO = Fe_3C + CO_2 \qquad (2.2.7)$$

$$\log_{10} \frac{CO^2}{CO_2} = -\frac{7510}{T} + 7.819 \qquad (2.2.8)$$

The question of whether carbon is present as graphite, or combined as carbide, cannot, therefore, be resolved by thermodynamics, and must also depend on kinetic factors. The thermodynamic data for iron carbon oxygen are summarised in Figure (2.1), due to Surman (1973).

Godfrey and Phennah (1968c) showed that there are also reactions involving thewater, hydrogen and methane which are inevitably found in

Table 2.3 Variation of equilibrium (CO^2/CO_2) with Temperature for reaction (2.2.2).

Temperature		Cameron (1958)	Direct Calculation (Appendix 1)
°C	K	CO^2/CO_2	CO^2/CO_2
200	473	1.9×10^{-10}	1.5×10^{-10}
300	573	3.8×10^{-7}	3.4×10^{-7}
400	673	7.6×10^{-5}	7.6×10^{-5}
500	773	3.9×10^{-3}	4.1×10^{-3}
600	873	8.2×10^{-1}	8.8×10^{-2}

Table 2.4 Variation of equilibrium CO/CO_2 for reaction (2.2.2) with pressure and temperature.

Temperature		P_{CO} bar	CO/CO_2	P_{CO} bar	CO/CO_2
°C	K	at 1 bar		at 20 bar	
200	473	1.4×10^{-5}	1.4×10^{-5}	6.2×10^{-5}	3.1×10^{-6}
300	573	6.1×10^{-4}	6.1×10^{-4}	2.7×10^{-3}	1.4×10^{-4}
400	673	8.7×10^{-3}	8.8×10^{-3}	3.9×10^{-2}	2.0×10^{-3}
500	773	6.1×10^{-2}	6.5×10^{-2}	2.8×10^{-1}	1.4×10^{-2}
600	873	2.5×10^{-1}	3.3×10^{-1}	1.2	6.6×10^{-2}

Based on Cameron (1958)

Table 2.5 Equilibrium values for reaction (2.2.7).

Temperature		Direct calculation	Cameron	p_{CO}(bar)	CO/CO_2	p_{CO}(bar)	CO/CO_2
°C	K	CO^2/CO_2	(2.2.8) CO^2/CO_2	at 1 bar		at 20 bar	
200	473	7.0×10^{-9}	8.8×10^{-9}	9.4×10^{-5}	9.4×10^{-5}	4.2×10^{-4}	2.1×10^{-5}
300	573	4.6×10^{-6}	5.2×10^{-6}	2.3×10^{-3}	2.3×10^{-3}	1.0×10^{-2}	5.1×10^{-4}
400	673	4.3×10^{-4}	4.6×10^{-4}	2.1×10^{-2}	2.2×10^{-2}	9.6×10^{-2}	4.8×10^{-3}
500	773	1.3×10^{-2}	1.3×10^{-2}	1.1×10^{-1}	1.2×10^{-1}	5.0×10^{-1}	2.6×10^{-2}
600	873	1.7×10^{-1}	1.7×10^{-1}	3.3×10^{-1}	4.9×10^{-1}	1.7	9.5×10^{-2}

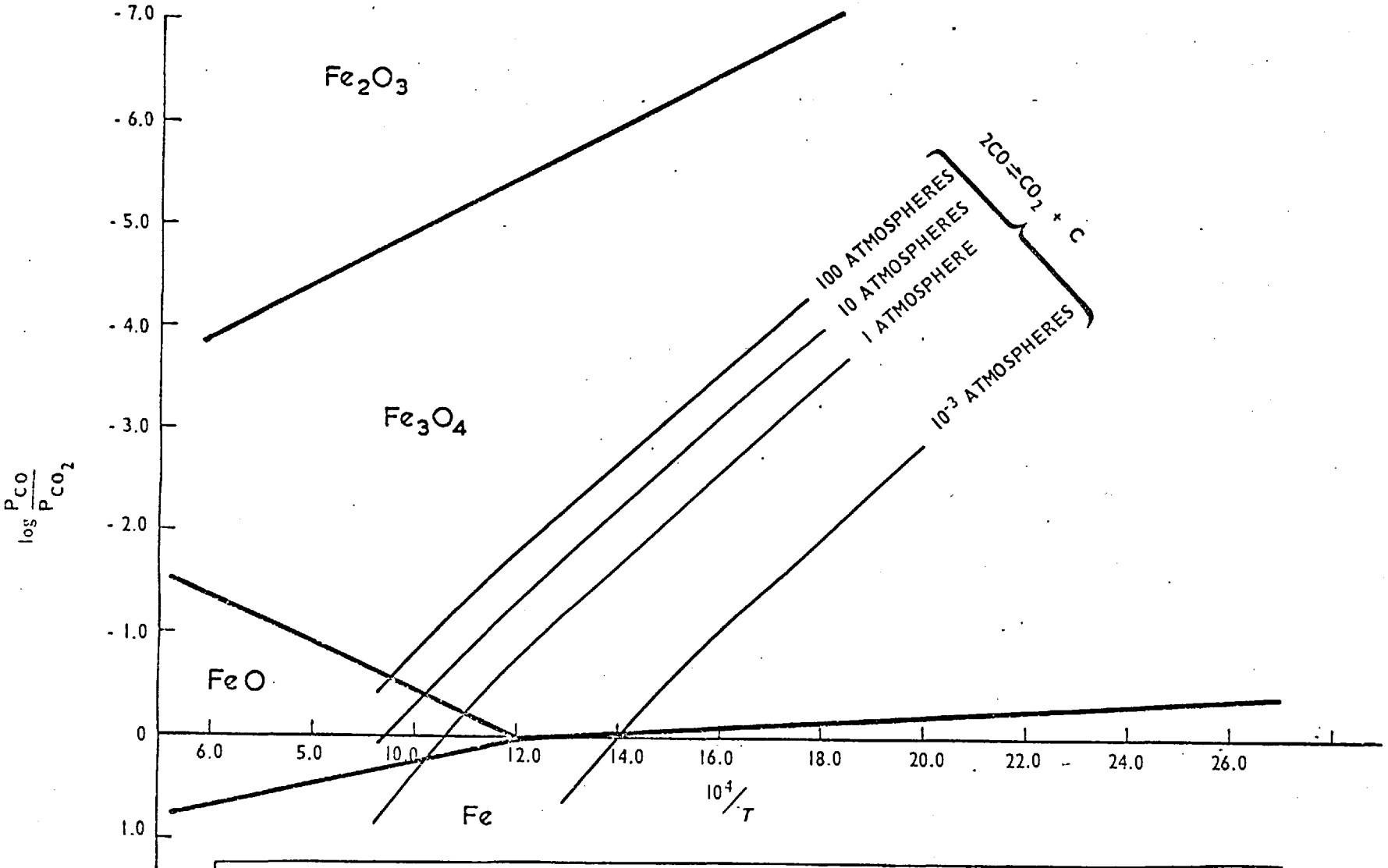

Figure 2.1 Equilibrium for iron and steel oxidation in CO_2
Reference Surman (1973)

the coolant gas of a Magnox reactor. Should equilibrium be attained by water and hydrogen present in small amounts it is likely to be established via the reaction (2.2.9).

$$H_2O + CO = H_2 + CO_2 \qquad (2.2.9)$$

This relates the hydrogen water ratio directly to the CO CO_2 ratio. Water and hydrogen can also react as in (2.2.10):

$$H_2O + C = H_2 + CO \qquad (2.2.10)$$

Both these reactions indicate possible ways in which water in the gas may affect the oxidation behaviour. Thermodynamic data for these reactions are given in Table (2.6).

2.3 Weight Gain data.

The motive for the initial work on the oxidation of mild steels in CO_2 atmospheres was to establish their resistance to corrosion in service under the conditions found in the CO_2-cooled 'Magnox' nuclear reactors. Much data collected for this purpose were summarised by Moore and Raine (1961). Their values for the outlet gas temperatures of the reactors then existing or being built are given in Table (2.7). The application of steels at these temperatures in the presence of CO_2 had not previously been required, so that no work had been carried out. In the practical situation, which makes it very difficult, and in many cases impossible, to replace or examine components of a nuclear reactor which have become active, Moore and Raine recognised that in order to obtain corrosion data at all, short-time trials would have to

Table 2.6 Equilibrium data for reactions (2.2.9-10).

Equation		(2.2.9)	(2.2.10)
°C	K	$K = \frac{(H_2)(CO_2)}{(H_2O)(CO)}$	$K = \frac{(H_2)(CO)}{(H_2O)}$
200	473	235	3.6×10^{-8}
300	573	40.5	1.4×10^{-5}
400	673	12.1	9.1×10^{-4}
500	773	5.05	2.1×10^{-2}
600	873	2.62	2.3×10^{-1}

Table 2.7 Reactor gas outlet temperatures and pressures.

	Temperature °C	Pressure	
		lb/in^2	bar
Calder Hall	340	100	(7.8)
Berkeley	350	125	(9.5)
Hunterston	395	150	(11.2)
Bradwell	390	150	(11.2)
Hinkley Point	375	180	(13.2)
Trawsfynydd	395	230	(16.6)
Windscale (AGR)	575	270	(19.4)

From Moore and Raine (1961) except for Windscale from Tyzack et al (1963).

be undertaken at temperatures above the service temperatures. The rates could then be corrected to the operating temperatures using the Arrhenius equation,

$$k = A \exp(-Q/RT) \qquad (2.3.1)$$

provided a linear plot ($\ln k$, T^{-1}) was obtained showing the activation energy, Q to be a constant. First results showed that this was not the case as has been confirmed by the more recent work of Gibbs, Pendlebury and Wootton (1974). The weight gain given by Moore and Raine are summarised in Tables (2.8-9), and cover a range of mild and low alloy steels, which were oxidised at up to 500°C at 150-300 lbs/ in^2 gauge ($\sim$ 10-22 bar). There were some discrepancies in data from different laboratories and in the compositions found on the analysis of steels made to the same specification. The results show, however, that at all temperatures the oxidation was initially parabolic and protective, following a weight gain law of the form

$$W = kt^n \qquad (2.3.2)$$

with n about 1/2. The oxidation rate increased if the CO_2 contained CO or water, both of which can be expected to be present under reactor conditions. In some cases an acceleration to a linear rate of oxidation, with n about 1, was observed. This was described as 'breakaway oxidation'. It occurred particularly with the low alloy steels used for heat exchanger construction, at temperatures of 400°C and above. A typical graph of weight gain with time is shown in

Figure (2.2). After discussion of possible mechanisms for this oxidation, Moore and Raine concluded that the steels examined were satisfactory for the duties required, up to temperatures between 360°C and 400°C, but that further investigation of the oxidation mechanism was desirable, especially if future reactors were to work at higher temperatures.

Later work was reported by Tyzack, Campbell and Trowse (1963), who assessed the materials compatibility problems associated with the Windscale Advanced Gas Cooled reactor. The design gas outlet temperature of this reactor is also shown in Table (2.7). While being concerned mainly with other components such as the high alloy steel fuel cans, these authors also discussed the components in the gas circuit. Further oxidation data were reported for a low alloy, 1% Cr ½% Mo steel, which had been observed to undergo breakaway at 600°C even in dry CO_2. These results, which are included in Table (2.9), caused some worry since the material was regarded as cheaper replacement for stainless steel, in those parts of the circuit where the operating temperature would be in the range 500-575°C. Mild steel was considered to be adequate for use in those parts of the heat exchanger, where its temperature would not exceed 320°C, although it was known that at higher temperatures the oxidation of mild steel became linear in character.

Results extending those reported by Moore and Raine (1961) were given by Antill et al (1964), who also provided a more detailed account of the work discussed by Tyzack et al (1963). Mild and low alloy

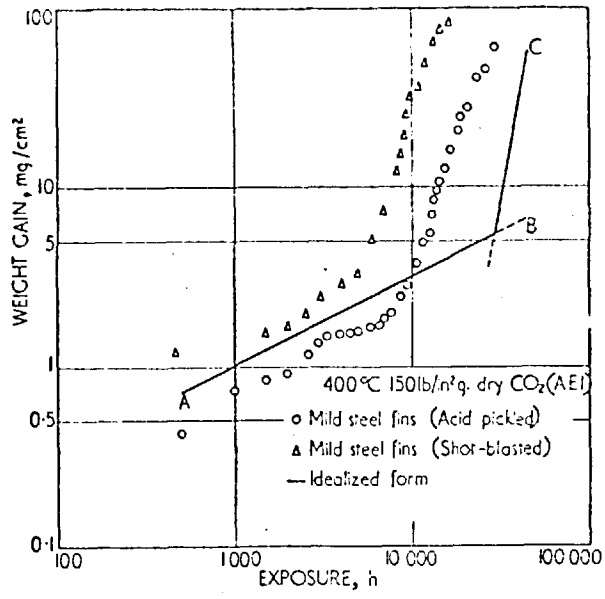

Figure 2.2 Transition from protective to breakaway oxidation
Reference Moore and Raine (1961)

steels were here oxidised at temperatures in the range 350-550°C, in up to 14.6 bar pressure of CO_2, both with and without additions of CO and water. The results are summarised in Table (2.11). The same pattern of initial parabolic oxidation was observed, with in many cases transition to a linear regime of constant rate. The resistance of mild steel proved to be particularly low. The factors tending to encourage breakaway were shown to be higher temperatures, the presence of water and, to a smaller extent, the presence of CO and higher total pressure.

At 350°C, the addition of water did not, however, increase the oxidation rate of any of the steels in CO_2/CO at 14.6 bar, and no breakaway was to be observed after 7000 h. Since, at higher temperatures, there was considerable variation in the oxidation time before breakaway occurred, with some specimens taking as long as 8000 h, the possibility remained that breakaway would occur eventually even at 350°C. These workers evidently appreciated the problems involved in extrapolating data to service conditions.

Cowen and Tyzack (1968) summarised a later conference on the metal-gas reactions in atmospheres containing CO_2. The behaviour of mild and low-alloy steels was known by this time to be sensitive both to the composition of the steel and of the gas, but the mechanisms involved were not apparent. Rimming steels showed poor resistance, and low alloy steels a great variability in performance. It was also appreciated from the thermodynamics that carbon-forming reactions could occur during oxidation, using as source the CO formed by the oxidation reaction itself.

Much long term testing of steels was reported by Goodison, Harris and Goldenbaum (1969). Tests of up to 8000 h were carried out at 350-450°C and 400-600 p.s.i. (25-40 bar), with controlled variations of CO and moisture content. The steels used were a range of low alloy and mild steels, but did not include the very low carbon rimming steel which is used in nuclear heat exchangers(Moore and Raine, 1961). At 350°C no breakaway was observed after 8000 h, but at 380°C breakaway to linear kinetics was observed on some specimens of both mild and low alloy steels, while at 400°C all the mild steels showed linear breakaway kinetics. Typical weight gain figures for these tests are summarised in Tables (2.8-9) and (2.11). The authors concluded that the most important factors which influence the linear oxidation rate of a given steel were temperature and the presence of water vapour in the gas, with total pressure and variation of CO in the gas being of lesser significance.

Antill, Peakall and Warburton (1968) reported further results, given in Tables (2.8-10), in agreement with the previous findings, except that some specimens which showed breakaway at 20 bar did not do so at 1 bar, when oxidised at 500°C in CO_2 with 2% CO and water. They discussed the need for other work than kinetic data to elucidate the mechanisms involved, and performed experiments to determine the behaviour of carbon within the oxide, together with marker experiments designed to show the locus of oxide growth in different circumstances.

Further work has concentrated on these mechanistic aspects of the oxidation, using as a basis the kinetic data established by previous authors. It is necessary to discuss in detail the physical

Table 2.8 Weight Gain Data for Mild Steel in CO_2

Pressure lb/in^2 g	Pressure bar	Temperature °C	Gas	Steel	Time hr	Wt Gain mg/cm^2	Oxidation	Reference
200	(14.6)	350	Moist	1,2,3	10^3 10^4	0.5 1.0	Protective	(1)
200	(14.6)	450	CO/CO_2	1,2	10^3 5×10^3	10 1000	Breakaway	
				3	10^3 10^4	2.0 20	Breakaway	
150	(11.2)	400	Dry CO_2	4,5,6	10^3 10^4	0.5 5	Transition to Breakaway	(1)
200	(14.6)	400	Moist CO/CO_2	"	10^3 10^4	0.5 2.0	Protective	
200	(14.6)	450	"	"	10^3 10^4	1.0 5.0	Protective	
400/600	(28.2/41.8)	350	CO_2/2% CO 250 ppm H_2O	4,5,6	8×10^3	0.2 - 0.4	Protective	(2)
400	(28.2)	380	"	"	8×10^3	0.5 - 1.6	Protective	
600	(41.8)	380	"	"	8×10^3	2.0 - 4.0	Transition	

Table 2.8 Continued

Pressure lb/in^2 g	Pressure bar	Temperature °C	Gas	Steel	Time hr	Wt Gain mg/cm^2	Oxidation	Reference
600	(41.8)	400	CO_2/2% CO 250 ppm H_2O	4,5,6	8×10^3	4 - 10	Breakaway	(2)
600	(41.8)	450	"	"	6×10^3	10 - 80	Breakaway	
400	(28.2)	450	"	"	6×10^3	5 - 40	Breakaway	
-	1	500	Moist CO_2/CO	1	2×10^3	4	Protective	(3)
-	20	500	Dry CO_2	1	10^3 10^4	7 12.6	Protective	
-	20	500	Moist CO_2	1	10^3 8×10^3	2 7.6	Protective	
-	20	500	Moist CO_2/CO	1	10^3 2×10^3	8 18	Breakaway	

References (1) - Moore and Raine (1961)
(2) - Goodison et al (1969)
(3) - Antill et al (1968)

Numbers in Steel column refer to types of steel in Table (1.3) but not necessarily to exact compositions.

Table 2.9 Weight Gain Data for Low Alloy Steels in CO_2

Pressure lb/in^2 g	Pressure bar	Temperature °C	Gas	Steel	Time hr	Wt Gain mg/cm^2	Oxidation	Reference
150	(11.2)	450	Moist CO/CO_2	7	10^3	2	Protective	(1)
150	(11.2)	500	"	7	10^3	3	Protective	
150	(11.2)	550	"	7	10^3	6	Protective	
not stated		500 550	Dry CO_2, CO_2/5% CO, CO_2/2% CO 300 ppm H_2O	7	2.2×10^4	< 20	Protective	(2)
400/600	(28.2/41.8)	350	CO_2/2% CO 250 ppm H_2O	7	8×10^3	0.2 - 0.3	Protective	(3)
400/600	(28.2/41.8)	380	"	7	8×10^3	0.5 - 1	Protective	
600	(41.8)	400	"	7	8×10^3	1 - 3	Protective	
400/600	(28.2/41.8)	450	"	7	6×10^3	2 - 20	Transition	

Table 2.9 Continued

Pressure lb/in^2 g	Pressure bar	Temperature °C	Gas	Steel	Time hr	Wt Gain mg/cm^2	Oxidation	Reference
-	20	500	Dry CO_2	various steels	10^4	7 - 12	Protective	(4)
-	20	500	Moist CO_2	"	8×10^3	8 - 13 100	Protective Breakaway	
"	20	500	Moist CO_2/CO	"	2×10^3	7 - 10	Breakaway	
"	1	500	Moist CO_2/CO	"	2×10^3	3 - 4	Protective	

References (1) - Moore and Raine (1961)
(2) - Tyzack et al (1963)
(3) - Goodison et al (1969)
(4) - Antill et al (1968)

Numbers in Steel column refer to types of steel in Table (1.3), but not necessarily to exact compositions.

Table 2.10 Weight Gain Data for Iron in CO_2

Pressure bar	Temperature °C	Gas	Time hr	Wt Gain mg/cm^2	Oxidation
20	500	Dry CO_2	10^3 10^4	7 18.5	Protective
20	500	Moist CO_2	10^3 8×10^3	4 10.6	Protective
20	500	Moist CO_2/CO	10^3 2×10^3	7 37	Breakaway
1	500	"	2×10^3	6	Protective

Reference Antill et al (1968)

Table 2.11 Weight Gain Rate Data for Steels in CO_2

Pressure lb/in^2 g	Pressure bar	Temperature °C	Gas	Steel	Time hr	Rate mg/cm^{2}hr x 10^{-3}	Oxidation	Reference
200	(14.6)	400	Dry CO_2/0.2% CO	1	13.5 x 10^3	0.11	Linear	(1)
				5	13.5 x 10^3	0.04	"	
				7	13.5 x 10^3	0.10	"	
200	(14.6)	450	Dry CO_2	1	12.5 x 10^3	0.35	Decreasing	
				5	12.5 x 10^3	0.16	"	
				7	12.5 x 10^3	0.20	"	
200	(14.6)	450	Dry CO_2/5% CO	1	19 x 10^3	1.60	Linear	
				5	19 x 10^3	0.14	"	
				7	19 x 10^3	0.57	"	
200	(14.6)	500	Dry CO_2/5% CO	1	8 x 10^3	2.1	Decreasing	
				5	8 x 10^3	0.25	Linear	
				7	8 x 10^3	0.60	Decreasing	

Table 2.11 Continued

Pressure lb/in^2 g	Pressure bar	Temperature °C	Gas	Steel	Time hr	Rate mg/cm^{2}hr x 10^{-3}	Oxidation	Reference
200	(14.6)	400	Moist CO_2/0.2% CO	1	13 x 10^3	6.0	Linear	(1)
				5	13 x 10^3	0.12	Increasing	
				7	13 x 10^3	0.30	Linear	
200	(14.6)	450	Moist CO_2	1	7 x 10^3	40	Linear	
				5	7 x 10^3	0.16	"	
				7	7 x 10^3	2.7	"	
200	(14.6)	450	Moist CO_2/5%CO	1	7 x 10^3	40	"	
				5	7 x 10^3	1.8	"	
				7	7 x 10^3	2.2	"	
200	(14.6)	500	Moist CO_2/5% CO	1	10^4	20 - 55	"	
				5	10^4	1 - 2	"	
				7	10^4	5.2	"	

Table 2.11 Continued

Pressure lb/in^2 g	Pressure bar	Temperature °C	Gas	Steel	Time hr	Rate mg/cm^{2}hr x 10^{-3}	Oxidation	Reference
600	(41.8)	380	CO_2/2% CO/ 250 ppm H_2O	3	8 x 10^3	0.8	Linear	(2)
600	(41.8)	400	"	3	8 x 10^3	1.63	"	
400	(28.2)	450	"	7	8 x 10^3	6.3	"	
600	(41.8)	450	"	3	8 x 10^3	18 - 21	"	
				7	8 x 10^3	4 -5.1	"	
450	(31.6)	450	CO_2/250 ppm H_2O	3	8 x 10^3	18 - 19	"	
				7	8 x 10^3	5.6	"	

References (1) - Antill et al (1964)
(2) - Goodison et al (1969)

Numbers in Steel column refer to types of steel in Table (1.3) but not necessarily to exact compositions.

characteristics of the oxides formed, and then the understanding of mechanisms which has grown from analysis of the results.

2.4 Physical Observations.

Gibbs, Pendlebury and Wootton (1974) have reviewed many observations of the oxidation of mild steels in carbon dioxide. They quote Moore and Raine (1961), who reported that X-ray crystallography showed that the oxide formed is Fe_3O_4, containing some carbon, either free or as carbide. This is consistent with the thermodynamic evidence of Section (2.1). The oxide formed in the early, protective, stages of oxidation, up to 100 h at 550°C, is nearly all formed at the gas oxide boundary; inert markers placed on the metal remain near to the metal surface. Examination in detail using a scanning electron microscope can sometimes reveal a thin layer of oxide formed inside the markers, at the metal-oxide interface. Surman (1973) has also reported this thin inner layer, as shown in Figure (2.3).

At longer times, Gibbs et al (1974) reported, the inner layer becomes relatively thicker, approaching a maximum of equal thickness with the outer layer. Under these conditions, inert markers are found at the interface between the two layers. The boundary between the layers tends to follow the original outline of the specimen, even where the metal-oxide boundary becomes comparatively irregular. Many such specimens have been found in practical situations, as well as on test pieces. The inner layer contains inclusions such as carbide particles which can be identified as having been originally in the metal. The inner layer grows more quickly at the corners of specimens, rounding off the corners. The oxide at this stage is still protective;

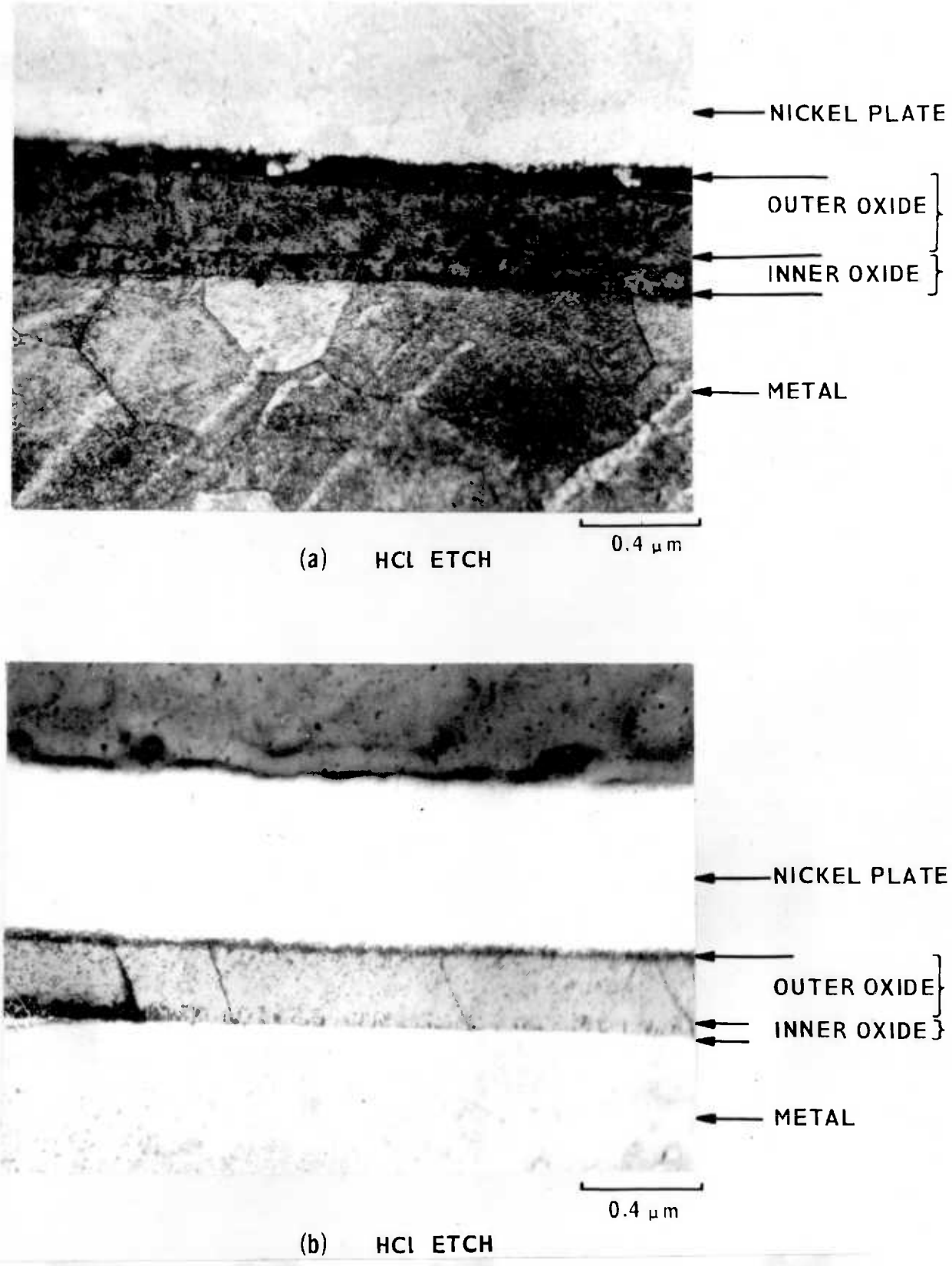

Figure 2.3 Two layer oxide formed on steel oxidised in CO_2
Reference Surman (1973)

PLATE 4 INNER TO OUTER OXIDE RATIOS OF 1:4 OBSERVED AFTER OXIDATION AT 500°C IN (a) 0.0125% CO/CO_2 AND (b) 10% CO/CO_2

Gibbs et al (1973) have shown that large stresses are not generated within it.

Gibbs et al (1974) also reported the contrasting situation when the oxide has become non-protective. Non-protective oxide is nucleated beneath the existing oxide, and may form either uniformly over the specimen or non-uniformly as a series of excrescences resembling volcanoes, which can push apart the protective oxide. This is shown in Figure (2.4), from work by Brown (1975). There is circumstantial evidence that this must be preceded by two layer protective growth. The excrescences are nucleated apparently at random, and then can grow together to form the uniform breakaway oxide. Gibbs et al (1973) demonstrated that after breakaway, compressive stresses are generated in the oxide.

2.4.1 Carbon formation.

Antill, Peakall and Warburton (1968) reported experiments to determine the oxidation kinetics and carbon content of protective and breakaway oxides formed on pure iron and on several different steels oxidised in CO_2 and CO/CO_2 mixtures at 500°C. They also investigated the effect on oxidation kinetics of saturating the gas with water vapour. Carbon made up about 0.5% of the weight gain for pure iron after protective oxidation in wet or dry CO_2, but contributed 5.4% by weight after breakaway oxidation in wet CO_2 containing 1-2% CO. The carbon percentages for steels were higher, but still showed corresponding increases in those situations where breakaway occurred.

The same authors also discussed experiments to investigate the conditions which favour carbon formation. Pure Fe powder was

Figure 2.4 Breakaway oxide excresence
Reference Brown (1975)

completely oxidised at 500°C in dry CO_2 at 1 bar. The product was then heated at 500°C in various atmospheres. Carbon formation was less than 90 p.p.m. for CO_2 containing 1-2% CO, either dry or saturated with water, at 1 or 20 bar. However, when the fraction of CO was increased to 30% $\pm$ 20% massive carbon deposits formed, at both pressures, in dry gas.

Similar experiments have been reported by Surman and Brown (1974). They studied the decomposition of CO over magnetite at 430°C and about 20 bar in CO/CO_2 mixtures in a sealed vessel. Samples of gas were analysed at intervals using a gas chromatograph. When the gas contained initially less than 30% of CO, the composition was found to be unchanged after 120 h and no carbon was formed. At 30% CO, some carbon was formed. With more than 30% CO, carbon was again formed and the gas composition changed until about 30% CO remained. The weight of carbon was consistent with reaction (2.2.2) being the only significant reaction. 30% CO is much higher than the equilibrium value of 0.2% calculated by the authors, and a similar value of 0.2% at 20 bar and 400°C, from Table (2.4).

Evidence for the distribution of the carbon formed during oxidation is given by Pritchard et al (1974). In a series of experiments at 500°C, specimens of mild steel were oxidised in CO_2 at 20 atmospheres pressure, and then further oxidised at 10 atmospheres in CO_2 containing $^{14}CO_2$. The specimens were then analysed, the total takeup of ^{14}C and its distribution being determined. The weight fraction of carbon in the oxide formed during the second oxidation was in the range 1-12%, varying between cases of oxidation in wet and dry gas, and the length of the first oxidation. When the distribution of the ^{14}C was

determined by counting the radioactivity, the greatest activity was found in the oxide near to the metal-oxide interface. In some cases there was a smaller peak near the oxide-gas boundary. A typical result is shown in Figure (2.5).

2.4.2 Physical properties of the oxide.

There is very little detailed information on the physical properties of the protective magnetite scale. The low weight gains (e.g 10 mg cm^{-2}) reported by Antill, Peakall and Warburton (1968) for protective oxidation mean that the oxide is too thin to be readily examined. Some workers have assumed that protective magnetite is non-porous (Price and Whittle, 1967), but others justify a low level of porosity on indirect evidence (Gibbs et al, 1974). No attempts to measure the porosity directly are available. It is clear, however, from the morphological evidence of Section (2.4), that the voidage of the protective oxide layer is either very small or zero.

Carbon content and porosity data have been reported by Gibbs et al (1974), for breakaway oxides. The density was appreciably less than the density of pure magnetite (5.18 gm cm^{-3}), as the mean carbon content was $5 \pm 1\%$ by weight, the voidage being $23 \pm 5\%$ including the carbon in the voidage. There are thus comparable volumes of void space and carbon in so-called breakaway magnetite.

Gibbs (1973) has set an upper bound for the porosity of pre-breakaway oxide based on a 5% difference in density from crystalline magnetite. This is derived from measurements of photographs of the oxide, and does not take into account other elements, such as carbon, present in the oxide.

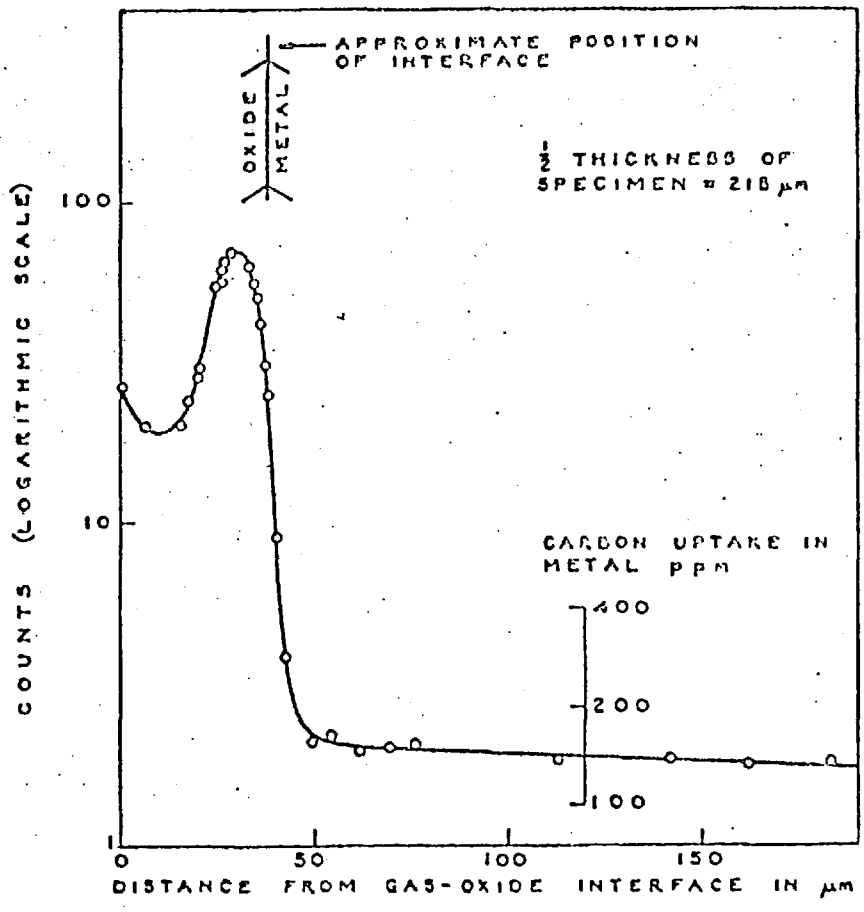

Figure 2.5 Carbon distribution in magnetite
Reference Pritchard et al (1974)

2.5 The Mechanism of Oxidation.

There has been a great deal of discussion of possible mechanisms for the oxidation of mild steel in CO_2, developing in parallel with the growth of experimental evidence. Thus, quite early in the investigations, Moore and Raine (1961) suggested that the protective film suffered a compressive stress which eventually caused it to rupture, thus causing breakaway. Price and Whittle (1967) considered this to be an inadequate model, and included reactions forming carbon. They suggested that disruption of the protective oxide is initiated by accumulation of hydrogen or CO beneath the film, thus disrupting it and allowing faster oxidation. In both of these papers lattice diffusion mechanisms only are considered for material transport in the protective oxide, that is to say, the oxide is regarded as wholly non-porous.

In their later work, Antill, Peakall and Warburton (1968) proposed that the outer layer of the two-layer protective oxide was formed by cation diffusion. The inner layer of ultimately equal thickness, formed either as a result of an anion transport mechanism or as a result of oxygen transport across closed pores. The latter was by dissociation and reformation of oxide, with CO or hydrogen acting as carrier within the pore. They favoured the latter mechanism, because other work suggested that anion diffusion in the lattice would be inadequate to account for the observed rates. Breakaway, they argued, might be caused by a build-up of H_2 or CH_4 within the oxide, or alternatively by the formation of carbon causing disruptive stresses. Discussion of high CO levels in pores and cracks enhancing carbon formation indicated some feeling that there might be voidage within the protective

oxide.

At the same period a radically different mechanism was proposed by Surman and Castle (1969). They argued by analogy with the situation in the oxidation of mild steel in steam, where they produced evidence of vapour phase transport of iron as volatile $Fe(OH)_2$ from the metal to form the outer layer of a two-layered oxide. A similar mechanism had also been used successfully to explain the corrosion of mild steel in alkaline solutions(Castle and Mann, 1966), and they now suggested that a similar vapour phase mechanism could apply to the case of steels in CO_2, with a volatile compound of iron, such as $Fe(CO)_5$, being responsible for the diffusion of iron through the oxide to form the outer layer.

In support of this general concept Castle, Emsley and Surman (1971) later reported movement of iron powder into a bed of alumina at 350°C when pure CO at 25 bar was passed through the bed.

A more recent paper by Gibbs (1973) goes so much further towards quantifying the different suggested mechanisms that it becomes possible to make distinguishing tests between them. He argues that the outer layer grows by metal lattice vacancy diffusion. In the temperature range of interest (350-550°C), iron diffusion is predominantly along 'short circuit' paths such as dislocations and grain boundaries in the oxide. The vacancies then accumulate at the metal interface, leading to the formation of voids and microporosity; this allows gas to reach the metal surface, thus allowing the inner layer oxidation to occur. Gibbs refers to the work of Channing and Graham (1972), who showed that a sufficient rate of iron diffusion across magnetite can occur to reduce

Fe_2O_3, under conditions of vacuum anneal, when solid but not vapour phase processes are possible; the activation energy of this process is within experimental error of that found for the parabolic rate constant for oxidation in CO_2. Cation diffusion, by a 'short circuit' mechanism, is therefore both an adequate and probable mechanism for outer layer magnetite formation.

In contrast Gibbs is in agreement with Surman and Brown (1974) that inner layer oxidation is a result of CO_2 gas access to the metal through microporosity in the oxide. Gibbs is able to set bounds on the diffusivity of the gases in porous magnetite needed to account for the observed oxidation rate and consistent with the magnetite densities found by Gibbs et al (1973) for prebreakaway oxide. These calculations showed that the diffusion of CO_2 is adequate for the observed oxidation; this requires, at low porosities, a large gas composition difference across the oxide. The high composition of CO is the most favourable for the formation of possible volatile iron compounds, as suggested by Surman and Castle (1969) as an alternative for outer layer oxidation: even under these circumstances, however, this mechanism is several orders of magnitude too small to contribute significantly to the oxidation.

At a recent conference, mild steel corrosion in CO_2 was reviewed by Leach (1974), who reported agreement that the protective oxide was formed in two layers, with the interface at the original metal surface, with some workers observing a single-layered initial stage. Both scales are magnetite, Fe_3O_4, and, after the initial period, both grow at approximately the same rate, the inner layer growing as a result

of oxidant access to the metal surface. The breakaway oxidation is initiated at the metal surface, and breaks up the duplex structure. A general survey of important variables shows that water has a significant effect, and that the levels in the metal of silicon, carbon, sulphur, phosphorus and manganese affect the oxidation.

There is some disagreement between the different groups of investigators about the mechanistic significance of the various factors. Gibbs et al (1974) and Surman and Brown (1974) both suggest mechanisms for breakaway where the significant factor is the development of a catalyst for the Boudouard reaction (2.2.2) at the metal surface, which thus causes an increase in the rate of carbon deposition. Pritchard et al (1974), however, suggest a mechanism involving hydrogen. None of these suggestions explains the role of silicon in the metal, nor the effects of water. Another significant difference is the nature of the rate-controlling step in the process. The critical factor is the diffusion of iron to form the outer layer. If the outer layer does not represent a barrier to diffusion, Leach considers there is no oxidation potential gradient to drive the iron diffusion, despite the agreement that the outer layer grows at the oxide gas interface.

Gibbs, Pendlebury and Wootton(1974), on the other hand extend the discussion of Gibbs (1973). They suggest that a key factor is the onset of breakaway is the formation of Boudouard catalysts, leading to carbon formation at a sufficient rate for the level of CO at the metal to actually fall, this accelerates the rate of oxidation, because the oxygen potential is now higher at the metal. Their qualitative

diagram is shown in Figure (2.6). The rapid formation of carbon prevents sintering of the oxide particles, which are therefore not limited to the volume made available by outward diffusion of iron. This means that the oxidation is no longer unstressed, and the existing two layer oxide is disrupted.

Surman and Brown (1974) agree with much of this mechanism, except that they have evidence that catalysts for the Boudouard reaction are no longer active below 30% CO in CO_2.

It is evident that there is not complete agreement on the mechanism of the oxidation of mild steel in CO and CO_2. One of the factors at issue is which of the steps controls the rate of the observed phenomena. In circumstances where several processes are occurring both in parallel and in sequence, there is no assurance that the control may not in fact be shared, in a way that may change in the course of the process. If that is the case, then measures of the overall kinetics, such as rate constants derived from (weight gain, time) graphs, give but a poor guide to the rates of the individual underlying steps of the mechanism. Further, changes in temperature may affect different steps in different ways, so that the overall activation energy for the process may not be a constant, but reflect a changing balance among several processes.

There is one factor which has not been fully considered in the development of the mechanisms reported. It is the development of a consistent mass balance, which must apply to the oxidation. Whatever the rate processes which are assumed to apply, the quantity of transfer

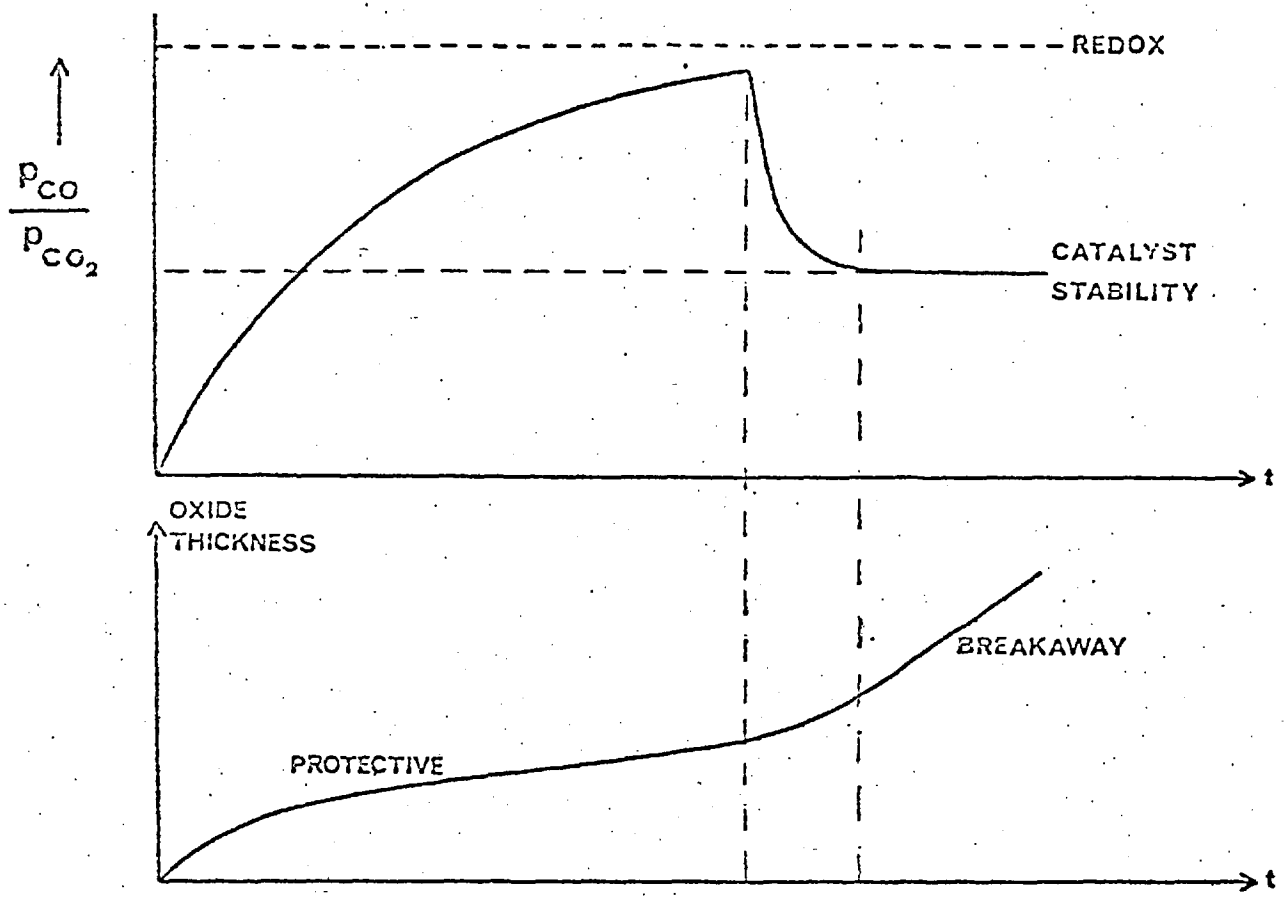

Figure 2.6 Suggested CO concentration-time profile
Reference Gibbs et al (1974)

at each step must be the quantity which is reacting and accumulating at the destination of that transfer. This is the simple but fundamental assumption which has been made in constructing an overall model for the oxidation. As far as possible, this has been done in such a way as to minimise the number of assumptions which limit the applicability of the overall mass balance to some mechanistic processes only. Thus the rate processes are considered separately, and can be incorporated at will in the mass balance. It is thus possible to consider alternative rate processes within the same framework.

3. Mathematical Modelling.

3.1 Introduction.

The process of corrosion is modelled by constructing a mass balance over the oxide layer. This accounts for all the mass flows, and allows for oxide growth, and the chemical reactions occurring. When this has been achieved, then the terms of the mass balance are related to the other variables of the system, using an appropriate physical model. For example, chemical reaction rates are modelled by rate 'laws' which are functions of the gas concentrations. In some cases, several alternative models have been considered.

It is possible to formulate the mass balance for any small element in the oxide layer, and to consider mass flows in three dimensions. Such an approach would be needed to account fully for the localised behaviour of the oxide in the later stages of oxidation, which has already been described in Section (2.4). At the earlier stages of oxidation considered here, the oxidation is much more uniform, as described in Section (2.4); the oxide is thin compared to the size of the metal involved. It is therefore justified to assume a planar oxide of uniform thickness at any time, and uniform properties at a constant distance from the surface, to formulate a model for the situation before 'breakaway' non-uniform oxidation occurs. This model can be formulated as a series of non-linear partial-differential equations in one space variable and time. Chemical reactions can be considered to take place throughout the oxide layer, and oxide properties such as voidage can be functions of the space variable, oxide depth. The results from this model would take the form of concentration profiles for the different

chemical components with depth, at different times.

The planar model is developed in Section (3.1.1), but it is reasonable to make some further simplifications. Evidence on the location of carbon deposits in oxidised specimens, discussed in Section (2.4.1) supports the view that carbon deposition takes place at the metal-oxide boundary. Evidence that the outer layer oxide is formed at the gas-oxide boundary has been discussed in Section (2.5). It has, therefore, been assumed that all significant chemical reactions are occurring at the appropriate boundary. There remain properties of the oxide which may vary with depth. However, in practice the thickness of the oxide is so small that its bulk properties are difficult to establish with any certainty, and no practical data are available on any variations with depth. Preliminary work with the system of partial differential equations showed that the solution of the non-linear differential boundary conditions arising from reaction at the metal-oxide boundary was particularly difficult. These reasons taken together justified consideration of a model with uniform oxide properties, where all reactions occur at the boundaries, and the chemical concentration profiles are assumed to be linear.

This two point model consists of a set of non-linear ordinary differential equations: the only independent variable is time. The mass balance is formulated only at the boundaries, and the equations incorporate alternative models for some of the rate processes. The set has been solved by well established numerical methods, to yield profiles with time of the oxide thickness, weight gain, and other significant variables. It is important that at no stage have assumptions been made

about the overall kinetics of the process, which is what is readily observable in experiments on oxidation. This means that the output from the model can be treated as raw data for the different types of curve fitting used by the oxidation chemist. The overall kinetics derived in this way are sometimes used to 'predict' the basic mechanism. That is not the case here - rather, the model is tested to see if it can produce the type of overall kinetics observed in experiment, and thus demonstrate which of the assumptions within the model leads to realistic behaviour.

There is a further difficulty, in that even the parameters needed for the simplified model are not all available. Some are determined by the physical situation, and others can be assigned values from other experiments, but there remain some to which can be assigned only a region of reasonable magnitude. In these cases, the model has been examined with a variety of values of each one, in the form of a factorial experiment. These results have been analysed to see which parameters have most effect on the various results.

If it is possible to establish more closely, by further experiment, what are the best values of these parameters, then it will be feasible to use the model in a more predictive way, for choices of assumptions about the rate processes which are thought to be reasonable.

3.1.1 The Mass Balance.

The evidence considered above suggests that the main chemical reactions to be considered in forming the mass balance are

(2.2.1) $3\,Fe + 4\,CO_2 = Fe_3O_4 + 4\,CO$ (1) at the metal-oxide boundary (C)

$Fe = Fe^*$ (2) at the metal-oxide boundary (C)

(2.2.2) $2\,CO = C + CO_2$ (3) in the inner oxide (B-C)

(2.2.1) $3\,Fe^* + 4\,CO = Fe_3O_4 + 4\,CO$ (4) in the outer oxide (A-B)

These are shown in Figure (3.1). Here Fe* represents a form of iron which can be transported from C to the outer oxide A-B. Possible forms for this to take were discussed in Section (2.5). These reactions have been incorporated into the planar model discussed in Section (3.1). The only difference in simplifying to the two-point model also discussed, is that reaction (3) now takes place exclusively at C, and reaction (4) at A.

A mass balance at a general plane, x, within the oxide for each of the transported species yields the following partial differential equations, in which N_A^x is the inward molar flux of species A through unit area distant x from the original metal surface, and $(A)^x$ is the molar concentration of species A at x.

Within oxide AB

$$-\frac{\partial N_{CO}^x}{\partial x} = -4r_4 + \varepsilon_{AB}\frac{\partial}{\partial t}(CO)^x + \varepsilon_{AB}(CO)^x\, k_4 r_4 \qquad (3.1.1)$$

$$-\frac{\partial N_{CO_2}^x}{\partial x} = +4r_4 + \varepsilon_{AB}\frac{\partial}{\partial t}(CO_2)^x + \varepsilon_{AB}(CO_2)^x\, k_4 r_4 \qquad (3.1.2)$$

$$-\frac{\partial N_{Fe*}}{\partial x} = +3r_4 + \varepsilon^*_{AB}\frac{\partial}{\partial t}(Fe*)^x + \varepsilon^*_{AB}(Fe*)^x\, k_4 r_4 \qquad (3.1.3)$$

Within oxide BC

$$-\frac{\partial N_{CO}^x}{\partial x} = 2r_3 + \varepsilon_{BC}\frac{\partial}{\partial t}(CO)^x + \varepsilon_{BC}(CO)^x\, k_3 r_3 \qquad (3.1.4)$$

$$-\frac{\partial N_{CO_2}^x}{\partial x} = -r_3 + \varepsilon_{BC}\frac{\partial}{\partial t}(CO_2)^x + \varepsilon_{BC}(CO_2)^x\, k_3 r_3 \qquad (3.1.5)$$

$$-\frac{\partial N_{Fe*}^x}{\partial x} = 0 + \varepsilon^*_{BC}\frac{\partial}{\partial t}(Fe*)^x + \varepsilon^*_{BC}(Fe*)^x\, k_3 r_3 \qquad (3.1.6)$$

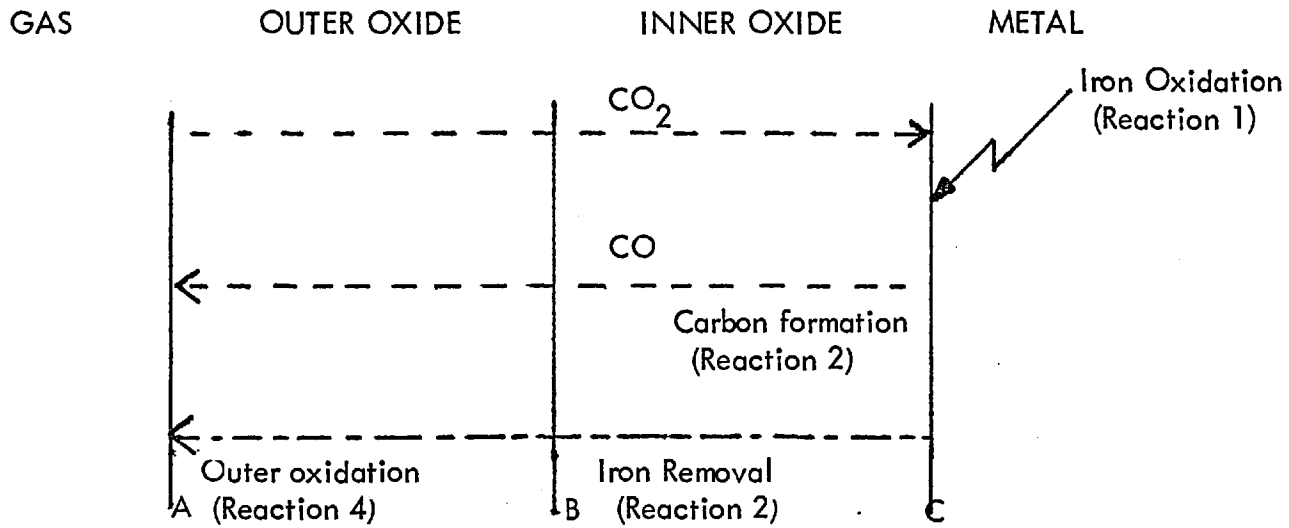

Figure 3.1 Schematic diagram of mass balance

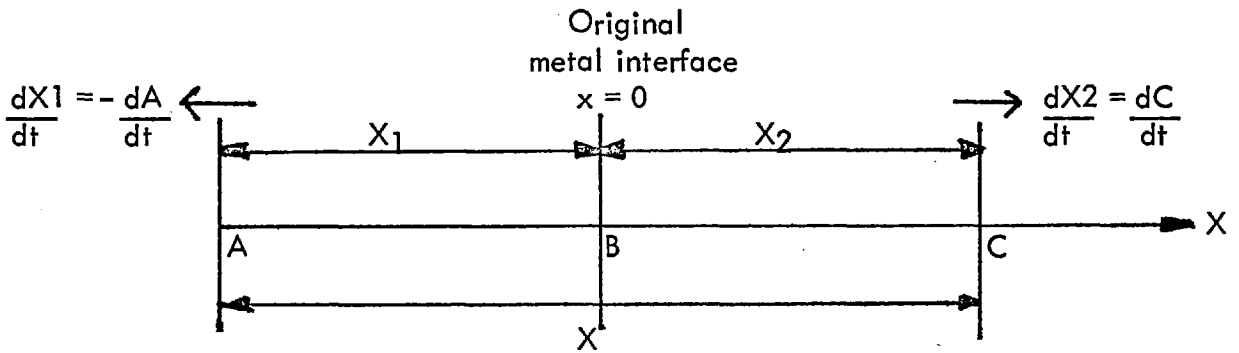

Figure 3.2 Schematic diagram of oxide growth

Each equation relates the change in the flux of one of the species to causes of change across the oxide. The first term is due to the species taking part in a chemical reaction, whose local reaction rate per unit volume of oxide is r_3 for reaction (3), etc. The second term accounts for the accumulation of the species because of changes in its local concentration, and the third term for the accumulation which occurs because the reaction taking place increases the size of the oxide, and therefore the space within it for accumulation. This increase will depend on the reaction rate, and also a constant, e.g. k_4, for reaction (4). Each of the last two terms will contain also the void fraction of the oxide, for the gases, ε_{AB} or ε_{BC} and for Fe*, an appropriate constant ε^*_{AB}.

These equations will be developed further in Section (3.3), after discussion of the order of magnitude of the processes involved. The boundary conditions are the same as those of the simpler, two-point, model. The external gas composition is assumed to be constant, as the work of Godfrey and Phennah (1968a) suggests that metal oxidation has no significant effect upon it. At the metal-oxide boundary, the total flux of gases is determined by the reactions occurring there, while some other concentrations are fixed by chemical equilibrium. These conditions are discussed in more detail in Section (3.3.1).

3.2 Order of magnitude of the processes involved.

As well as formulating the mass balance, each of the transport steps involved must be analysed, in order to construct a model for it. It is also necessary to estimate from reported data the rate of oxidation typically observed, to ensure that the models are reasonable.

The transport steps include the diffusion of gases outside and within the oxide, both of which depend on estimates of the diffusion coefficients of CO and CO_2 in their mixtures. The remaining transport is that of iron to form the outer layer of oxide. Suggested mechanisms have been discussed in Section (2.5) and these are now to be quantified.

3.2.1 Estimation of the Mass Transport Required.

The results of Antill et al (1968) are among those already discussed in Section (2.3); their results are summarised in Tables (2.8-10). Specimens of pure iron oxidised in various atmospheres at 20 bar showed protective oxidation following parabolic kinetics; typical weight gains after 500 h were in the range 2-5 mg cm^{-2}.

If parabolic kinetics for weight gain are assumed:

$$W^2 = k\,t \qquad (3.2.1)$$

and a value of W of 2 mg cm^{-2} (20 g m^{-2}) is used, then

$$k = 0.8\ g^2\ m^{-4}\ h^{-1}. \qquad (3.2.2)$$

The instantaneous rate of weight gain is given by

$$\frac{dW}{dt} = \frac{k}{2w} = 0.02\ g\ m^{-2}\ h^{-1} = 5 \times 10^{-11}\ g\ mm^{-2}\ s^{-1} \qquad (3.2.3)$$

This weight gain will consist largely of oxygen, supplied by the reduction of CO_2. The required transport of CO_2 from the gas to the oxide surface is therefore

$$N^A_{CO_2} = \frac{44}{16} \times 5 \times 10^{-11}\ g\ mm^{-2}\ s^{-1} = 3 \times 10^{-12}\ gmol\ mm^{-2}\ s^{-1} \qquad (3.2.4)$$

At a pressure of 20 atmospheres and 700K the ideal gas concentration, C_{tot}, is

$$C_{tot} = 3.49 \times 10^{2} \text{ gmol m}^{-3} = 3.49 \times 10^{-7} \text{ gmol mm}^{-3}. \quad (3.2.5)$$

These figures correspond with similar estimates made by Gibbs (1973). He gives an approximate figure for the oxygen "molecules" transported as CO_2 to the metal-oxide interface of

$$9.2 \times 10^{17} \text{ molecules m}^{-2} \text{ s}^{-1} = 1.5 \times 10^{-12} \text{ gmol mm}^{-2} \text{ s}^{-1} \quad (3.2.6)$$

This corresponds to a total requirement for the whole oxide of 6×10^{-12} gmol mm^{-2} s^{-1} of CO_2, and the agreement is satisfactory.

As the oxide is mainly formed by a reaction in which Fe_3O_4 replaces Fe, the weight gain for unit thickness of oxide is made up of the oxygen incorporated from the gas, together with any carbon deposit. This weight gain is about 1.4×10^{-3} g mm^{-3} of oxide formed. A weight gain of 2 mg cm^{-2} (20 g m^{-2}) corresponds to an oxide thickness of 1.3×10^{-2} mm (13 μm).

3.2.2 Estimation of the Gas Diffusion Coefficient.

The diffusion of gases in porous solids is discussed by Satterfield (1970), who distinguished between two distinct regimes of diffusion. In large pores, the gas molecules are colliding mainly with other gas molecules, and the diffusion process is similar to diffusion in a bulk gas. In the case of very small pores, collisions between gas molecules and the walls occur more often than collisions with gas molecules, and diffusion is no longer similar to bulk diffusion. At intermediate pore sizes, a mixed type of diffusion occurs. The problem

here is to identify which of these cases applies, and then to estimate the relevant diffusion coefficient. The bulk gas coefficient is in any case of relevance to discussion of gas diffusion outside the oxide.

Satterfield (1970) gave formulae for both bulk and Knudsen diffusion coefficients. In the case of bulk diffusion he quoted the Lennard-Jones formula:

$$D_{12}P = \frac{1.858 \times 10^{-3} \; T^{3/2} \; \left(\frac{m_1 + m_2}{m_1 m_2}\right)^{1/2}}{\sigma_{12}^2 \; \Omega_D} \; cm^2 \; bar \; s^{-1} \qquad (3.2.7)$$

where m_1 and m_2 are the molecular weights, T is in Kelvin, and the values of σ_{12} and Ω_D depend upon detailed treatment of the Lennard-Jones potential theory. Hirschfelder et al (1954) discussed this problem in more detail, and pointed out that this is an approximate solution to an integral problem. They suggested the following mixing rules to calculate the parameters σ_{12} and ε_{12} for the interactions between unlike molecules in a gas mixture:

$$\sigma_{12} = \frac{1}{2}(\sigma_1 + \sigma_2) \qquad (3.2.8)$$

$$\varepsilon_{12} = (\varepsilon_1 \varepsilon_2)^{1/2} \qquad (3.2.9)$$

where σ and ε are the parameters in the Lennard-Jones potential equation:

$$\Phi(r) = 4\varepsilon \left[(\sigma/r)^{12} - (\sigma/r)^6 \right] \qquad (3.2.10)$$

This applies only approximately even to spherical non-polar molecules,

although values can be assigned for other molecules.

Hirschfelder et al (1954) gave values of σ_{12} and ε_{12} for the $CO-CO_2$ mixture, together with calculated and experimental values of the diffusion coefficient at 273K and 1 bar. These are given in Table (3.1), together with extrapolation to 700K using the temperature dependence of Equation (3.2.7). The authors consider the agreement between the experimental and calculated values for a range of mixtures to be reasonable.

For Knudsen pore diffusion the different gases can be considered to diffuse independently. Satterfield here quoted the dimensional formula:

$$D_k = 19400 \frac{\varepsilon}{S_g \rho_p} \left(\frac{T}{m}\right)^{\frac{1}{2}} \quad cm^2\ s^{-1} \qquad (3.2.11)$$

where T is in Kelvin, m the molecular weight and the following parameters are properties of the solid phase through which diffusion is taking place: ε, the voidage fraction, S_g, the specific surface area ($cm^2\ g^{-1}$) and ρ_p the density ($g\ cm^{-3}$). The last of these is known to be 5.18 $g\ cm^{-3}$ for magnetite, but there is considerable uncertainty about the correct values to be used for ε and S_g. Equation (3.2.11) can be written

$$D_k = K \frac{\varepsilon}{S_g} \quad mm^2\ s^{-1} \qquad (3.2.12)$$

when S_g is expressed in $m^2\ g^{-1}$, K is 187 for CO and 149 for CO_2 at 700K.

When diffusion within a solid is being considered, all of these diffusion coefficients are in terms of the cross-section of gas path available and a correction must be applied to give an effective diffusion coefficient in terms of a fixed cross-section of oxide. The form for

Table 3.1 Diffusion coefficient for CO/CO_2.

Temperature (K)	Pressure (bar)	D_{12} ($mm^2\ s^{-1}$)	
273.2	1	13.7	(experimental)
273.2	1	12.8	(calculated)
700	1	52.5	(extrapolated)
700	20	2.62	(extrapolated)

this given by Satterfield (1970) is

$$D_{eff} = \frac{\varepsilon}{\zeta} D \qquad (3.2.13)$$

where ε is the void fraction, and ζ is a factor to allow for tortuosity. This is applied to both bulk and Knudsen diffusion coefficients, so that the basis of calculation can be a unit area of metal exposed to oxidation. Thus a combination of Equation (3.2.13) with either Equation (3.2.12) or the values of Table (3.1) provide estimates for further calculation of gas diffusion.

3.2.3 Gas diffusion outside the oxide.

The practical situation outside the oxide is one of a gas flow containing a mixture of components. It has already been discussed in Section (3.1.1) that the gas composition can be assumed to be a boundary condition for any model of the oxide. This will hold at a point sufficiently far from the oxide surface for the gas composition to be unaffected by the chemical reactions occurring. It must, however, be considered whether there is a significant difference between the bulk gas composition, and the composition in contact with the oxide: i.e. whether there is a significant boundary layer effect.

Such an effect is significant unless the concentration gradient involved is much smaller than any concentration gradient within the oxide itself. The mass transport involved is of the same order of magnitude: all the weight gain of the oxidation must cross the gas-oxide boundary, while up to half of the growth is in the inner layer, and must therefore be transported across the oxide, from the discussion of Section (2.5). Expressing both these mass fluxes approximately as

steady state equimolar diffusion, using the notation of Section (3.1.1):

$$N_{CO}^{A} = - D_{12} \frac{(CO)^{Bulk} - (CO)^{A}}{\delta} \text{ gmol mm}^{-2} \text{ s}^{-1} \qquad (3.2.14)$$

$$N_{CO}^{C} = - D_{eff} \frac{(CO)^{A} - (CO)^{C}}{X} \text{ gmol mm}^{-2} \text{ s}^{-1} \qquad (3.2.15)$$

where D_{eff} is the appropriate value from Equation (3.2.13), X the oxide thickness and δ the notational gas boundary layer. If N_{CO}^{C} is taken to by half of N_{CO}^{A}, i.e., the layers are growing at equal rates, then from Equations (3.2.14-15), the concentration gradients are in inverse ratio to the diffusion coefficients:

$$\frac{(CO)^{Bulk} - (CO)^{A}}{(CO)^{A} - (CO)^{C}} \cdot \frac{X}{2\delta} = \frac{D_{eff}}{D_{12}} \qquad (3.2.16)$$

The ratio can only approach unity when, from Equation (3.2.13), $\frac{\varepsilon}{\zeta}$ also approaches unity, i.e. the oxide is very porous, so that flow within it resembles that in the gas. The evidence of Section (2.4.2) is that such high voidages are found after breakaway, but not earlier in the oxidation. The concentration of CO can be expressed in terms of its mole fraction, C, and the total gas concentration C_{tot}, from Equation (3.2.5); substituting in Equation (3.2.14) yields:

$$N_{CO}^{A} = - D_{12} C_{tot} \frac{C^{Bulk} - C^{A}}{\delta} \text{ gmol mm}^{-2} \text{ s}^{-1} \qquad (3.2.17)$$

Using values of C_{tot} and D_{12} at 700K and 20 bar, from Sections (3.2.1-2),

an estimate of the mole fraction gradient needed to support the flux calculated in Section (3.2.1) can be obtained:

$$\frac{C^A - C^{Bulk}}{\delta} = \frac{N^A_{CO}}{D_{12}\, C_{tot}} = 3.3 \times 10^{-6} \ mm^{-1} \qquad (3.2.18)$$

This is extremely small compared with the gas mole fraction of 0.015 CO in CO_2 observed in reactors: the implication is that whenever the oxide is porous enough to be comparable as a barrier with the gas film, then the gas composition at the metal-oxide interface is essentially the same as the external gas. In these circumstances, either chemical reaction or metal transport must be controlling the oxidation. This calculation is effectively independent of pressure, because the diffusion coefficient, D_{12}, and the gas concentration are multiplied together, and their pressure dependences cancel out. In terms of mole fractions the effect is the same. This means that the external gas concentration can be used as a boundary condition when there is significant oxide resistance to gas diffusion, without the need to consider a gas boundary layer.

3.2.4 Gas diffusion across the oxide.

The gas diffusion coefficients calculated in Section (3.2.2) can now be used to determine which of the diffusion regimes applies in the less porous pre-breakaway oxide. Equation (3.2.15) can be written in terms of mole fractions:

$$N^C_{CO} = -\frac{D}{X} C_{tot} (C^A - C^C) \qquad (3.2.19)$$

Using the values of C_{tot} and X from Section (3.2.1), and N^C_{CO} as half N^A_{CO},

this becomes:

$$D(C^C - C^A) = D\Delta C = \frac{N^C_{CO} X}{C_{tot}} = 5.5 \times 10^{-8} \qquad (3.2.20)$$

From their work discussed in Section (2.5), both Gibbs et al (1974) and Surman and Brown (1974) agreed that the mole fraction difference, ΔC, is appreciable during pre-breakaway protective oxidation. This was based both on the need to explain the transport occurring at porosities known to be low, and also because of the observation that carbon deposition does occur, and that the experiments of Surman and Brown (1974) showed that it did not form under reactor conditions of temperature, pressure and composition. Gibbs et al (1974) suggest values approaching the equilibrium value for reaction (2.2.1) established as approximately 0.5 in Section (2.2). Taking a value of 0.3, and using Equation (3.2.13) together with the bulk and Knudsen diffusion coefficients calculated in Section (3.2.2), the gas diffusion regime can be ascertained, together with bounds to the values of ε and ζ needed to sustain the transport.

For the bulk diffusion coefficient, at 700K and 20 bar, substitution in Equation (3.2.20) gives:

$$\frac{\varepsilon}{\zeta} = \frac{5.5 \times 10^{-8}}{0.3 \times 2.62} = 6.0 \times 10^{-8} \qquad (3.2.21)$$

Satterfield (1970) gave an equation for the radius of the equivalent tubular pore for a solid of given voidage, density and specific surface area:

$$r_e = \frac{2\varepsilon}{S_g \rho_p} = 0.386 \frac{\varepsilon}{S_g} \quad m \qquad (3.2.22)$$

where S_g is in $m^2\ g^{-1}$. Substituting Equation (3.2.21) for ε in Equation (3.2.22) gives

$$r_e = 2.3 \times 10^{-8} \frac{\zeta}{S_g} \quad m \qquad (3.2.23)$$

For the Knudsen diffusion coefficient, substituting Equation (3.2.12) into Equation (3.2.13), taking K as 187 for CO and substituting in Equation (3.2.20) gives

$$\frac{\varepsilon^2}{S_g \zeta} = \frac{5.5 \times 10^{-8}}{0.3 \times 187} = 0.98 \times 10^{-9}\ g\ m^{-2} \qquad (3.2.24)$$

and in this case the equivalent pore radius is given by

$$r_e = 0.386\ (0.98 \times 10^{-9} \frac{\zeta}{S_g})^{1/2} = 3.9 \times 10^{-6} (\frac{\zeta}{S_g})^{1/2} \qquad (3.2.25)$$

The mean free paths of CO and CO_2 at 700K and 20 bar are approximately 10^{-2} μm and 7×10^{-3} μm respectively, calculated from room temperature data(Hodgman, 1960). For a pore diameter smaller than this, Knudsen diffusion will normally predominate over bulk diffusion. These values can be used with the pore radius Equations (3.2.23and25) to find the value of ζ/S_g for transition from bulk to Knudsen diffusion, although in fact there would not be a sharp transition. The ultimate lower limit on pore size for Knudsen diffusion is the size of the diffusing molecules, 4×10^{-4} μm, and this also provides a bound on ζ/S_g. These bounds are very sensitive to the assumed value of ΔC, and are given in Table (3.2) for values of 0.3 and 0.03. The lowest limit is not sensitive to pressure, but the transition limit is, as the mean free path varies

Table 3.2 Limits of gas diffusion regimes.
Pressure is 20 bar

Mole fraction difference	Lower limit on ζ/Sg for Knudsen diffusion $g\ m^{-2}$	Transition ζ/Sg from Knudsen to bulk diffusion $g\ m^{-2}$
0.03	100	5×10^4
0.3	1600	5×10^5

inversely with pressure.

These values have been used to estimate a consistent set of parameters of the oxide, under which the observed transport is sustained by the estimated concentration difference and diffusion coefficient. Values of the tortuosity do not normally exceed 10, and using this with a tentative estimate of the surface area of the oxide as in the range 0.01 - 0.1 $m^2\ g^{-1}$ Surman (1972) gives a very low value of about 10^{-5} for the voidage, ε , and a regime of Knudsen diffusion within micropores. The expectation of Knudsen diffusion is confirmed by substituting a value of 10 for ζ in Equation (3.2.21), which gives the extremely low value of 6×10^{-9} for bulk flow voidage. This is not reasonable; bulk pore diffusion is not compatible with a significant concentration gradient.

This calculation is an approximate one only, and not a substitute for measurements to establish more accurate values of the parameters. It does, however, set guidelines for values to be used in the modelling process. The values above yield an estimated effective diffusion coefficient, D, which is comparable at $2 \times 10^{-7}\ mm^2\ s^{-1}$ with values quoted by Satterfield (1970) for gases diffusing in zeolites with very small pores.

3.2.5 Transport of metal across the oxide.

The work discussed in Section (2.5), exemplified by Gibbs (1973), has concluded that metal is transported outwards across the oxide to form the outer layer, and that this transport is by 'short circuit' iron vacancy diffusion down grain boundaries and dislocations in the magnetite. No direct work has been done to produce a quantitative

measure of this diffusion; Castle and Surman (1969), however, investigating oxygen self-diffusion in magnetite, proposed Equation (3.2.26) for the concentration of iron

$$C^{o}_{Fe} = k\ (CO_2 / CO)^{1/n} \quad n = 3 \qquad (3.2.26)$$

vacancies, C^{o}_{Fe}, in magnetite in equilibrium with a mixture of CO and CO_2. If the iron vacancy concentration is assumed to be in equilibrium with the external gas at the gas-oxide boundary, and to be fixed at the metal-oxide boundary by the solid-solid equilibrium, then there is a concentration gradient of vacancies in the oxide, and the flux can be represented by a simple diffusion equation:

$$N^{C}_{Fe*} = D_{Fe}\ \frac{((C^{o}_{Fe})^{C} - (C^{o}_{Fe})^{A})}{X} \qquad (3.2.27)$$

Tomashov (1966) quoted the stoichiometic range of magnetite as 27.4 to 27.7% oxygen by weight, with an exact stoichiometric value of 27.64% oxygen by weight. Assuming that all the range is due to iron vacancies, the maximum fractional vacancy concentration, f, is

$$f = 0.3/72.36 = 0.004 \qquad (3.2.28)$$

This will occur when the ratio CO_2/CO is at the limit of stability of Fe_3O_4 with respect to Fe_2O_3, which is at a ratio of approximately 10^5. The maximum vacancy concentration is therefore given by:

$$C^{o}_{Fe,max} = 3\ f\ \rho o/M = 2.68 \times 10^{-7}\ g\ atom\ mm^{-3} \qquad (3.2.29)$$

and k in Equation (3.2.26) by the concentration when CO_2/CO is unity:

$$k = 2.68 \times 10^{-7}/10^{5/3} = 5.6 \times 10^{-9} \text{ g atom mm}^{-3} \qquad (3.2.30)$$

The transport in Equation (3.2.27) can now be calculated if a value for the diffusion coefficient, D_{Fe}, can be calculated. Birchenall (1968) gave a value of the self diffusion coefficient of iron in Fe_3O_4 of 10^{-9} mm^2 s^{-1} at 800°C, which extrapolates to much lower values in the temperature range 350 - 550°C. The value needed can be estimated using the estimates of required transport from Section (3.2.1) with the maximum possible concentration difference, from Equations (3.2.29-30):

$$D_{Fe} = \frac{N_{Fe^*} X}{C_{Fe}} = 0.75 \times 10^{-7} \text{ mm}^2 \text{ s}^{-1} \qquad (3.2.31)$$

This is larger than the value above, and thus there is agreement with the discussion in Section (2.5), where Gibbs' (1973) proposal of enhanced diffusion is mentioned. In the absence of any definite values, D_{Fe} has been treated in the model as an unknown parameter, to be varied over a range of significant values.

Since in this model the vacancy concentration is fixed by chemical equilibrium at both the inner and outer boundaries, these provide boundaries for Equation (3.2.27). The model presented here is not valid when the oxide is very thin, when the rate would be limited by other mechanisms, probably chemical rates.

3.3 Development of the Model.

The evidence already discussed in Section (2.5) suggests that the inner oxide, (B-C) in Figure (3.1), is formed at the metal-oxide boundary,

and the outer oxide, (A-B), at the gas-oxide boundary. There is also evidence, from Section (2.4), of the stress free nature of protective oxide and that the inner oxide is not more voluminous than the metal which it replaces. This means that the volume of inner oxide which can be formed is limited to the space made available by all the oxidation. The specific volume of magnetite per iron atom is larger than that of iron itself, and thus if the transport of iron to form the outer layer is insufficient, this limit will be reached. The volume available is still further reduced by the formation of carbon in the inner oxide. This has a large specific volume and can appreciably lower the mean density of the inner oxide.

The question of the volume available for new inner oxide can be tackled in various ways. In early versions of the model it was assumed that the metal transported at any time to form the outer oxide was just enough to release the space needed for the inner oxide and carbon. No separate model for the iron transport was included, and control was divided between the gas diffusion and chemical reaction processes. Later the model of Section (3.2.5) was introduced to represent the iron transport, and the possibilities for control of the inner oxidation became more complex.

When the oxide is thin, as at the start of oxidation, the rate of iron transport, which is inversely proportional to thickness (cf. Equation (3.2.27)), will be very high, while the chemical reaction to form the inner oxide will be bounded by the value attained when there is no significant resistance to gas flow through the oxide. For extremely thin oxide the outer layer reaction must

also be the controlling factor here, but this has been assumed always to attain equilibrium (cf. Section (3.2.5)). At these early stages, the inner oxide will be unable to grow fast enough to fill the available space. Carbon deposition will also be low, for any models which assume that this increases as the CO mole fraction at the metal increases, because the gas will still be comparatively uniform in composition throughout the oxide thickness.

As the oxide becomes thicker, the iron transport falls inversely with thickness, always controlling the outer layer. The inner layer oxidation rate also falls as the barrier to gas diffusion increases, but does so in a more complex manner, as there are two steps involved, diffusion and reaction. If it falls more slowly, then eventually it is limited by the volume available, and competes for this space with the formation of carbon. In extreme cases all the volume available is used for carbon, and here the model becomes inadequate, and might be extended.

These mechanisms are incorporated into the two point model in the following sections, but it is first necessary to consider the simplifications of Equations (3.1.1-6), to form such a two-point model.

3.3.1 Simplification to two-point model.

In Section (3.1) it is explained why reactions (3) and (4) can be assumed to take place at (C) and (A) respectively. This means that the local reaction rates within the oxide, r_3 and r_4, are both zero, when the terms containing them in Equations (3.1.1-6) all vanish. All the reaction rates are represented as boundary conditions on the equations, at the appropriate boundary; R_1, R_2, R_3 and R_4, the first

3 at (C), and the last at (A), are the reaction rates per unit area of oxide. Equations (3.1.1-6) can now all be integrated across the oxide to yield the equations:

$$N^A_{CO} - N^B_{CO} = \varepsilon_{AB} \frac{\partial}{\partial t} \int_A^B (CO)^x \, dx \qquad (3.3.1)$$

$$N^A_{CO_2} - N^B_{CO_2} = \varepsilon_{AB} \frac{\partial}{\partial t} \int_A^B (CO_2)^x \, dx \qquad (3.3.2)$$

$$N^A_{Fe*} - N^B_{Fe*} = \varepsilon^*_{AB} \frac{\partial}{\partial t} \int_A^B (Fe*)^x \, dx \qquad (3.3.3)$$

$$N^B_{CO} - N^C_{CO} = \varepsilon_{BC} \frac{\partial}{\partial t} \int_B^C (CO)^x \, dx \qquad (3.3.4)$$

$$N^B_{CO_2} - N^C_{CO_2} = \varepsilon_{BC} \frac{\partial}{\partial t} \int_B^C (CO_2)^x \, dx \qquad (3.3.5)$$

$$N^B_{Fe*} - N^C_{Fe*} = \varepsilon^*_{BC} \frac{\partial}{\partial t} \int_B^C (Fe*)^x \, dx \qquad (3.3.6)$$

The integrals must be made within the differentiation since the position of A and C will move with time, relative to B, the original metal surface (cf. Sections (3.3) and (3.1.1)). These integrals all represent gas or vacancies accumulating in the growing oxide. If each

of the pairs of equations for the same component is added together and the voidages assumed to be the same for each layer, then the equations become:

$$N^{A}_{CO} - N^{C}_{CO} = \varepsilon \frac{\partial}{\partial t} \int_{A}^{C} (CO)^{x} \, dx \qquad (3.3.7)$$

$$N^{A}_{CO_2} - N^{C}_{CO_2} = \varepsilon \frac{\partial}{\partial t} \int_{A}^{C} (CO_2)^{x} \, dx \qquad (3.3.8)$$

$$N^{A}_{Fe*} - N^{C}_{Fe*} = \varepsilon^{*} \frac{\partial}{\partial t} \int_{A}^{C} (Fe*)^{x} \, dx \qquad (3.3.9)$$

Using the relationship

$$\frac{\partial}{\partial t} \int_{A}^{C} f(x)dx = f(C) \frac{dC}{dt} - f(A) \frac{dA}{dt} + \int_{A}^{C} \frac{\partial f(x)}{\partial t} \, dx \qquad (3.3.10)$$

these become

$$N^{A}_{CO} - N^{C}_{CO} = \varepsilon(CO)^{C} \frac{dC}{dt} - \varepsilon(CO)^{A} \frac{dA}{dt} + \varepsilon \int_{A}^{C} \frac{(CO)^{x}}{t} \, dx \qquad (3.3.11)$$

$$N^{A}_{CO_2} - N^{C}_{CO_2} = \varepsilon (CO_2)^{C} \frac{dC}{dt} - \varepsilon (CO_2)^{A} \frac{dA}{dt} + \varepsilon \int_{A}^{C} \frac{(CO_2)^{x}}{t} \, dx \qquad (3.3.12)$$

$$N^{A}_{Fe*} - N^{C}_{Fe*} = \varepsilon^{*}(Fe*)^{C}\frac{dC}{dt} - \varepsilon^{*}(Fe*)^{A}\frac{dA}{dt} + \varepsilon^{*}\int_{A}^{C}\frac{(Fe*)^{x}}{t}\,dx \quad (3.3.13)$$

The movement of A and C is related to the changes in thickness of the two oxide layers, as shown in Figure (3.2), using B as a reference point

$$\frac{dX_1}{dt} = \frac{dA}{dt} \quad (3.3.14)$$

$$\frac{dX_2}{dt} = \frac{dC}{dt} \quad (3.3.15)$$

It is now necessary to make the assumption of a linear concentration profile for each component discussed in Section (3.1). This takes the same form for each, e.g.

$$\frac{(CO)^{x} - (CO)^{A}}{(CO)^{C} - (CO)^{A}} = \frac{x - A}{C - A} \quad (3.3.16)$$

where $$C - A = X_1 + X_2 = X \quad (3.3.17)$$

and X is the total oxide thickness (cf. Figure (3.1)).

Hence $$(CO)^{x} = (CO)^{A} + \left[(CO)^{C} - (CO)^{A}\right]\frac{(x - A)}{X} \quad (3.3.18)$$

and $$\frac{\partial (CO)^{x}}{\partial t} = \frac{\partial}{\partial t}(CO)^{A} + \frac{\partial}{\partial t}\left[(CO)^{C} - (CO)^{A}\right]\frac{(x - A)}{X} \quad (3.3.19)$$

Then, on integration with respect to x

$$\int_A^C \frac{\partial (CO)^x}{\partial t} dx = X \frac{\partial}{\partial t} (CO)^A + \frac{\partial}{\partial t} \left[(CO)^C - (CO)^A\right] \frac{1}{X} \int_A^C (x - A)\, dx \quad (3.3.20)$$

$$= X \frac{\partial}{\partial t} (CO)^A + \frac{X}{2} \frac{\partial}{\partial t} \left[(CO)^C - (CO)^A\right] \quad (3.3.20a)$$

$$= \frac{X}{2} \left[\frac{\partial}{\partial t} (CO)^A + \frac{\partial}{\partial t} (CO)^C\right] \quad (3.3.21)$$

And for CO_2 and Fe*

$$\int_A^C \frac{\partial}{\partial t} (CO_2) dx = \frac{X}{2} \left[\frac{\partial}{\partial t} (CO_2)^A + \frac{\partial}{\partial t} (CO_2)^C\right] \quad (3.3.22)$$

$$\int_A^C \frac{\partial}{\partial t} (Fe^*) dx = \frac{X}{2} \left[\frac{}{t} (Fe^*)^A + \frac{\partial}{\partial t} (Fe^*)^C\right] \quad (3.3.23)$$

These can be further simplified using as boundary conditions the external gas composition, as discussed in Section (3.2.3), and the concentrations of iron vacancies, which are controlled by chemical equilibrium, as discussed in Section (3.2.5). These conditions are:

$$(CO)^A = (CO)^{ext} \quad (3.3.24)$$

$$(CO_2)^A = (CO_2)^{ext} \quad (3.3.25)$$

$$(Fe^*)^A = C^o_{Fe}A \quad (3.3.26)$$

$$(Fe^*)^C = C^o_{Fe}C \quad (3.3.27)$$

when all the derivative terms except those in $(CO)^C$ and $(CO_2)^C$ are zero. Equations (3.3.11-13) then become:

$$N^A_{CO} - N^C_{CO} = \varepsilon(CO)^C \frac{dX}{dt}2 + \varepsilon(CO_{ext}) \frac{dX}{dt}1 + \varepsilon\frac{X}{2}\frac{\partial}{\partial t} (CO)^C \quad (3.3.28)$$

$$N^A_{CO_2} - N^C_{CO_2} = \varepsilon(CO_2)^C \frac{dX}{dt}2 + \varepsilon(CO_{2ext}) \frac{dX}{dt}1 + \varepsilon \frac{X}{2}\frac{\partial}{\partial t} (CO_2)^C \quad (3.3.29)$$

$$N^A_{Fe*} - N^C_{Fe*} = \varepsilon^*(C^o_{Fe})^C \frac{dX}{dt}2 + \varepsilon^*(C^o_{Fe})^A \frac{dX}{dt}1 \quad (3.3.30)$$

These equations have the boundary conditions that at C the reactions (1), (2) and (3) take place, so that

$$N^C_{CO} = -4R_1 + 2R_3 \quad (3.3.31)$$

$$N^C_{CO_2} = 4R_1 - R_3 \quad (3.3.32)$$

$$N^C_{Fe*} = -R_2 \quad (3.3.33)$$

and reaction (4) at A:

$$N^A_{Fe*} = -3R_4 \quad (3.3.34)$$

The terms R_i are the reaction rates per unit area at the appropriate boundary.

3.3.2 Justification of further simplification.

It can now be shown that the terms on the righthand sides of Equations (3.3.28-30) can be neglected in comparison with Equations (3.3.31-33), so that the fluxes at A are effectively equal to those at C. Dividing Equations (3.3.28-30) by Equations (3.3.31-33) respectively, we obtain:

$$\frac{N^A_{CO} - N^C_{CO}}{N^C_{CO}} = \frac{\varepsilon}{-4R_1 + 2R_3}\left[(CO)^C \frac{dX_2}{dt} + (CO)^A \frac{dX_1}{dt} + \frac{X}{2}\frac{\partial}{\partial t}(CO)^C\right] \quad (3.3.35)$$

$$\frac{N^A_{CO_2} - N^C_{CO_2}}{N^C_{CO_2}} = \frac{\varepsilon}{4R_1 - R_3}\left[(CO_2)^C \frac{dX_2}{dt} + (CO_2)^A \frac{dX_1}{dt} + \frac{X}{2}\frac{\partial}{\partial t}(CO_2)^C\right] \quad (3.3.36)$$

$$\frac{N^A_{Fe*} - N^C_{Fe*}}{N^C_{Fe*}} = \frac{\varepsilon^*}{-R_2}\left[(C^o_{Fe})^C \frac{dX_2}{dt} + (C^o_{Fe})^A \frac{dX_1}{dt}\right] \quad (3.3.37)$$

If the growth of the two oxide layers is assumed as an approximation to be due only to the formation of oxide whose specific volume is $V\ mm^3\ gmol^{-1}$, then

$$\frac{dX_1}{dt} = VR_4 \quad \text{and} \quad \frac{dX_2}{dt} = VR_1 \quad (3.3.38)$$

Using these values, neglecting carbon formation (reaction (3)), and

introducing C for the mole fraction of CO, then Equations (3.3.35-36) become

$$\frac{N^A_{CO} - N^C_{CO}}{N^C_{CO}} = \frac{\varepsilon C_{tot}}{-4R_1}\left[CVR_1 + CVR_4 + \frac{X}{2}\frac{\partial}{\partial t}C\right] \qquad (3.3.39)$$

$$\frac{N^A_{CO_2} - N^C_{CO_2}}{N^C_{CO_2}} = \frac{\varepsilon C_{tot}}{4R_1}\left[(1-C)VR_1 + (1-C)VR_4 - \frac{X}{2}\frac{\partial}{\partial t}C\right] \qquad (3.3.40)$$

If $R_1 \sim R_4 \simeq 10^{-12}$ gmol/mm^{2}s, $X \sim 10^{-2}$mm, $C_{tot} = 3 \times 10^{-7}$ gmol/mm^3 as discussed in Section (3.2.1) and $V \simeq 45 \times 10^3$ mm^3/gmol, for Fe_3O_4, and $\varepsilon \simeq 10^{-4}$ as discussed in Section (3.2.4), then these equations become:

$$\frac{N^A_{CO} - N^C_{CO}}{N^C_{CO}} = -3 \times 10^{-11}\left[\frac{1}{4} C\, 45 \times 10^2\ \ 2 + \frac{10^{-2}}{8.10^{-12}}\frac{\partial C}{\partial t}\right] \qquad (3.3.41)$$

$$\frac{N^A_{CO_2} - N^C_{CO_2}}{N^C_{CO_2}} = +3 \times 10^{-11}\left[\frac{1}{4}(1-C)\,45 \times 10^3\ \ 2 - \frac{10^{-2}}{8.10^{-12}}\frac{\partial C}{\partial t}\right] \qquad (3.3.42)$$

$$\frac{N^A_{CO} - N^C_{CO}}{N^C_{CO}} = 7 \times 10^{-7}\ C - 0.04\frac{\partial C}{\partial t} \qquad (3.3.43)$$

$$\frac{N^{A}_{CO_2} - N^{C}_{CO_2}}{N^{C}_{CO_2}} = + 7 \times 10^{-7} \ (1 - C) - 0.04 \ \frac{\partial C}{\partial t} \qquad (3.3.44)$$

As $0 \leq C \leq 1$, the first terms can be neglected. The second term will also be negligible in all situations except very early in the oxidation, because the time units are seconds, compared to the hours of oxidation, for CO change. But, the value of X is lowest, and R_1 highest, early in oxidation, so that even then the effect is small. In the case of Equation (3.3.37), if it is conservatively assumed that the appropriate voidage for iron vacancies, ε^{*} is

$$\varepsilon^{*} = 1 - \varepsilon \qquad (3.3.45)$$

i.e. that all the oxide is available for diffusion, then

$$\frac{N^{A}_{Fe*} - N^{C}_{Fe*}}{N^{C}_{Fe*}} = (C^{o}_{Fe})^{C} \ V \frac{R_1}{R_2} + (C^{o}_{Fe})^{A} \ V \frac{R_4}{R_2} \qquad (3.3.46)$$

When using the values discussed in Section (3.2.5) $(C^{o}_{Fe})^{C} \quad 10^{-7}$, $(C^{o}_{Fe})^{A} \simeq 10^{-9}$, with $R_1 \simeq R_4 \simeq \frac{R_2}{3}$

$$\frac{N^{A}_{Fe*} - N^{C}_{Fe*}}{N^{C}_{Fe*}} \simeq 10^{-3} \qquad (3.3.47)$$

which can be neglected in comparison with the assumptions made in Section (3.2.5).

In particular, from Equations (3.3.33-34) and Equation (3.3.47)

$$- R_2 = N^C_{Fe*} = N^A_{Fe*} = - 3R_4 \qquad (3.3.48)$$

3.3.3 Incorporation of the volume mechanism.

It is now possible to quantify the discussion of Section (3.3), and apply it to Equations (3.3.31-33), using the assumption justified in Section (3.3.2), that the lefthand sides of Equations (3.3.28-30) are equal to zero, and thus Equations (3.3.31-33) apply throughout the oxide. Equation (3.3.38) for the oxide growth rate can be stated more accurately as

$$\frac{dX}{dt}1 = K_1\, 3R_4 = K_1\, R_2 \qquad (3.3.49)$$

and

$$\frac{dX}{dt}2 = K_2\, 3R_1 + K_C\, R_3 \qquad (3.3.50)$$

Here K_1 and K_2 are related to the molecular volumes of the pure oxide, V, by the Equation (3.3.51), and K_C is the molecular volume of carbon.

$$\begin{aligned} K_1 &= V/3\,(1 - \varepsilon) \\ K_2 &= V/3\,(1 - \varepsilon - \varepsilon_C) \\ V &= 44.7 \times 10^3 \text{ mm}^3/\text{gmol} \\ K_C &= 6.0 \times 10^3 \text{ mm}^3/\text{gmol} \end{aligned} \qquad (3.3.51)$$

where ε_C is the volume fraction of carbon in the inner oxide. All of these coefficients are constant except K_2 and ε_C. If a variable Z is defined

$$Z = {}^{R_3}/_{R_1} \qquad (3.3.52)$$

Then the mass fraction of carbon in new inner oxide being formed, Cn, is

$$Cn = M_C Z/(M_C Z + M_{Fe_3O_4}) \qquad (3.3.53)$$

where M_C and $M_{Fe_3O_4}$ are the molecular weights. The density of the oxide formed is given by

$$\rho = (1 - \varepsilon)/(Cn/\rho_C + (1 - Cn)/\rho_O \qquad (3.3.54)$$

where ρ_O and ρ_C are the bulk densities of Fe_3O_4 and carbon. Then

$$\varepsilon_C = Cn\rho/\rho_C \qquad (3.3.55)$$

and thus ε_C and K_2 depend upon R_3/R_1.

The inner oxide cannot grow faster than the volume made available for it by the removal of iron from the metal, as discussed in Section (3.3). This can be represented by

$$\frac{dX}{dt}2 \leq K_3 (3R_1 + R_2) \qquad (3.3.56)$$

where K_3 is the molecular volume of the metal.

$$K_3 = V_{Fe} = 7.1 \times 10^3 \text{ mm}^3/\text{gmol} \qquad (3.3.57)$$

Substituting Equation (3.3.50) in Equation (3.3.56), the inequality becomes:

$$K_3 (3R_1 + R_2) \geq 3K_2 R_1 + K_C R_3 \qquad (3.3.58)$$

Auxiliary variables S and Q are defined to be the ratios, respectively, of the two oxidation reactions, and the rates of growth of the two layers.

$$S = \frac{R_4}{R_1} = \frac{R_2}{3R_1} \tag{3.3.59}$$

$$Q = \frac{dX_1}{dt} \Big/ \frac{dX_2}{dt} \tag{3.3.60}$$

Using Equation (3.3.59) in Equation (3.3.58), this inequality can be expressed in a simple form where the only variables are S, R_3 and R_1, together with the slight dependence of K_2 on ε_c.

$$S \geq \frac{K_2}{K_3} - 1 + \frac{K_c R_3}{3K_3 R_1} \tag{3.3.61}$$

Similarly, Equations (3.3.49-50) can be substituted into Equation (3.3.60) to yield

$$Q = \frac{K_1 R_2}{3K_2 R_1 + K_c R_3} = \frac{\frac{K_1}{K_2} S}{1 + \frac{K_c R_3}{3K_2 R_1}} \tag{3.3.62}$$

The weight gain rate of the oxide, $\dot{W}$, depends on the reaction rates, and also on the atomic weights of oxygen and carbon

$$\frac{dW}{dt} = \dot{W} = 4(16)(R_1 + R_4) + (12)R_3 \tag{3.3.63}$$

$$= 64R_1(1 + S) + 12 R_3 \tag{3.3.64}$$

and the oxide growth rate F can be expressed

$$F = \frac{dX_1}{dt} + \frac{dX_2}{dt} = (1 + Q)(3K_2 R_1 + K_c R_3) \tag{3.3.65}$$

3.3.4 The two-point model.

The equations needed for the model outlined in Section (3.3) have now been derived. The basic Equations are (3.3.61-65) together with Equation (3.3.31). The conclusion of Section (3.3.2) that Equation (3.3.43) can be neglected means that Equation (3.3.31) can be written

$$N_{CO} = -4R_1 + 2R_3 \qquad (3.3.66)$$

where the flux term now applies throughout the oxide.

The inequality of Equation (3.3.61) has been treated in two ways, corresponding to the discussion of Section (3.3). First, S can be made always equal to the right hand side of Equation (3.3.61), in which case the rate of reaction (2) is determined by that of reactions (1) and (3), providing just enough space for the inner oxide. The alternative is to assume a separate mechanism for reaction (2), as discussed in Section (3.2.5). In this case the inequality can apply, when the inner oxide does not use all the volume available, and the equality of Equation (3.3.61) means that the inner layer growth is restricted to the volume available.

It is unnecessary to consider the corresponding equation for CO_2, because the sum of the mole fraction is unity and the total pressure is constant at all points in the oxide. The Equation for Fe* is given as (3.3.48).

In deriving these equations, no particular form has been assumed for the reaction rate expressions. The equations cannot be solved

without rate expressions, but the approach maintains the greatest possible flexibility in trying alternatives. Many of the transport models were discussed in Sections (3.2) to (3.2.5). These, and others for the chemical reactions, can now be substituted into the model.

3.4 The models for rate processes.

3.4.1 Oxidation reactions.

The oxidation reaction at the metal-oxide boundary, reaction (1), is assumed to depend upon the local concentration of CO, and the value at which CO and CO_2 are both in equilibrium with the metal and oxide. This value can be estimated from the thermodynamic data of Section (2.2) to be approximately 1:1 of CO to CO_2 at a temperature of 350-550°C. A simple equation based upon this thermodynamic argument is

$$R_1 = r_1 ((CO)^{eqm} - (CO)^{C}) \qquad (3.4.1)$$

where r_1 is a rate constant which must be estimated. The equation provides a maximum value, which is not reached when the separate mechanism for reaction (2) is limiting, as discussed in Section (3.3.4).

The outer layer oxidation, at the gas-oxide boundary, is assumed to be controlled by the rate of iron transport, with reactions (2) and (4) at chemical equilibrium, as discussed in Section (3.2.5). In Section (3.3) it is concluded that this may not be valid when the oxide is very thin.

Two different assumptions have been made for this rate: the first is when S is determined by Equation (3.3.61) (cf. Section (3.3.4)), then no rate expression is needed. In the second the following expression is

used, derived from Section (3.2.5):

$$-N_{Fe*} = R_2 = \frac{D_{Fe}\, k}{X}\left[\left(\frac{CO_2}{CO}\right)^{1/n}_{ext} - \left(\frac{CO_2}{CO}\right)^{1/n}_{eqm}\right] \qquad (3.4.2)$$

where n = 3.

3.4.2 Carbon formation.

Evidence on the formation of carbon in the oxide discussed in Section (2.4.1) shows that carbon formation depends upon the concentration of CO, and that very little carbon is formed at low levels of CO. Several alternative models are used. The first assumes that the ratio of reaction (3) to reaction (1) is constant, i.e.

$$R_3 = ZR_1 \;;\; Z \text{ constant} \qquad (3.4.3a)$$

This does not depend upon CO in the suggested manner, but is simpler mathematically and was used in development of the numerical solution.

The alternatives are to use first or second order dependence on the CO.

$$R_3 = r_{31}\,(CO)^C \qquad (3.4.3b)$$

$$R_3 = r_{32}\,((CO)^C)^2 \qquad (3.4.3c)$$

where r_{31} and r_{32} are rate constants to be estimated. Equation (3.4.3c) has been used because it better represents as a smooth function the experimental evidence available, that carbon formation is low when the CO level is low(Surman and Brown, 1974).

3.4.3 Gas diffusion.

The model for the flux of CO is the Equation (3.2.15) of Section (3.2.3). This uses as a driving force for transport the linear gradient of CO across the oxide.

$$N_{CO} = \frac{D_{eff}}{X} \left((CO)^C - (CO)^A\right) \qquad (3.4.4)$$

3.5 The assembled model.

The equations are now in the form of a set of ordinary differential equations in time. They are non-linear, and must be solved numerically: they are restated here for convenience. These are Equations (3.3.64-65) and Equation (3.3.50), with a separate integration to sum the carbon formed.

$$\frac{dW}{dt} = \dot{W} = 64R_1 (1 + S) + 12 R_3 \qquad (3.5.1)$$

$$\frac{dX}{dt} = F = (1 + Q) (3 K_2R_1 + K_CR_3) \qquad (3.5.2)$$

$$\frac{dX_2}{dt} = 3 K_2R_1 + K_CR_3 \qquad (3.5.3)$$

$$\frac{dW}{dt}C = 12R_3 \qquad (3.5.4)$$

The auxiliary Equations (3.3.61-62) are also needed:

$$S \geq \frac{K_2}{K_3} - 1 + \frac{K_C R_3}{3K_3R_1} \qquad (3.5.5)$$

$$Q = \frac{\frac{K_1 S}{K_2}}{(1 + \frac{K_C R_3}{3K_2 R_1})} \qquad (3.5.6)$$

Another essential equation is Equation (3.3.66), which must be solved at every time, to determine the concentration of CO which balances the various rates:

$$N_{CO} = -4R_1 + 2R_3 \qquad (3.5.7)$$

These equations, together with the models for the rate processes, Equations (3.4.1-4), can now be solved numerically. The initial conditions are $X = W = W_C = 0$ at $t = 0$, with X set equal to a small value, to avoid numerical difficulties.

3.5.1 Effectiveness factors.

It is possible to define effectiveness factors for the different causes of weight gain, in comparison with the weight gain which would result from a clean metal surface oxidising by the mechanism of Equation (3.4.1) only, when in contact with gas of the bulk composition. The weight gain, $\dot{W}^*$, and the oxidation rate, R_1^*, for this are given by

$$\dot{W}^* = 64R_1^* = 64\, r_1\, ((CO)^{eq} - (CO)^{ext}) \qquad (3.5.8)$$

Then for reaction (1), the effectiveness factor E_1 is

$$E_1 = \frac{R_1}{R_1^*} \qquad (3.5.9)$$

and for the outer layer, reaction (4),

$$E_4 = \frac{R_4}{R_1^*} = \frac{R_1}{R_1^*} S \qquad (3.5.10)$$

and for carbon formation, on a weight basis

$$E_C = \frac{12\, R_3}{64\, R_1^*} = \frac{3}{16} \frac{R_3}{R_1} \frac{R_1}{R_1^*} \qquad (3.5.11)$$

These are defined so that their sum gives a total effectiveness.

$$E_{tot} = \frac{\dot{W}}{\dot{W}^*} = \frac{R_1}{64\, R_1^*} \left(64\,(1 + S) + 12\, \frac{R_3}{R_1}\right) \qquad (3.5.12)$$

$$= E_1 + E_4 + E_C$$

An integrated effectiveness factor can also be defined

$$E^I_{tot} = \frac{W}{\dot{W}^* t} = \frac{W}{64\, R_1^* t} \qquad (3.5.13)$$

The volume available for the inner layer growth can also be accounted for in this way. The total volume available if reaction is occurring according to Equation (3.5.8) would be given by Equation (3.5.14). This represents a theoretical maximum.

$$V_P = 3\, K_3\, R_1^* \qquad (3.5.14)$$

The actual volume available, and the volumes taken up by carbon and inner

layer oxide are given respectively by Equations (3.5.15-17).

$$V_A = K_3 (3R_1 + R_2) \tag{3.5.15}$$

$$V_C = K_C R_3 \tag{3.5.16}$$

$$V_{OX} = 3 K_2 R_1 \tag{3.5.17}$$

These can be combined with Equation (3.5.14) to provide dimensionless volume factors G_A, G_C and G_{OX} given by Equations (3.5.18-20).

$$G_A = \frac{(3 R_1 + R_2) K_3}{3 K_3 R_1^*} = E_1 + E_4 \tag{3.5.18}$$

$$G_C = \frac{K_C R_3}{3 K_3 R_1^*} = \frac{K_C}{3 K_3} \cdot \frac{R_3}{R_1} \cdot E_1 = 0.28 Z E_1 \tag{3.5.19}$$

$$G_{OX} = \frac{3 K_2 R_1}{3 K_3 R_1^*} = \frac{K_2}{K_3} \cdot E_1 = 2.1 E_1 \tag{3.5.20}$$

As the volume available must be sufficient for the oxide and carbon, Equation (3.5.21) is equivalent to Equation (3.3.58).

$$G_A \geq G_C + G_{OX} \tag{3.5.21}$$

and if G_C were to approach G_A there would be no volume left for oxide growth. This corresponds to carbon forming most of the inner layer.

3.5.2 Conclusion.

It has now been possible to quantify the discussion of Section (3.3), to the point where the mass balance differential equations to be solved have been stated in Section (3.5). The transport processes of Section (3.2) have been restated, in a suitable form for incorporation in the mass balance, in Section (3.4). The dimensionless equations of Section (3.5.1) provide a means for analysing the results of numerical solution of the model. An important objective has therefore been achieved: the construction of a mass balance model of the protective oxidation process.

4. Numerical solution of the model.

4.1 Introduction.

The model developed in the previous chapter consists of a set of four ordinary differential equations, (3.5.1-4), together with Equations (3.5.5-7) and the models of Equations (3.4.1-4) for the different rate processes. These equations are non-linear, and have been solved numerically.

The numerical solution can be considered in two distinct sections. First, numerical analysis is needed to convert the equations to a form in which the derivatives of Equations (3.5.1-4) can be evaluated. For this the main requirements are the values of X and CO^C. X is available at any time from the integration of Equation (3.5.2); the value of CO^C, however, can only be obtained from the solution of Equation (3.5.7), for the chosen set of models for N_{CO}, R_1 and R_3. This forms a subsidiary problem, which can in some cases be solved analytically, but in others must also be solved numerically. In general, such numerical solution is more complicated when the separate model for R_2, Equation (3.4.2), is used, because then the inequality of Equation (3.5.5) must be tested in the course of the solution of Equation (3.5.7).

The second part of the solution is to use the derivatives evaluated in the first part, in a suitable integration method, in such a way as to provide reliable estimates of the true, but unobtainable, solution of the equations. These estimates are not available continuously, but at discrete intervals of the independent variable, time. Continuous curves can be generated numerically from these

discrete solutions, in order to provide a comparison with similar continuous curves fitted to experimental data.

4.2 Evaluation of the derivatives.

Equation (3.5.7) must be solved before the derivatives can be evaluated. The equation can be written

$$0 = 4R_1 - 2R_3 - \frac{D_{eff}}{X} C_{tot} (C - C_{ext}) \qquad (4.2.1)$$

where C_{tot} is the total gas concentration calculated in Section (3.2.1), and C the mole fraction of CO at interface C. Six solutions of Equation (4.2.1) are given, corresponding to the combination of any one of Equations (3.4.3a-c) for carbon formation with either the equality of Equation (3.5.3), or Equation (3.4.2). These are summarised in Table (4.1).

For each of the Cases Ia, Ib, and Ic, there are analytical solutions to Equation (4.2.1).

CASE Ia.

For Case Ia, after substituting Equations (3.4.1), (3.4.3a) and (3.4.5) in Equation (4.2.1)

$$0 = 4r_1 C_{tot} (C_{eq} - C) (1 - \frac{Z}{2}) - \frac{D_{eff}}{X} C_{tot} (C - C_{ext}) \qquad (4.2.2)$$

$$C = \frac{D_{eff} C_{ext} + X C_{eq} 4r_1 (1 - \frac{Z}{2})}{D_{eff} + X 4r_1 (1 - \frac{Z}{2})} \qquad (4.2.3)$$

Table 4.1 Cases of solution of Equation (4.2.1).

Carbon equation	Equality of (3.5.5)	Equation (3.4.2)
(3.4.3a)	Ia	IIa
(3.4.3b)	Ib	IIb
(3.4.3c)	Ic	IIc

CASE Ib.

In Case Ib, Equations (3.4.1), (3.4.3b) and (3.4.5) are substituted in Equation (4.2.1).

$$0 = 4r_1 C_{tot} (C_{eq} - C) - 2r_{31} C \; C_{tot} - \frac{D_{eff}}{X} C_{tot} (C - C_{ext}) \quad (4.2.4)$$

$$C = \frac{D_{eff} C_{ext} + X C_{eq} 4r_1}{D_{eff} + X (4r_1 + 2r_{31})} \quad (4.2.5)$$

CASE Ic.

For Case Ic, Equations (3.4.1), (3.4.3c) and (3.4.5) are substituted into Equation (4.2.1)

$$0 = 4r_1 C_{tot} (C_{eq} - C) - 2r_{32} C^2 C_{tot}^2 - \frac{D_{eff}}{X} C_{tot} (C - C_{ext}) \quad (4.2.6)$$

This can be written as a quadratic in C

$$0 = (2r_{32} C_{tot})C^2 + (4r_1 + \frac{D_{eff}}{X})C - (4r_1 C_{eq} + \frac{D_{eff}}{X} C_{ext}) \quad (4.2.7)$$

The solution of this is

$$C = \frac{- (4r_1 + \frac{D_{eff}}{X}) \pm \left[(4r_1 + \frac{D_{eff}}{X})^2 + 8r_{32} C_{tot} (4r_1 C_{eq} + \frac{D_{eff}}{X} C_{ext}\right]^{1/2}}{4r_{32} C_{tot}} \quad (4.2.8)$$

This always has a positive real root for the positive sign of the square root, for positive values of the constants.

Analysis shows that in each of these cases the solution if the carbon production rate becomes negligible is

$$C = \frac{(4r_1 C_{eq} + \frac{D_{eff}}{X} C_{ext})}{(4r_1 + \frac{D_{eff}}{X})} \qquad (4.2.9)$$

This is a solution in which C is initially C_{ext} and becomes close to C_{eq} as the time becomes large.

For these three cases it is now possible to use the value of C to evaluate S and Q using Equations (3.5.5-6),

$$S = \frac{K_2}{K_3} - 1 + \frac{K_C R_3}{3K_3 R_1} \qquad (4.2.10)$$

$$Q = \frac{\frac{K_1}{K_2} S}{(1 + \frac{K_C R_3}{3K_2 R_1})} \qquad (4.2.11)$$

since R_1 and R_3 can be evaluated from Equation (3.4.1) and the appropriate one of Equations (3.4.3a-c), and K_2 from Equations (3.3.51-55). It is then possible to evaluate the derivatives using Equations (3.5.1-4). This procedure is shown in the Program Flowsheet of Appendix 2.

CASES IIa, IIb and IIc.

In the cases of type II, the calculation is carried out as for the corresponding type I case e.g. Case Ia for Case IIa. R_2 is then calculated from Equation (3.4.2) and S_D given by

$$S_D = R_2/3R_1 \tag{4.2.12}$$

is compared with S from Equation (4.2.10). If S_D is greater than S, then there is sufficient volume, for reaction (1) to occur at it's calculated rate; S is then replaced by S_D, and Q calculated using Equation (4.2.11). The derivatives are now calculated as before. If, however, S_D is less than S, the reaction (1) is now limited by reaction (2), and the Case I solution for C is not valid.

The process for recalculating C, and the reaction rates R_1 and R_3, when reaction (1) is limited, is shown in detail in Appendix 2. The rate R_2 is fixed, and C and R_1 must be found so that

$$S = \frac{R_2}{3R_1} = \frac{K_2}{K_3} - 1 + \frac{K_C R_3}{3K_3 R_1} \tag{4.2.13}$$

so that Equation (3.5.7) is satisfied.

CASE IIa.

Case IIa is straightforward, because K_2 and R_3/R_1 are constant. Then

$$R_1 = \frac{R_2 K_3}{(3K_2 - 3K_3 + K_C Z)} \tag{4.2.14}$$

and substituting this and Equation (3.4.3a) into Equation (4.2.1)

$$0 = 4R_1 \left(1 - \frac{Z}{2}\right) - \frac{D_{eff}}{X} (C - C_{ext}) C_{tot} \qquad (4.2.15)$$

Note that here, as R_1 is proportional to R_2, and R_2, from Equation (3.4.2) depends upon $1/X$, then C will be independent of X.

$$C = C_{ext} + \frac{4R_1 X \left(1 - \frac{Z}{2}\right)}{D_{eff} C_{tot}} \qquad (4.2.16)$$

CASES IIb and IIc.

For the remaining cases, IIb and IIc, Equation (4.2.13) cannot be solved directly, because K_2, R_3 and R_1 can all now vary. Instead a numerical method must be used. If estimates for C and K_2 are available, from previous calculation or initial values, then Equation (3.4.3b) or (3.4.3c) can be used to find R_3, and R_1 found from

$$R_1 = \frac{(K_3 R_2 - K_C R_3)}{3(K_2 - K_3)} \qquad (4.2.17)$$

From these Z, C_n, ρ_2, ε_C and a new value of K_2 can be found using Equations (3.3.51-55). Equation (4.2.1) can now be solved numerically using a Newton-Raphson technique, e.g. Jenson and Jeffreys (1963), for if

$$G = 4R_1 - 2R_3 - \frac{D_{eff}}{X} (C - C_{ext}) C_{tot} \qquad (4.2.18)$$

then

$$\frac{dG}{dC} = 4\frac{dR_1}{dC} - 2\frac{dR_3}{dC} - \frac{D_{eff}}{X}C_{tot} \qquad (4.2.19)$$

and a new estimate for C can be found to make G zero from

$$C_{new} = C - \frac{G}{\frac{dG}{dC}} \qquad (4.2.20)$$

The calculation is repeated until C_{new} is sufficiently close to C, when G will be close to zero. The derivative needed in Equation (4.2.20) can be an approximation to Equation (4.2.19) as long as this does not become zero. In fact the dependence of R_1 on C through Equation (4.2.17) has been neglected in using Equation (4.2.20).

The final values for C and K_2 are used to evaluate R_3, R_1, Q and the derivatives using Equations (3.4.3 b or c), (4.2.17), (3.5.6) and (3.5.1-4). All the alternatives are shown in Appendix 2. The values for the derivatives are passed to the integration routine, to be discussed in the next section.

4.3 Choice of integration Algorithm.

An algorithm for the numerical integration of the Equations (3.5.1-4) must satisfy several criteria. It must be able to generate a succession of points which are within a bounded error of the 'true', but unobtainable, continuous solution of the differential equations. This means that it must be stable to the propagation of

numerical errors from one step to the next, so that the error on any one step has a decreasing influence on the following steps. This is the most important criterion, but it is also important that a reasonable desired accuracy should be achieved as economically as possible, and that the method should be suitable for a range of problems without failure. In order to achieve these objectives, some means of estimating the local errors of the integration is needed, both to adjust the integration step length to a suitable size, such that the desired accuracy is just obtained, and also to detect and indicate cases where the errors are becoming too serious for the integration to continue. The algorithm must be available in the form of a program which is free from errors, and which will satisfactorily solve a series of test problems, such as those suggested by Fox (1972). Crane and Fox (1969) discussed in more detail the problem of comparing different algorithms, and concluded that the results can depend very much upon the actual computer program, and the computer system used. There can thus be no final conclusion as to the best algorithm, and factors such as availability and ease of use will count in the actual practical choice.

In this case, the equations involved pose no great problems for integration, except that for a given error, a much shorter step length is needed at the start than is sufficient later in the integration. Thus significant economy is made by changing from a fixed to a variable step length. The method used is the Merson (1957) modification of the fourth order Runge-Kutta, which is discussed by Fox and Mayers (1968). This algorithm readily generates an estimate

of the local error which can be used to control the step length. An equation

$$\dot{y} = f(x,y) \tag{4.3.1}$$

is being integrated from (x_r,y_r) with step h. The estimate of the local error in the value of y_{r+1} is given by $\grave{e}_{r+1}$, and is of order h^5 (Fox and Mayers, 1968). The algorithm is given in Equation (4.3.2), where each of the variables k, f, y, ę can represent a vector if there is more than one equation.

$$\begin{aligned}
k_1 &= h\, f(x_r,y_r) \\
k_2 &= h\, f(x_r+h/3, y_r+k_1/3) \\
k_3 &= h\, f(x_r+h/3, y_r+k_1/6+k_2/6) \\
k_4 &= h\, f(x_r+h/2, y_r+k_1/8+3k_3/8) \\
k_5 &= h\, f(x_r+h, y_r+k_1/2-3k_3/2+2k_4) \\
y_{r+1} &= y_r+k_1/6+2k_4/3+k_5/6 \\
x_{r+1} &= x_r+h \\
e_{r+1} &= k_1/15-3k_3/10+4k_4/15-k_5/30
\end{aligned} \tag{4.3.2}$$

Kinsey (1972) has suggested a method of using an error estimate, e, to modify the step length, which is more flexible than the usual step halving and doubling, and achieves more closely the maximum permissible

step length for a given desired accuracy, E. At each step the quantity

$$w = \alpha (E/e)^{1/5} \qquad \alpha = 0.999 \tag{4.3.3}$$

is calculated.

The step length is multiplied by w to obtain the new step length

$$h' = wh \tag{4.3.4}$$

$$\text{If} \quad w \geq \alpha \tag{4.3.5}$$

$$\text{i.e} \quad e \leq E$$

then the step is accepted and integration proceeds from (x_{r+1},y_{r+1}). Otherwise, the step is repeated from (x_r,y_r), using the reduced step length h'.

The error, e, at any step to be used in Equations (4.3.3) and (4.3.5) can be defined either as an absolute error

$$e = \underset{i}{\text{Max}} \, (\text{ABS}(e_{r+1,i})) \tag{4.3.5a}$$

i.e an absolute error, or as a relative error

$$e = \underset{i}{\text{Max}} \, (\text{ABS}(e_{r+i,i}/y_{r+1,i})) \tag{4.3.5b}$$

Here the suffix i denotes the number of the equation, so that the

largest error is chosen to compute Equation (4.3.3).

The integration is performed by a program which applies Equations (4.3.1-5) to any set of simultaneous ordinary differential equations, such as Equations (3.5.1-4), for which the derivatives can be evaluated. This program is written as a sub-routine which is documented in Appendix 3, and it has been applied also to various test problems to the extent that it is considered reliable, and to satisfy the criteria outlined earlier in this section.

4.3.1 Test performance of the integration routine.

The routine described in Section (4.3) was tested using the problems

$$\frac{dy_1}{dx} = -y_1 \qquad y_1(0) = 1 \tag{4.3.6}$$

and

$$\frac{dy_1}{dx} = y_2 \qquad y_1(0) = 1 \tag{4.3.7}$$

$$\frac{dy_2}{dx} = y_1 \qquad y_2(0) = -1$$

These both have the solution

$$y_1 = e^{-x}$$

$$(y_2 = -e^{-x} \text{ for Equation (4.3.7)}) \tag{4.3.8}$$

but the second has a parasitic solution

$$y_1 = Ae^{x} \tag{4.3.9}$$

which will swamp the true solution if rounding errors become serious so that A is not zero. This problem has been used by Donovan and Willbe (1974) and also by Crane and Fox (1969). The results of integrating both of these problems to x=5 are shown in Table (4.2), for both fixed and variable step length versions of a program using Equation (4.3.2). The fixed step length calculation took one hundred steps to reach x=5, and gave a final relative error calculated by Equation (4.3.10) of less than 10^{-7} in all cases, where

$$\text{Relative Error} = \text{Abs}\left[\frac{\text{Calculated} - \text{Exact}}{\text{Exact}}\right] \qquad (4.3.10)$$

The variable step length version used a local relative error criterion of 10^{-7}, using Equation (4.3.5b) to calculate the error estimate, and took in each case thirty-six steps and one failed step to calculate the result with a final relative error of at most 3×10^{-6}, from Equation (4.3.10).

4.3.2 Performance in integrating the model.

The routines described in Section (4.3) have been used to integrate the model described in Sections (3.5) and (4.2). Runs with a fixed step length indicate that relative errors are highest at the start of the integration, with typical values of about 10^{-4}, decreasing to 10^{-7} or less at the end of a simulation of 500 h of oxidation, using 1000 s steps. This takes 1800 integration steps. Results identical to 4 figure accuracy can be achieved with a variable step length, and

Table 4.2 Test results for the integration algorithm.

Problem	Fixed Step Length (100 Steps)	Relative error at $x = 5$	Variable Step Length (Local relative Error interior, 10^{-7})	Relative error at $x = 5$	No. of Steps
Equation (4.3.6) to $x = 5$	6.7379473×10^{-3}	5×10^{-8}	6.7379655×10^{-3}	2.8×10^{-6}	36 + 1 fail
Equation (4.3.7) to $x = 5$	6.7379474×10^{-3} $-6.7379472 \times 10^{-3}$	3×10^{-8} 6×10^{-8}	6.7379665×10^{-3} $-6.7379645 \times 10^{-3}$	3.0×10^{-6} 2.6×10^{-6}	36 + 1 fail
Exact Answer at $x = 5$	6.7379470×10^{-3}	-	6.7379470×10^{-3}	-	

a relative error criterion of 10^{-4}, taking about fifty steps. This criterion has therefore been used as a standard, and the results presented can be treated as reasonable numerical solutions to the model equations presented.

The only cases where the integration terminates before the final time specified are situations where the rate of reaction (1) becomes very small, while the rate of reaction (3) is finite. These are cases where the rate of reaction (2) is limiting the inner oxide, and the rate of reaction (1) is calculated from Equation (4.2.17), which does not exclude the possibility of R_1 approaching zero. This corresponds with the case where carbon takes up the whole of the inner layer, as mentioned in Section (3.3). Thus these cases indicate a point where the model might be extended, rather than failure of the numerical procedure for integration.

Repeated steps, failing the test of Equation (4.3.5), usually occur only in the initial stages of the integration, where small steps are needed, and also around the point where the result of comparing S_D with S, from Equations (4.2.10) and (4.2.12) changes. At the point of equality, corresponding with the equality sign in Equation (3.5.5), the reaction rates are the same by either method of calculation, following Equation (4.2.12), and thus at that point the derivatives given by Equations (3.5.1-4) are the same. Before and after that point, however, the rates calculated by the two methods differ increasingly, and thus steps which straddle the change usually fail. This is where the advantages of a variable step length approach are felt most fully,

because such a straddling step is reduced by the algorithm until it is ending at or near the changeover point, because calculation of the derivatives in different parts of the step by the different methods increases the local error. Once a step end is near enough to the changeover point, the local error becomes acceptable, and the next step is almost entirely beyond the changeover, and thus also has acceptable error. This process of adjustment is shown schematically in Figure (4.1). Without this feature there would be unacceptable total error in putting such switches within the derivative routine. The changeover is accompanied by a sharp change in the slope of the CO concentration graph, but not of the weight gain curve.

4.4 Implementation of the model.

The model equations and the algorithm described in Sections (3.4-5) and (4.2) are programmed in FORTRAN and run on the IBM 370 system of the Central Electricity Generating Board.

The calculations are carried out in double precision, because single precision on the IBM 370 would give only 7 significant figures accuracy at any stage; double precision gives 16 significant figures.

The program has been written in such a way that the separate sections are self contained; a flowsheet is given in Appendix 2. This enables modifications to be made separately to the different parts of the program. In particular, changes can be made to the model integrated, by changing the routine DYBDX, without the need to alter the integration routines. This is achieved by passing information

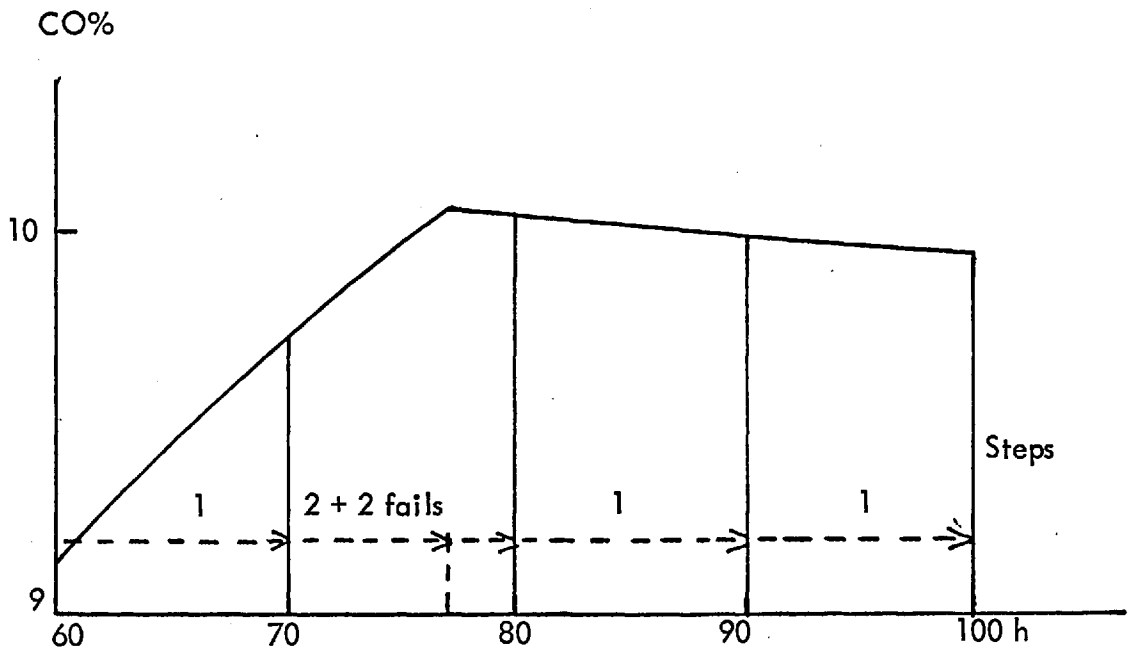

Figure 4.1 Schematic diagram of numerical integration progress
Data from Run 5624 case 5

direct to DYBDX from the main program, by extensive use of COMMON blocks. Because this routine is evaluated many times, care is taken to avoid recalculation of constant factors, by calculating them once and storing the results, wherever possible.

To examine the effect of the variation of parameters, it was necessary to perform a large number of runs. The presentation of results thus becomes a significant problem; any processing of the results which is of interest has of necessity to be repeated many times also, and is therefore incorporated into the program, and calculated with each case. The output from each case is presented in a number of clearly defined sections. First, the parameter values and options of the case are set out clearly, followed by a table of the integration results, and messages about the integration performance. The next section is a set of line printer graphs and curves fitted by different methods, and finally there is a table summarising the results of the case. At the end of each run, there is a table summarising in one line the results of each case. A sample set of output is given in Appendix 4.

The error philosophy is that as far as possible the failure of a case for any reason will give clear diagnostic messages, and exit to the next case without halting the run. In some cases this involves modifying or omitting the data analysis stages, if insufficient data has been calculated for analysis to be possible.

Data input for the large number of cases was usually performed by a separate program, which generated a factorial permutation of parameters, from only a small number of input cards. This avoided large problems

of data preparation which would otherwise have occurred. The input is arranged in such a way that input direct to the main program is compatible.

The whole philosophy of the program is to make the computer perform as many as possible of the routine tasks from data preparation through calculation to results presentation, leaving the user free for tasks that cannot be delegated: the choice of the parameter ranges of interest, and the interpretation of the results. To achieve this, advantage was taken of many of the facilities of the IBM 370 system, some of which are not available in exactly the same form on other computer systems such as the ICL 1900 series. In many applications this would be a severe disadvantage, in that it prevents the ready transfer of the program to other computer installations. This disadvantage is by no means so severe in this case. The program is mainly of interest within a large organisation sponsoring the work, with a central computer facility made widely available throughout its departments by the use of computer terminals with access to the central computer site.

The computer time involved is not constant in view of the variable step length integration but a typical case, simulating 36 cases for 500 h of oxidation, took 33 seconds of central processor time on the IBM 370/155, with a processor utilisation of 39%. The total time for the job was 43 seconds, and it generated 11,000 lines of output.

5. Results.

5.1 Cases computed.

The model as described in Sections (3.5) and (4.2) has been solved numerically by the method described in Section (4.3). In many cases the values of the parameters needed have been estimated in Section (3.2), and in others they are derived from practical considerations. In some cases a range of values has been used for a parameter in order to examine the effect of its variation on the performance of the model. The values used are summarised in Table (5.1), which includes reference to previous mention of the parameters and defining equations.

Pressure, temperature, and the external gas concentration are referred to as 'practical' parameters, because they are the only factors which can be varied independently in a practical experiment. All the other parameters in Table (5.1) are, in principle, either measurable constants, or have a functional dependence on temperature and pressure. In practice, these relationships are not well enough known to be directly incorporated, and constant values have been used. Only in the case of the oxidation and carbon reaction rate constants is there no information available to suggest reasonable values, and in these cases the chosen numerical values are such as to show oxidation of the right order of magnitude to compare with experiment.

The combinations of parameters computed in each run reported here are shown in Table (5.2). In each case all combinations of the different parameters were used, as a factorial experiment. The runs

Table 5.1 Values of parameters used in the model.

Name	Symbol	Defining Section		Range used	Value Estimated	Units
		Section	Equation			
Pressure	P	-		1,20	1,20 bar Practical	bar
Temperature	T	-		700 (427°C)	700K Practical	K
Voidage		3.2.4		10^{-4}	10^{-4}	
Gas diffusion coefficient	$D_{eff.}$	3.2.2		10^{-6}-10^{-8}	10^{-6}-10^{-7}	$mm^2\ s^{-1}$
Oxidation Rate Constant	r_1	3.4.1	3.4.1	10^{-5}-10^{-6}	?	$mm\ s^{-1}$
Equilibrium mole fraction of CO	$(CO)^{eq}$	3.4.1	3.4.1	50	50	%
External mole fraction of CO	$(CO)^{ext}$	3.4.1	3.4.1	.1 - 40	0 - 10% Practical	%
Critical mole fraction of CO	$(CO)^{crit.}$	5.1.1		30	30	%
Carbon rate constants	r_{31}	3.4.2	3.4.3b	not used	?	mm/s
	r_{32}		3.4.3c	1 - 1000	?	$mm^4/gmol\ s$
Iron diffusion coefficient	D_{Fe}	3.2.5		10^{-10}-10^{-15}	?	$mm^2\ s^{-1}$
Exponent on Fe diffusion		3.2.5		1/3	1/3	-

Table 5.2 Details of runs reported here.

Run Number	Variables							
	Final time hr	r_{32}	r_1	D_{eff}	CO_{ext}	P	D_{Fe}	No. of Cases
6888	500	100,1000	$10^{-5},10^{-6}$	$10^{-6},10^{-7},10^{-8}$	.1,1,10	1	$10^{-10},10^{-11},10^{-12}$	108
6888a	500	100	$10^{-5},10^{-6}$	$10^{-6},10^{-7},10^{-8}$	.1,1,10	1,20	-	36
6970	500	1,10	$10^{-5},10^{-6}$	$10^{-6},10^{-7},10^{-8}$	.1,1	20	$10^{-10},10^{-11},10^{-12}$	72
6984	50000	1,10	$10^{-5},10^{-6}$	$10^{-6},10^{-7}.10^{-8}$	.1,1	20	$10^{-10},10^{-11},10^{-12}$	72
7056	500	1000	10^{-6}	10^{-7}	1.25-40 in factors of 2	1	10^{-10}-10^{-15} in powers of 10	36
7085	5000	1,10	$10^{-5},10^{-6}$	$10^{-6},10^{-7},10^{-8}$	.1,1	20	$10^{-13},10^{-14},10^{-15}$	72
5624	500	10	10^{-6}	10^{-7}	.625-20 in factors of 2	20	10^{-10}-10^{-15} in powers of 10	36

Most runs vary 5 or 6 parameters, including D_{Fe}.

6888a does not include D_{Fe}, and uses coupled iron diffusion.

7056 and 5624 are designed to investigate D_{Fe} and CO in more detail, varying these only.

were usually made for the first 500 h of oxidation, but in some cases for longer periods. Particular cases will be referred to by the run numbers shown in Table (5.2).

The important conclusions drawn from the results do not depend critically on the exact value of any one parameter, but on the degree of control exercised by different processes in competition. The range of parameters covered shows that a range of different control regimes is possible, thus making clear the possibilities of rate control during experimental oxidations.

5.1.1 Results from each case.

For each case the results consist of a list of the case parameters, together with a table of the variation of the output variables with time. The output variables are listed in Table (5.3), and a sample of the case output is given in Appendix 4. This is accompanied by graphs of weight gain, oxide thickness and CO concentration against time, and analysis of the weight gain data according to the methods described in Section (5.2.1). Finally, each case has a brief summary, and each run has an overall summary of all the cases. Samples of the output are given in Appendix 4. For runs where the integration was completed for all the cases, it is possible to perform a factorial analysis of several of the dependent variables, in terms of the changes in the independent variables. This is described in Section (5.3.1).

A further test provided on the results from each case is to check when the CO level at the oxide first exceeds the critical value suggested by Surman and Brown (1974) as being necessary for the formation

of catalysts for the Boudouard reaction as discussed in Section (2.5). This value is included as an extra parameter in Table (5.1).

5.2 Analysis of weight gain data.

Several methods have been used to fit overall curves to the weight-gain time data obtained from the integrations, because of the importance of this approach in practical work. The usual means of establishing the parameters of a simple model with a few parameters is to apply the 'least squares' method, i.e. to minimise the sum of squares of the differences between the model's prediction, and the results to be fitted. Himmelblau (1970) discusses this method, and shows that it has limitations when both independent and dependent variables are liable to random error, and also where the errors are not randomly distributed, but successive errors instead display some degree of correlation. In the case of weight gain data, both in simulation and in practice, each increment of weight gain is added on to the previous value, and the error contribution of the increment is then carried forward in the sum. This means that any error is likely to be cumulative, and successive errors may well be correlated, even if the model is accurate. For such a case, Himmelblau (1970) shows that although the model parameters of a least-squares fit may be reasonably accurate, the estimate of the uncertainty will be optimistic, showing the model as better than it actually is. He quotes a method of Durbin and Watson (1951), which can be used to check for the correlation of the residuals, and thus the degree of systematic variation from a model fitted by least squares. The least squares and Durbin-Watson tests are detailed in Appendix 5.

Table 5.3 Output dependent variables from the model.

Name	Symbol	Units	Defining section and equation		Notes
CO	C	percent			*
CARBON	W_C	g/mm^2	3.5	3.5.4	
Weight gain	W	g/mm^2	3.5	3.5.1	*
Weight gain rate	$\dot{W}$	g/mm^2s	3.5	3.5.1	
Oxide depth	X	mm	3.5	3.5.2	
Oxide growth rate	F	mm/s	3.5	3.5.2	*
Rate of reaction 1	R1	mm/s	3.4.1	3.4.1	
Ratio R3/R1	Z	-	3.3.3	3.3.5	
Ratio X1/X2	-	-	5.4.1		
Steps successful	-	-	-	-	+
Failures	-	-	-	-	+

* Final values used for factorial analysis.

\+ For information on integration performance.

In practice, the problem of correlation is particularly severe with the comparatively small numerical errors of the numerical integration, and the Durbin-Watson test suggests correlated results, even when a good fit is in fact found. To overcome this problem, the models have also been fitted by Chebyshev polynomials, which minimise the maximum difference between the polynomial and the data points. The size of this maximum error provides a parameter of the accuracy of fit to the data. This method is discussed by Fox and Mayers (1968), and a method described by Curtis and Frank (1959) has been used to calculate such 'Minimax' polynomials. Some details are given in Appendix 5.

5.2.1 Models fitted to weight gain data.

The following are the few parameter models which have been fitted using the methods of Section (5.2).

A) Least squares method

A.1) Linear model

$$W = A_{11} + B_{11}\, t \qquad (5.2.1)$$

This simple model is only in a few cases a good description of the simulation. The residuals are always highly correlated.

A.2) Parabolic model

The simple model

$$W^2 = k\, t \qquad (5.2.2)$$

can be generalised to remove the assumption that the parabola starts at t=0 to become

$$(W+W_0)^2 = k\,(t+t_0) \qquad (5.2.3)$$

where $(-W_0,-t_0)$ is the parabola vertex. This can be rearranged to give

$$W^2 + 2WW_0 = kt \qquad (5.2.4)$$

since $W_0^2 = k\,t_0$, assuming W=0 when t=0, and then

$$W = k\left(\frac{t}{W}\right) - 2W_0 \qquad (5.2.5)$$

Hence, if the model

$$W = A_{12} + B_{12}\left(\frac{t}{W}\right) \qquad (5.2.6)$$

is fitted the constants k, W_0 and t_0 can all be evaluated. This method succeeds in estimating the parabolic rate constant, but the residuals are still correlated. There is the further disadvantage that the new independent variable in the regression, t/W, is subject to the errors in W, and the least squares analysis is not strictly valid.

A.3) Logarithmic model

$$W = A_{13}\,t^{B_{13}} \qquad (5.2.7)$$

or $$\log_{10} W = \log_{10} A_{13} + B_{13}\log_{10} t$$

is also fitted by linear regression. This assumes that the best line passes through the origin, and also places undue emphasis on the points at lower values of t, when equally spaced points are used. It is, however, included for completeness, because it is used to establish empirical equations from experimental data.

B) Mininax method

This method is applied after normalisation of the time and

weight-gain data to the range 0 to 1, in order to avoid the numerical problems of powers of numbers differing widely in magnitude, and to make the coefficients of the polynomials all multiply terms of comparable magnitude.

B.1) Linear models

The linear models

$$W = A_{21} + B_{21}\, t \qquad (5.2.8)$$

and

$$t = A'_{21} + B'_{21}\, W \qquad (5.2.9)$$

are both fitted, and give identical estimates of the first order rate constant.

B.2) Parabolic models

The models of Equations (5.2.10-11) are fitted.

$$W = A_{22} + B_{22}\, t^{\frac{1}{2}} \qquad (5.2.10)$$

$$t = A'_{22} + B'_{22}\, W + C'_{22}\, W^2 \qquad (5.2.11)$$

Equation (5.2.11) is the equivalent of Equation (5.2.6) and does not assume the position of the parabola origin. With simulated data with a low level of random error it is possible to extend the polynomials in W to higher order to examine whether the residual error in Equation (5.2.11) can be accounted for empirically. This cannot be consistently achieved, but it can be established that the form of Equation (5.2.11) is likely to be a good model when its maximum error is a large factor less than the maximum error of Equation (5.2.9).

Further details of the methods used are given in Appendix 5.

5.2.2 Results of weight gain data analysis.

The results of fitting the models described in Section (5.1.2) to one particular case are summarised in Table (5.4), and shown in full in the sample output of Appendix 4. The graphs show data points as (+), with the line fitted by least squares as (*), and the mean point as (0). There are three estimates of each of the two rate constants, linear and parabolic. In general, the parabolic estimates fit more closely, even when only two, rather than three, parameters are used, in Equation (5.2.10). The results are summarised for each case, in terms which state the closeness of agreement between the least squares and minimax values in the summary at the end of the case.

5.3 Comparison of the models.

The first result to be considered is the comparison of the two distinct models developed in Section (3.4.1), i.e either with or without the separate iron diffusion Equation (3.4.2). The weight gain results from the two models are different in shape, as shown in the plots of comparable cases in the logarithmic plot of Figure (5.1), and the linear plot of Figure (5.2). The calculated parameters of the cases plotted are given in Table (5.5). Graphs with separate iron diffusion show a consistent pattern, with a slope on the logarithmic plots of 0.5 ± 0.05. In the cases without Equation (3.4.2), the slope of the logarithmic plots are variable between 0.5 and 1.0, and parabolic kinetics can only be fitted by assuming that the parabola origin is not at the start of oxidation (cf. Section 5.2).

Table 5.4 Model Fitting Results for case 5 of Run 5624

Model Equation	COEFFICIENTS A	B	C	Rate Constant Linear	Parabolic	UNITS
5.2.1	6×10^{-6}	1.1×10^{-11}		1.1×10^{-11}	-	g/mm^2 s
5.2.6	2×10^{-6}	3.6×10^{-16}	-	-	1.30×10^{-2}	mg^2/cm^4 h
				-	3.61×10^{-16}	g/mm^4 s
5.2.7	8.8×10^{-9}	.5509	-	-	-	
5.2.8	-2.0×10^{-1}	1.1	-	1.22×10^{-11}	-	g/mm^2 s
5.2.9	1.8×10^{-1}	0.90	-	1.22×10^{-11}	-	g/mm^2 s
5.2.10	-3.7×10^{-2}	1.03	-	-	1.27×10^{-2}	mg^2/cm^4 h
					3.52×10^{-16}	g/mm^4 s
5.2.11	3.8×10^{-3}	6.2×10^{-2}	0.93	-	1.28×10^{-2}	mg^2/cm^4 h
					3.54×10^{-16}	g^2/mm^4 s

Agreement between (5.2.1) and (5.2.9) at 10%

Agreement between (5.2.6) and (5.2.11) at 10%

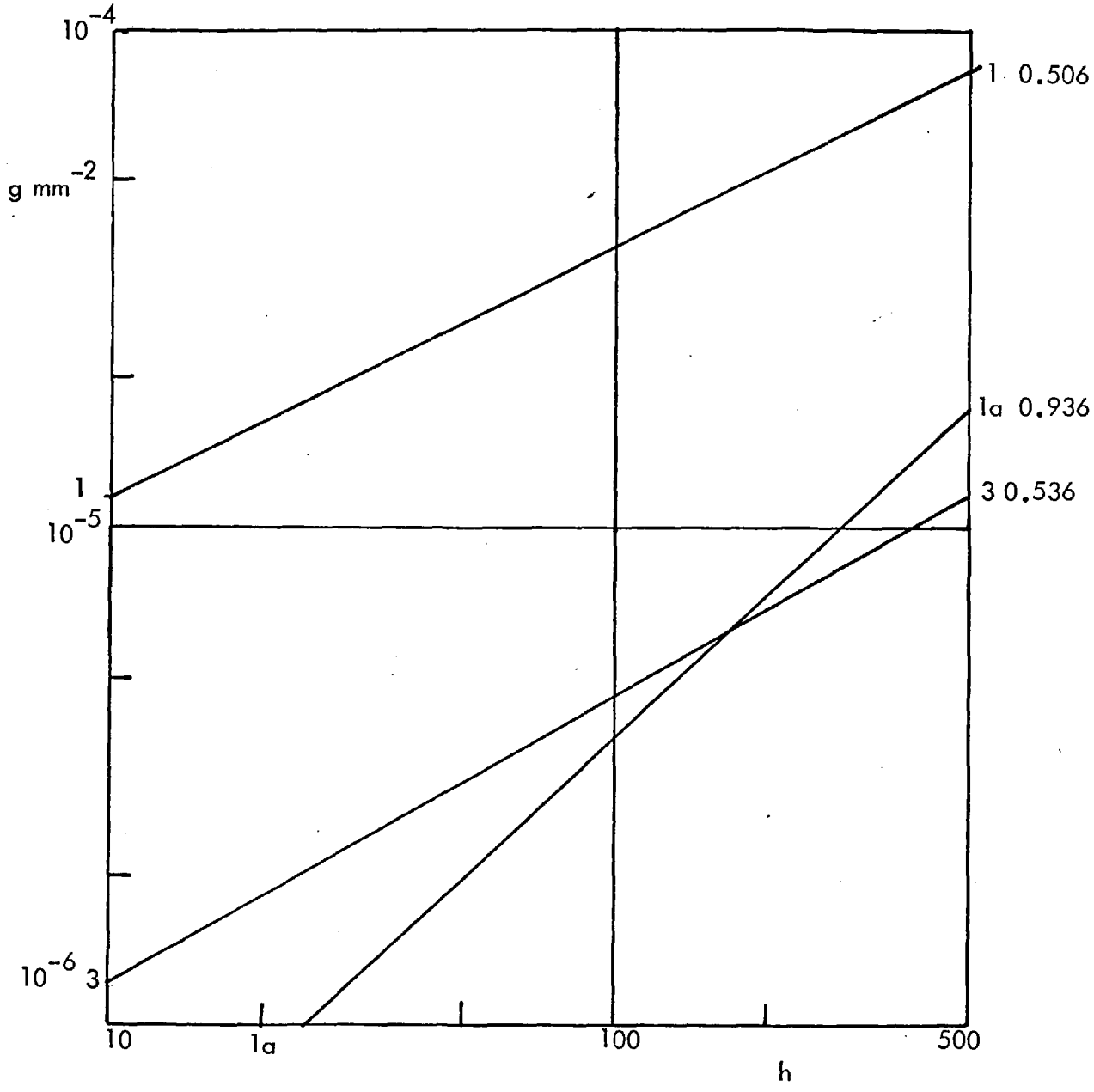

Figure 5.1 Logarithmic graph of weight gain for cases from Runs 6888 & 6888a

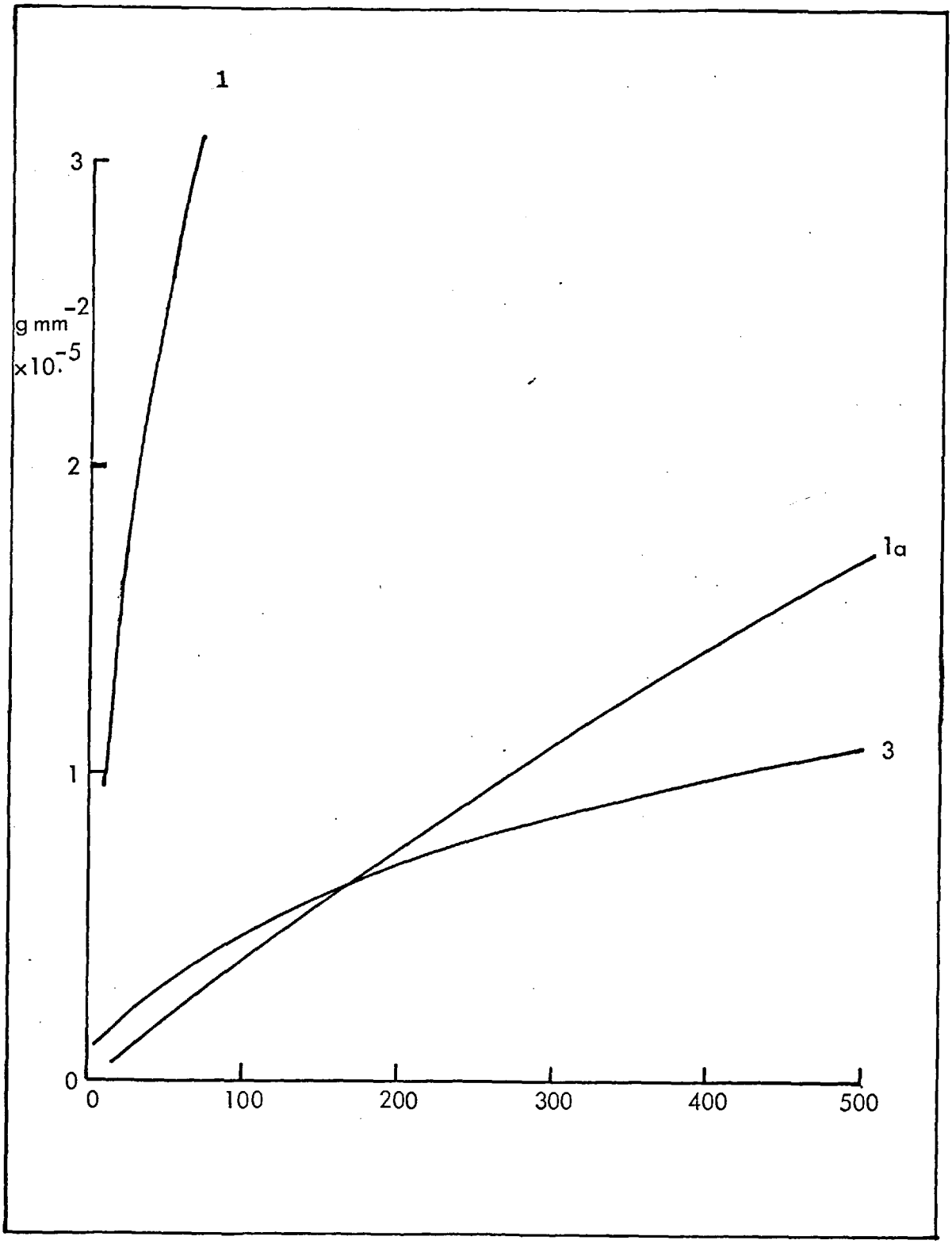

Figure 5.2 Graph of weight gain for cases from Runs 6888 & 6888a

Table 5.5 Rate constants of cases plotted in Figures (5.1-2)

Run	6888	6888	6888a	
Case	1	3	1	
Slope of log - log plot (B_{13} in Equation (5.2.7))	0.5064	0.5475	0.9365	
Parabolic rate constant (B_{12} in Equation (5.2.6))	1.43×10^{-1} 3.98×10^{-15}	2.69×10^{-3} 7.47×10^{-17}	3.05×10^{-2} 8.47×10^{-16}	mg^2/cm^4 h g^2/mm^4 s
Co-ordinates of Parabola origin (W_o)	-6.0×10^{-7}	-4.2×10^{-7}	-3.6×10^{-5}	g/mm^2
(t_o)	-0.025	-0.67	-432	h

Comparison with the experimental data of Section (2.3) shows that the practical data is parabolic in form with slopes of about $\frac{1}{2}$ for the protective region of oxidation. Thus the extra complexity of separate control of the iron diffusion is more in agreement with experiment.

5.3.1 Factorial analysis of parameter variation.

Comparison of the two models, with separate and coupled iron diffusion, can be carried further by examination of the results of complete runs by factorial analysis, described in Appendix 5, to see which of the parameters has most effect on the results. Results of the analysis are given for several runs. Tables (5.6-10) show the relative sizes of the mean squares terms for different variables, with the total sums of squares as 100. These show that the pattern of large effects is different. A key to these tables is given in Table (5.11). With separate iron diffusion, for the runs shown in Tables (5.6-9), the significant factors for weight gain are clear: the principle factor is the iron diffusion coefficient, with a smaller effect of the external CO concentration, there being some interaction between them. The oxide thickness shows a very similar effect, which is to be expected except when carbon deposition becomes very high, as the oxide density will be constant except for the effect of carbon. The parabolic rate constant also shows the same dependence, with less interaction. The pressure has not been varied within these runs, but there are some differences between the run at 1 bar, Run 6888 in Table (5.6), and the series at 20 bar, covering different final times and two ranges of iron diffusion coefficient, in Tables (5.7-9). The results for the remaining

Table 5.6 Factorial Analysis Results for Run 6888
Pressure 1 bar Time 500 h

	Wt gain g mm^{-2}	Oxide thick mm	CO Level	Log_{10} (K_p)
Mean Value	2.6×10^{-5}	18.7×10^{-3}	22.5%	-2.19
F	35.4	35.4	7.85	40.7
G	8.92	8.91	0.24	8.92
D	-	-	17.82	-
R	0.10	0.11	24.57	0.30
S	-	-	7.56	-
FG	2.80	2.80	-	-
FD	-	-	0.40	-
GD	-	-	0.24	-
FR	-	-	1.60	-
GR	-	-	0.54	-
DR	-	-	0.28	-
FDR	-	-	0.21	-
FRS	-	-	0.16	-

For parameters see Table (5.2)

For key see Table (5.11)

Table 5.7 Factorial Analysis Results for Run 6970
Pressure 20 bar Time 500 h

	Wt gain g mm^{-2}	Oxide thick mm	CO Level	Log_{10} (K_p)
Mean Value	3.8×10^{-5}	2.6×10^{-3}	16%	-1.83
F	44.1	44.1	20.5	47
G	6.36	6.33	1.28	5.42
D	0.23	0.19	18.0	-
R	0.20	0.21	0.89	-
S	-	-	3.32	-
FG	1.71	1.71	-	-
FD	0.12	0.10	2.22	-
FR	0.15	0.17	0.65	-
FS	-	-	0.45	-
DS	-	-	1.35	-
FGD	-	-	0.14	-

For parameters see Table (5.2)

For key see Table (5.11)

Table 5.8 Factorial Analysis Results for Run 6984
Pressure 20 bar Time 50,000 h

	Wt gain g mm^{-2}	Oxide thick mm	CO Level	Log_{10} (K_p)
Mean Value	40.9×10^{-5}	288×10^{-3}	10.4%	-1.82
F	44.47	44.56	20.9	47.12
G	6.55	6.53	2.18	5.63
D	0.11	-	8.01	-
R	-	-	-	-
S	-	-	15.4	-
FG	2.00	2.05	0.64	-
FD	-	-	0.91	-
GD	-	-	0.10	-
FS	-	-	4.88	-
GS	-	-	0.64	-
DS	-	-	3.11	-
FDS	-	-	0.60	-

For parameters see Table (5.2)

For key see Table (5.11)

Table 5.9 Factorial Analysis Results for Run 7085
Pressure 20 bar Time 5000 h

	Wt gain g mm^{-2}	Oxide thick mm	CO Level	Log_{10} (K_p)
Mean Value	0.43×10^{-5}	3.02×10^{-3}	0.7%	-4.80
F	44.34	44.4	7.25	46.9
G	6.87	6.72	40.7	6.02
D	-	-	7.15	-
R	-	-	-	-
S	-	-	-	-
FG	2.22	2.20	1.37	-
FD	-	-	5.13	-
GD	-	-	1.41	-
FGD	-	-	0.96	-

For parameters see Table (5.2)

For key see Table (5.11)

Table 5.10 Factorial Analysis Results for Run 6888a
Pressure 1 and 20 bar Time 500 h Coupled Iron diffusion

	Wt gain g mm^{-2}	Oxide thick mm	CO Level	Log_{10} (K_p)
Mean Value	8.04×10^{-5}	58×10^{-3}	21.7%	-0.92
G	-	-	0.67	0.51
D	-	-	7.45	1.74
R	27.56	27.56	71.22	15.52
P	48.43	48.34	-	50.77
RP	23.84	23.96	0.55	14.29
GR	-	-	0.25	0.62
DR	-	-	0.45	2.09
GP	-	-	0.20	0.43
DP	-	-	3.20	1.27
DRP	-	-	1.56	1.708
GRP	-	-	-	0.70

For parameters see Table (5.2)

For key see Table (5.11)

Table 5.11 Results of Factorial Experiments.

Key to Tables (5.6-10)

Key to Parameters from Tables (5.1-2)

F	D_{Fe}
G	CO Level
D	D_{eff}
P	P - Pressure
R	r_1
S	F_{32}

All figures shown in Tables (5.6-10) are the

$$\frac{\text{mean squares for the term x 100}}{\text{total sum of squares for that run}}$$

Figures less than 0.1 are shown -

variable, CO level, are far more complex, and change markedly even between two runs with the same parameters, but to different times, Run 6970 in Table (5.7) and Run 6984 in Table (5.8). Clearly the dependence of the CO level on parameter changes is not straightforward.

For the Run 6888a in Table (5.10), with coupled iron diffusion, the weight gain and oxide thickness also show a pattern of a few large effects. In this case they depend most sensitively on the pressure and the oxidation rate constant. The CO level and parabolic rate constant both show rather confused effects. In the latter case this reflects the fact that the fitted parabolae do not have their origins at the oxidation graph origins.

5.3.2 Further examination of significant effects.

The largest effects of parameter variation, isolated by the factorial analysis of Section (5.3.1), can be examined in more detail, using the full results of particular cases. Figure (5.3) shows a logarithmic plot of the weight gain for four cases from Run 6888a, illustrating the effect of variation of pressure and the oxidation rate constant, r_1; these are the most significant parameters in the coupled iron diffusion model.

A similar comparison for the separate iron diffusion model is shown in Figures (5.4-5), with cases from two runs which analyse in detail the effect of variation of D_{Fe} and external gas composition. These runs are Run 7056 at 1 bar and Run 5624 at 20 bar; four cases are given on each graph.

Each of the graphs of Figures (5.3-5) is labelled with the value of

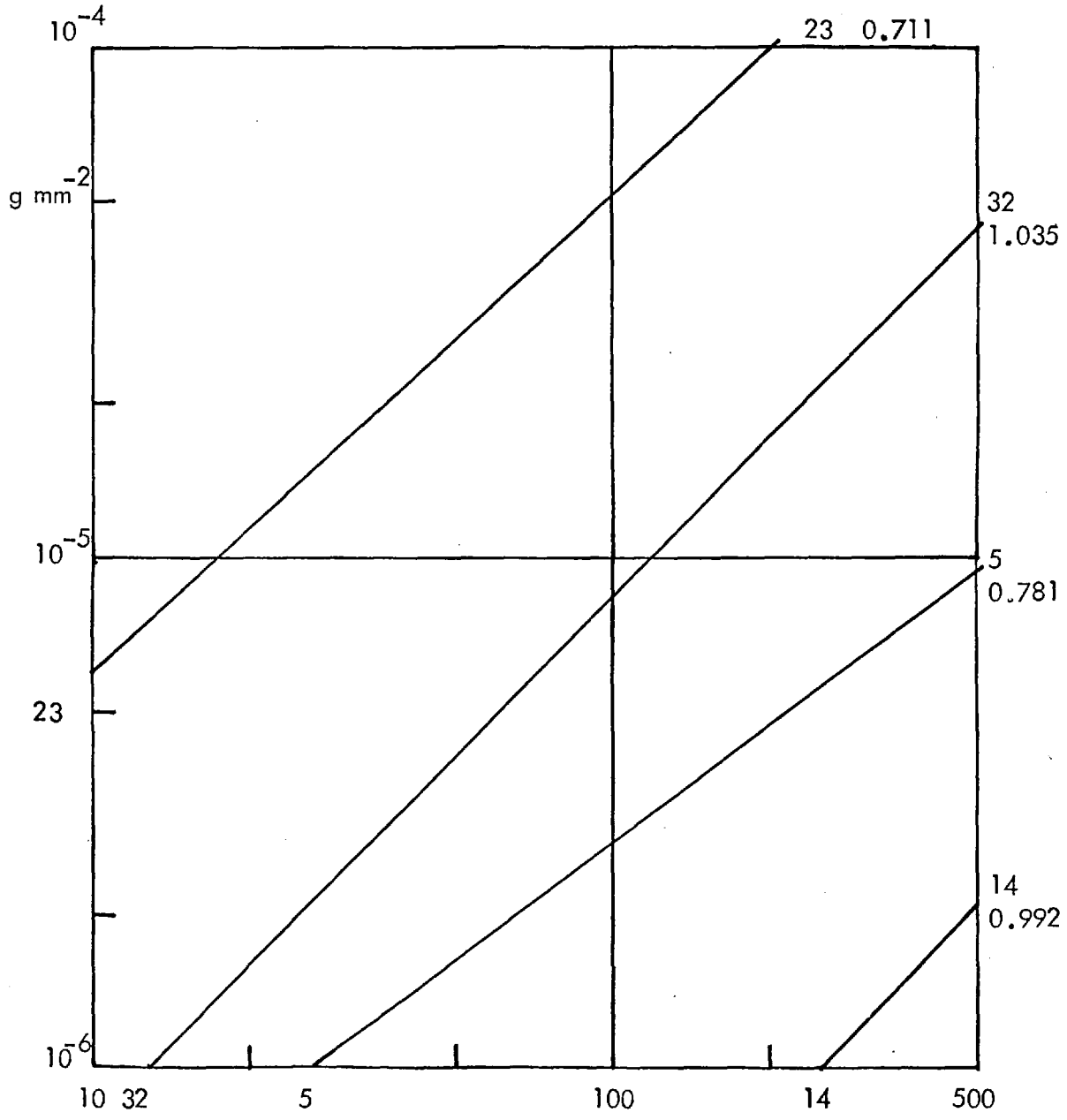

Figure 5.3 Graph of weight gain for cases 5, 14, 23 & 32 of Run 6888a
(5,14) (23,32) have same pressure
(5,23) (14,32) have same r_1

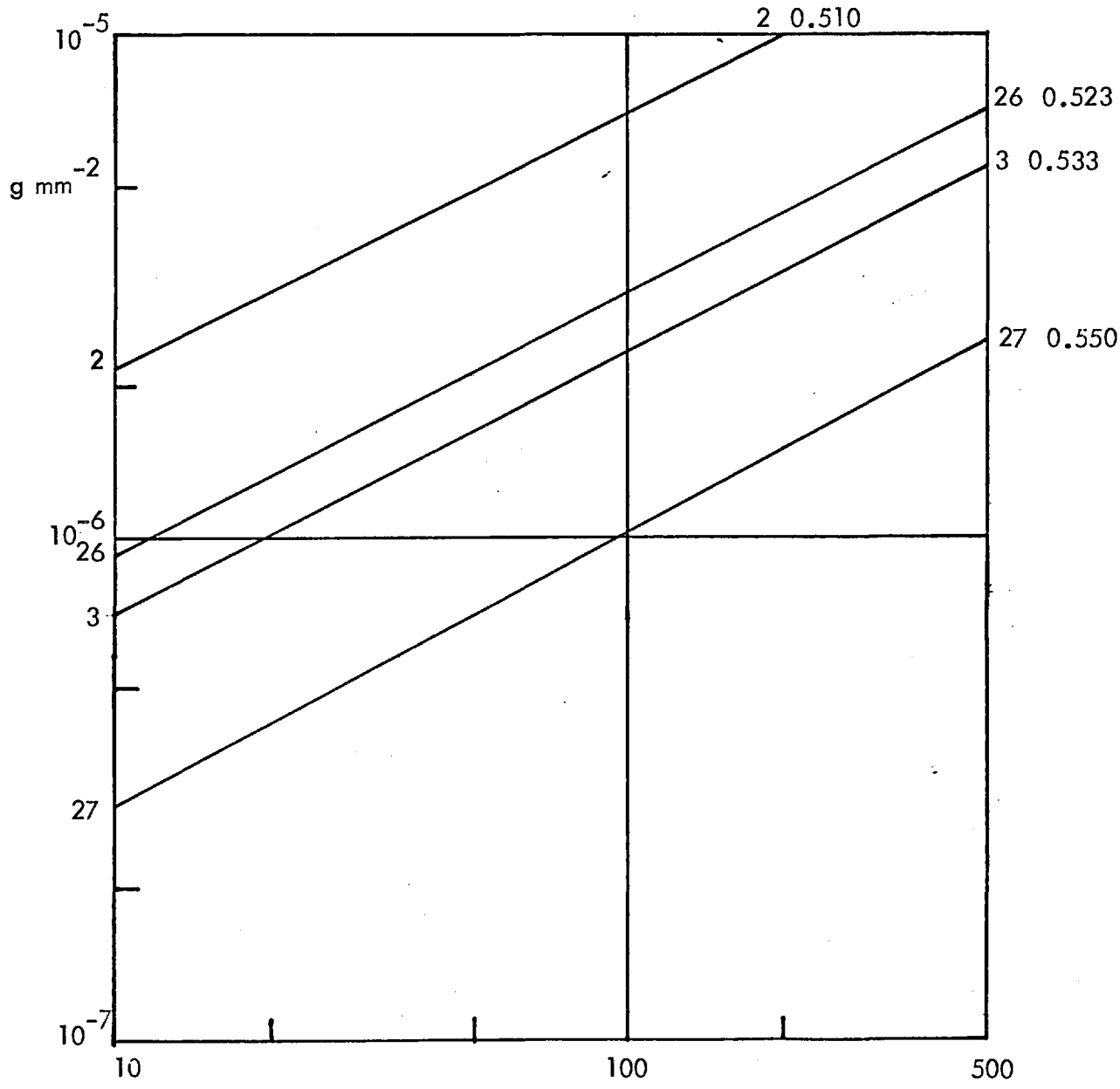

Figure 5.4 Graph of weight gain for cases 2, 3, 26, 27 of Run 7056

(2,3) (26,27) have same value of CO
(2,26) (3,27) have same value of D_{Fe}

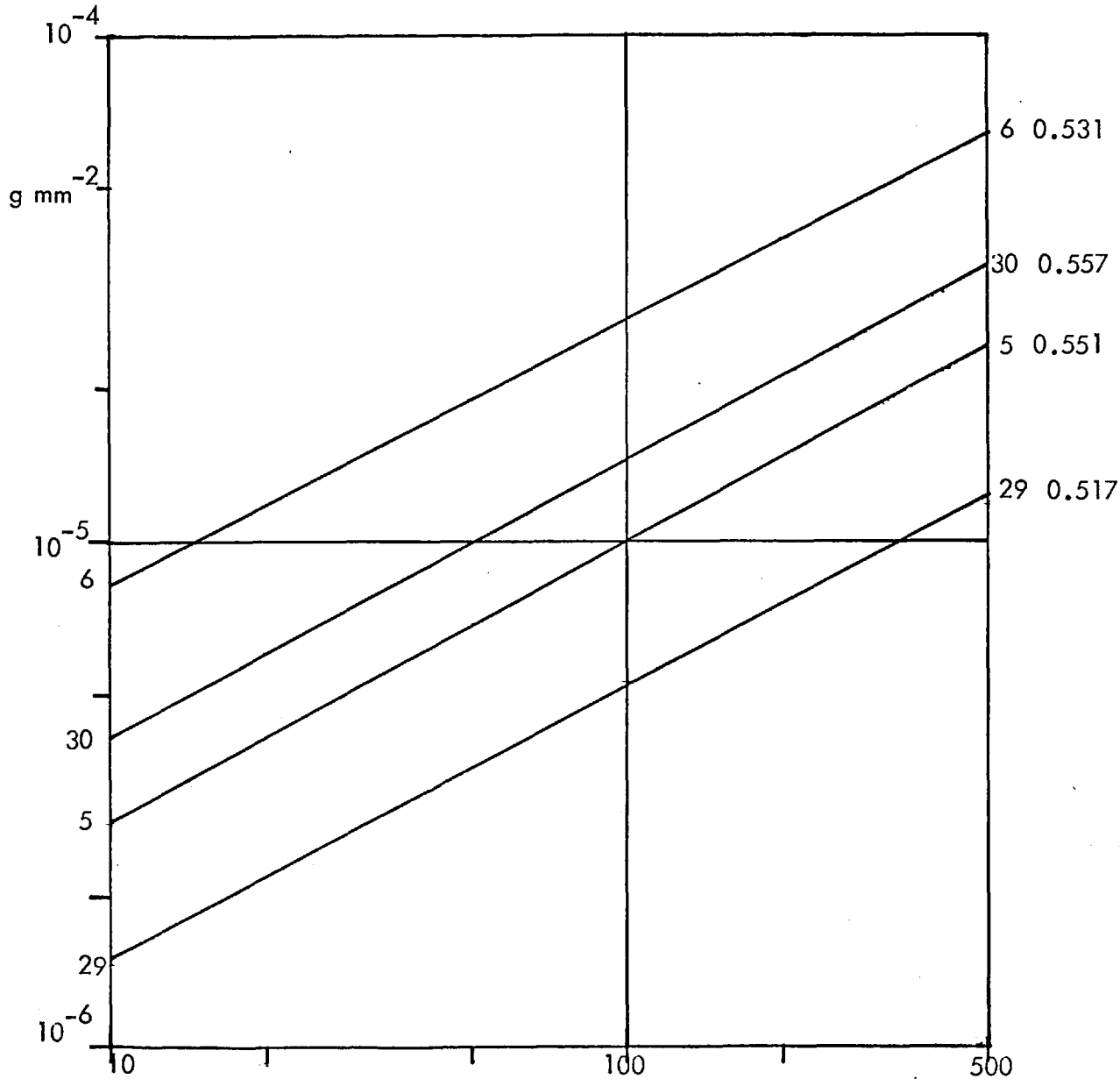

Figure 5.5 Graph of weight gain for cases 5, 6, 29 & 30 of Run 5624

(5,6) (29,30) have same value of CO
(5,29) (6,30) have same value of D_{Fe}

the slope of the logarithmic Equation (5.2.7). These confirm the conclusion of Section (5.3) that only the separate iron diffusion model is in agreement with the experimental observation of parabolic protective oxidation, with a value of about 0.5. Further examination of the results is therefore confined to this model.

5.4 Detailed results.

The results of the factorial analysis of Section (5.3.1) for the separate iron diffusion model are given in Tables (5.6-9). The relatively simple dependence of oxide weight gain on two parameters only, the iron diffusion coefficient and the external gas composition, is discussed in Section (5.3.1) and shown in Figures (5.4-5). The oxide thickness and parabolic rate constant show very similar patterns; this is reasonable given their direct relationships to the weight gain. These results have been used to confirm that the model results are not inconsistent with experimental observation.

The results of Tables (5.6-9) also show a more complex pattern of dependence of the CO concentration upon the parameters. There is clearly considerable variation, but the interactions are not clear from an overall analysis of this type. There is a need, therefore, to look more closely at the performance of the model, by examining the changes with time for typical cases of some of the subsidiary dependent variables, such as the CO concentration and the ratio of the two oxide layers. It can also be established which mechanism controls oxidation at each stage of the simulation.

This closer analysis enables a comparison to be made with certain

experimental results and mechanistic predictions, with useful results. This in turn makes posssible the use of the model in a predictive manner.

5.4.1 Relative sizes of the two oxide layers.

One of the dependent variables listed in Table (5.3) is the ratio, X1/X2, of the outer to inner oxide thickness. Experimental observation, discussed in Section (2.4), is that the inner layer is thinner than the outer layer in the early stages of oxidation, but that they become approximately equal in thickness as the oxidation proceeds. None of the mechanisms discussed in Section (2.5) has attempted to explain this observation. Computed results show that this ratio is large in the early stages, but declines during the oxidation in an asymptotic mannner to a limiting value, in many cases between 1.1 and 1.2, in general agreement with observation. Typical results for a number of cases from Run 5624 are shown in Figure (5.6). In cases where significant amounts of carbon, greater than about 5% by weight, are present in the inner oxide, the ratio passes through a minimum, and then increases slowly as the reaction continues. This is in general agreement with experimental observation.

5.4.2 CO concentration and carbon formation.

It is apparent from the mechanistic discussion of Section (2.5) that considerable significance has been attached to the concentration of CO at the metal-oxide interface, and to the role of CO in carbon formation, leading to breakaway oxidation. Gibbs et al (1974) have suggested qualitatively that the CO concentration should increase with time and then decrease, as shown in Figure (2.6).

In most of the cases examined, computed results show two distinct regimes of variation of the CO concentration. Initially, the concentration rises at a rate which decreases continuously but does not fall to zero. There is then a sharp change to a constant value, or a decrease which flattens out to a slow fall. This sharp change can occur at a wide variety of times, from close to the beginning, to after the end of the simulated period. Typical graphs, which illustrate a number of different cases, from Run 5624 are shown in Figure (5.7). These curves are very similar to those predicted, but not quantified, by Gibbs et al (1974).

In the computed results, carbon formation is given by Equation (3.4.3c), and thus depends directly on the square of the CO concentration. The two dependent variables which indicate the carbon formation are the weight of carbon, W_C, and the ratio, Z, of the rates of reactions 3 and 1. Graphs of Z, for the same cases from Run 5624 as are shown in Figure (5.7), are given in Figure (5.8). The ratio Z continues to rise even when the concentration of CO is falling.

5.4.3 Inner layer volume.

The question of the volume available for inner oxide growth is discussed in Section (3.3). That discussion can now be compared with the computed results. Equations (3.5.18-20) in Section (3.5.1) define the dimensionless volume factors G_A, G_C and G_{OX}, which compare the volume available, and that taken up by carbon and inner oxide, with the theoretical value of clean metal reacting given in Equation (3.5.14). Results for a particular case from Run 5624 are shown in Figure (5.9).

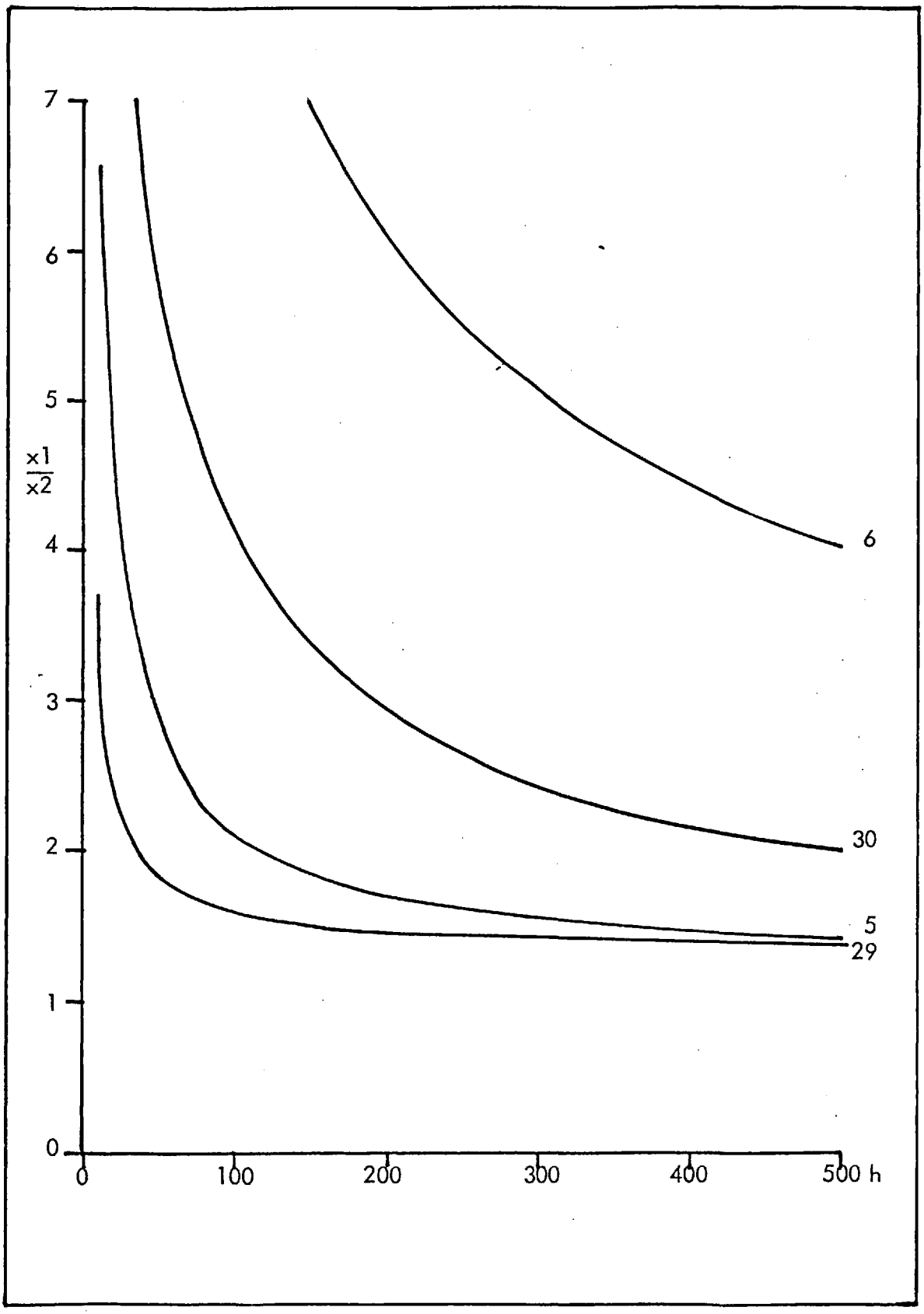

Figure 5.6 Graph of x1/x2 for cases 5, 6, 29, 30 of Run 5624

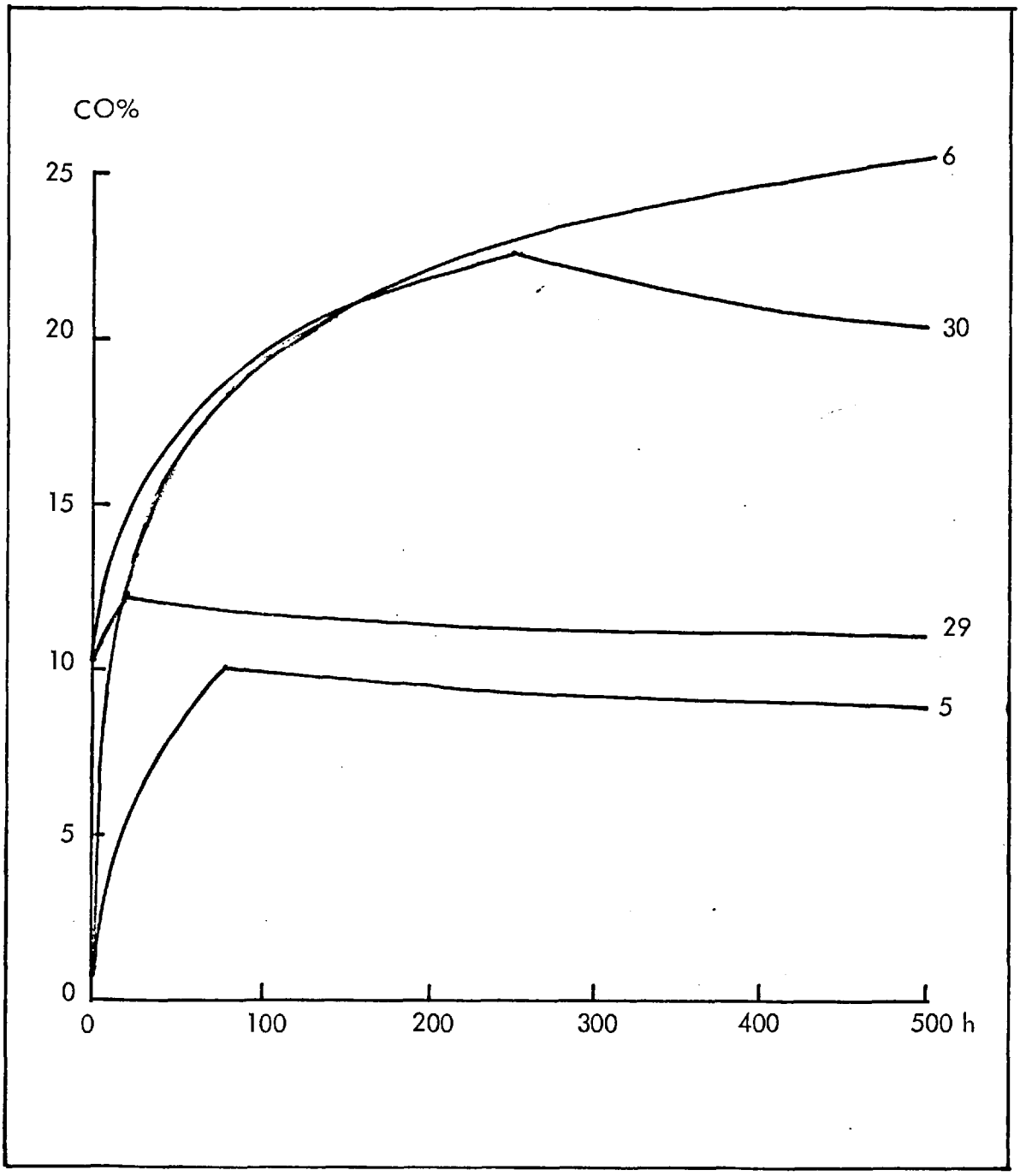

Figure 5.7 Graph of CO for cases 5, 6, 29 & 30 of Run 5624

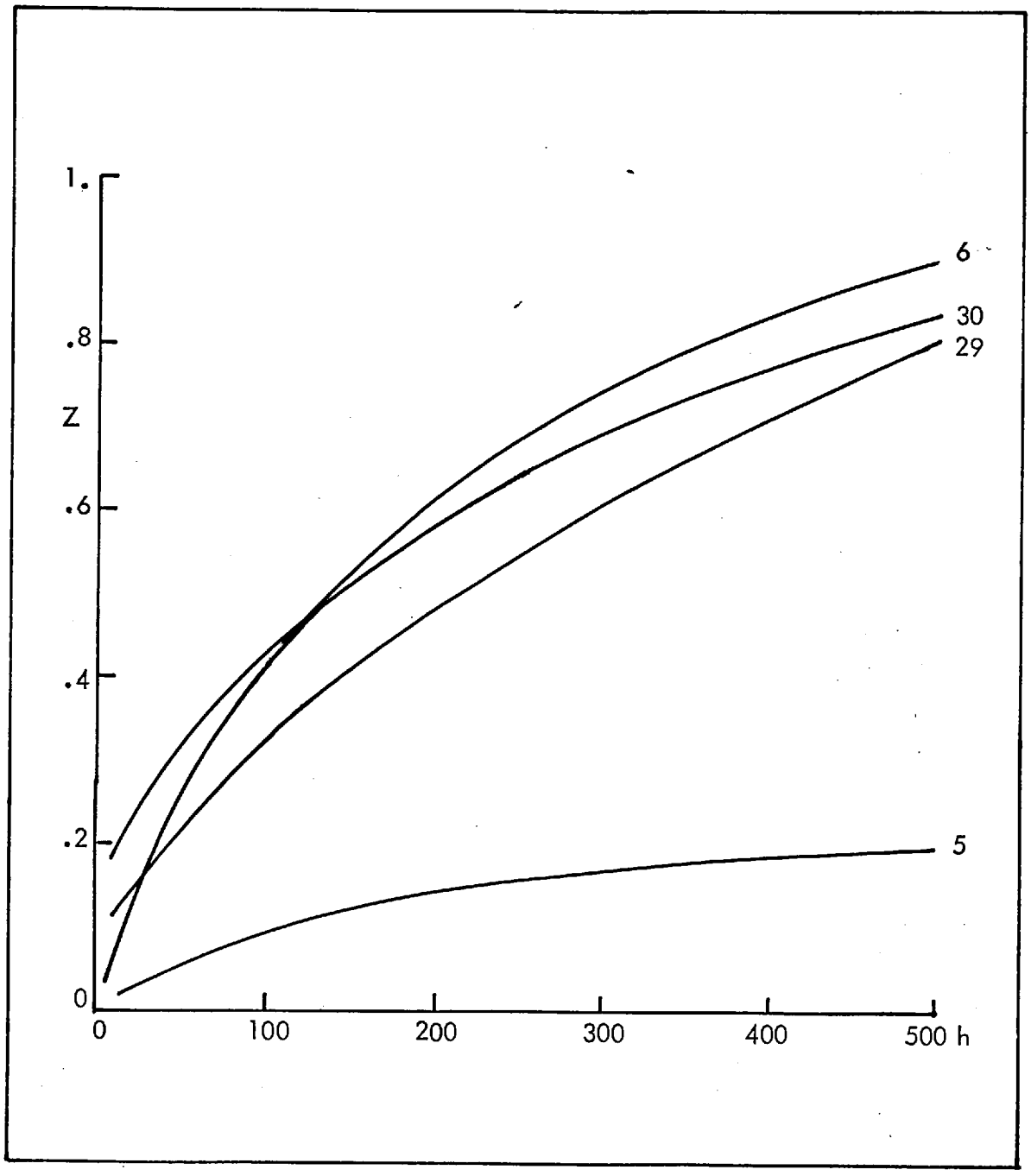

Figure 5.8 Graph of Z for cases 5, 6, 29 & 30 of Run 5624

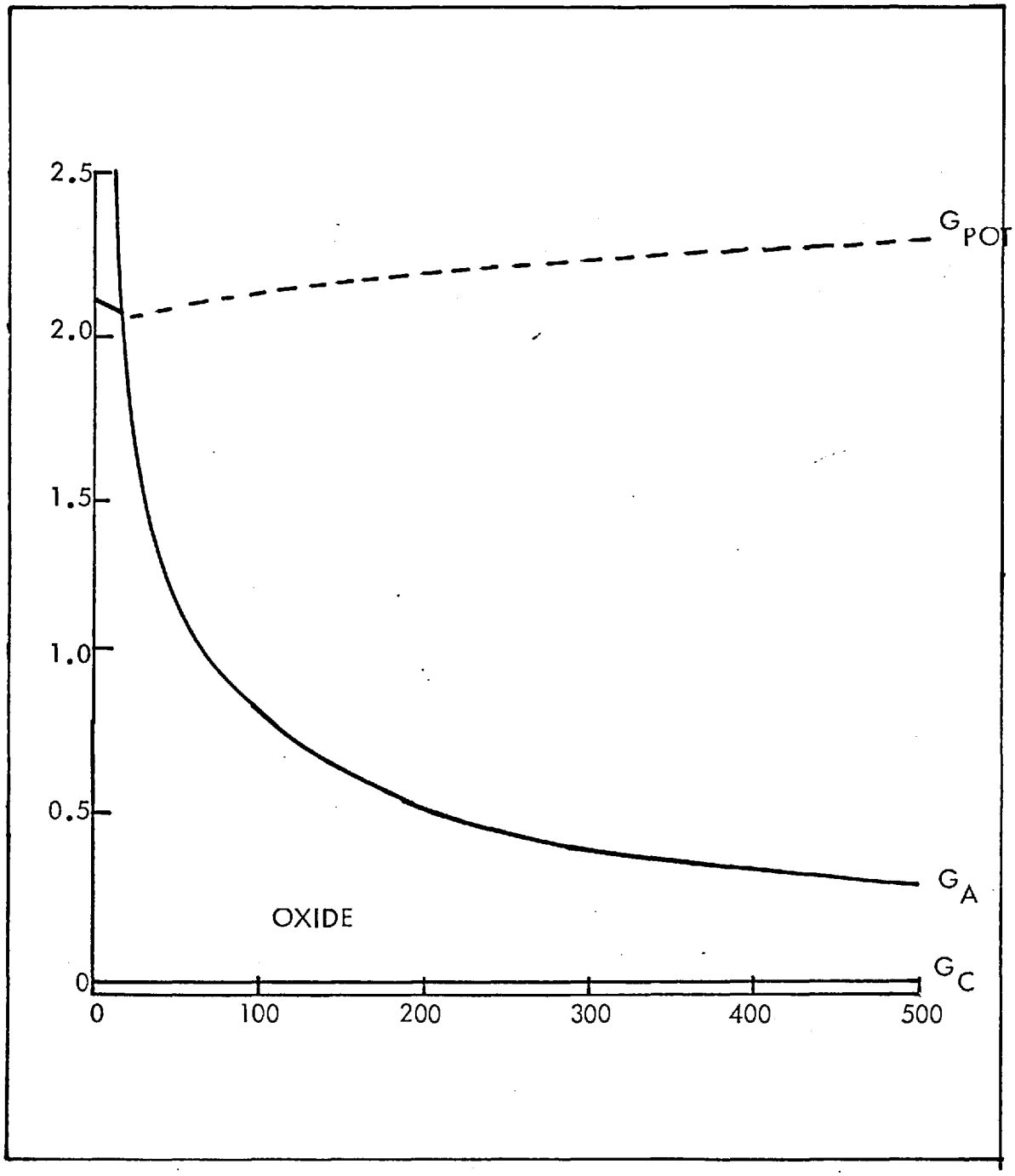

Figure 5.9 Graph of Dimensionless groups for case 29 of Run 5624

The graphs plotted are G_A, G_C and $G_C + G_{OX}$, the latter being the volume actually used, which cannot exceed G_A, the volume available, for the stress free growth which is observed in protective oxidation (cf. Section (2.4) and Equation (3.5.21)). The graph of $G_C + G_{OX}$ is continued as a dotted line after point A, representing the volume which would be required if the chemical reaction were not assumed to be limited to the volume available. The significance of this graph is not in the particular values plotted, but in the manner in which the volume available controls and reduces the inner layer oxidation after point A, until carbon forms all of the inner layer. This process depends upon the form of these two curves, one reaching a slow descent as shown in Figure (5.9) and determined by Equation (3.4.3c), and the other determined by the rates of reactions (1) and (2), from Equation (3.5.18). The rate of reaction (2) is given by Equation (3.4.2), and thus decreases with increasing oxide thickness, X, while the rate of reaction (1) is itself controlled after point A by the volume available. The model predicts that these two curves must eventually meet for any case with finite carbon formation, provided the simulation is carried on long enough. This is in agreement with the result in Section (5.4.2), that Z should continue to rise, even when the CO concentration, and thus carbon formation, is falling slowly.

5.4.4 Rate controlling processes.

In Sections (5.4.2-3) it is apparent that both the CO concentration and the inner layer volume follow two regimes of behaviour successively. In Section (5.4.3), the change of regime can be

identified by the point at which solid state transport limits the inner layer; inspection of each case shows that the change from increasing CO concentration, to a falling or steady concentration coincides with this change.

The model therefore predicts a two stage process for protective oxidation. In the first stage, the CO concentration rises, and the inner and outer layers are controlled independently, by chemical reaction and solid state diffusion respectively. In the second stage the solid state diffusion controls the volume available for the inner layer, which is increasingly filled with carbon.

At this stage Equation (3.4.1) predicts a much larger rate of oxidation at the metal than is allowed in the volume available. Both Gibbs (1973) and Surman and Brown (1974) have suggested that increasing quantities of carbon may cause the volume control mechanism to break down, ending stress-free protective oxidation and allowing a sudden increase in the oxidation rate. The situation predicted here, with increasing carbon in the inner layer, favours this possibility, as whatever critical level of carbon is needed will eventually be reached. The time at which it will be achieved will vary greatly, depending on the particular values of the parameters.

5.5 Conclusion.

The results show that the model with separate iron diffusion produces results in broad agreement with observations in the temperature range of interest, although the results cannot be made quantitative, because the correct values for many of the parameters have not been

established. The model gives a consistent pattern of parabolic growth and the relative sizes of the two layers are predicted to change in precisely the way observed in experiment. The effects of variation of some of the parameters have been examined. The results show a clear pattern of dependence on a few particular parameters. The most interesting results are the prediction of an initial rise in the level of CO, followed by a fall, because of the change in the rate controlling step for inner layer oxidation, and the prediction that carbon will eventually fill the inner layer, giving rise to conditions favourable for stresses to develop in the oxide.

6. Conclusions.

6.1 Discussion and limitations.

The main aim of this work has been to improve the understanding of the reaction mechanisms which control the oxidation behaviour of mild steels in oxidising mixtures of CO_2 and CO. This cannot be accomplished directly here, because no experimental work was undertaken. It can, however, be achieved less directly, by the incorporation of the mechanistic ideas, developed by experiment, into an overall framework of the law of conservation of mass. While a very simple model can be used in cases where only one process controls the mass transport, when, as here, there are known to be several such processes, it becomes difficult with a simple model to allow in the correct way for the interactions between processes. Indeed, it may be that a simple model is unable to account at all for the observed effects.

It is in these circumstances that a more comprehensive approach to mathematical modelling may be justified by the importance of the problem. Such is the case here, but the method has important limitations. First, the method cannot prove a mechanism to be correct: that can only be tested by experiment. The results can only be of a secondary nature. They can test assumptions, and show some to be misleading or wrong. Subject to the assumptions made, the results can predict effects, for which experimental tests can then be made. This is probably the most that can be claimed for this type of model, and it is made more difficult here by the limitations and uncertainties of the situation.

Secondly, it is difficult to find the correct degree of complexity for the model. This has already been discussed for this problem in Section (3.1), but in more general terms too little complexity means that the model cannot account for the phenomena observed, while too much means that the model is either too expensive to be useful, or too demanding of information. It is a matter of engineering judgement on the accuracy to which information is needed, and the price which the information is worth. Thus the degree of need, as well as the actual problem, can determine the method used.

It is important to consider the nature of what has been attempted, and what has resulted. This is important not only for the particular problem at hand, but for the development of a general approach to problems which are in many ways not well defined, but where an understanding, however tenuous, is worth considerable effort to attainment, because of the potential benefits that would be made available. What the approach amounts to is constructing a model of the situation which is simple enough to be soluble with the limited information available, while being at the same time true enough to the essential features of the problem to give answers in accord with the real situation. Without simplicity the problem will only be soluble by huge assumptions about missing information; without truth the exercise is one of imagination only. The important thing for the achievement of the correct level of simplification is an exercise of engineering judgement, which is partly logical and numerical, and partly intuitive.

The first can in principle be tested directly by inspection of results, though it is arguable whether the interaction of the parameters could be carried through. Such analysis of interactive parameters requires a feel for the problem. Making such intuition available for inspection and test has required recognition that this aspect of the study is synthetic rather than analytic. Detailed cases apart, the exemplification of this synthesis is the essential contribution of the present thesis. This is believed to be the first occasion on which such methods have been applied to a corrosion problem.

6.2 The current situation.

It is important not to overstate the numerical significance of the results that have been calculated. It has been shown that the model reproduces in outline the oxidation behaviour observed in experiment, and reproduces without this being assumed, the type of two layer behaviour shown on micrographs of specimens. The results cannot, however, be claimed as fully quantitative, because of the uncertainties in the values of the parameters. Despite this, it is possible to demonstrate two areas where the model can elucidate the mechanism of the oxidation, and thus point the way toward further experimental investigations. These two areas are the quest for the rate controlling step, and the concentration of CO near to the metal. Taken together, they allow some extensions of the theories of Gibbs (1973) towards an understanding of the nucleation of breakaway.

It is striking that the shape of the computed CO curve is very similar to the predictions of Gibbs et al (1974) discussed in

Section (2.5). There he suggests that breakaway nucleation should be associated with a situation where the oxygen potential is increased by some mechanism, so that the inner layer can grow faster. In fact here the model produces the desired increase of potential in a situation where the inner oxide is constrained by the volume available, and competing for space. If, for any reason, the constraint of space should cease to operate, the inner oxidation rate could increase, thus occupying more volume than is available, and disrupting the outer oxide layer. Thus the model provides a situation in which the mechanism of Gibbs et al (1974) is a viable one.

There is, however, a problem to be resolved, which was discussed by Leach (1974), as mentioned in Section (2.5). The work of Surman and Brown (1974) suggested that the Boudouard reaction (2.2.2) is not catalysed by magnetite when the CO concentration is below 30%, and thus carbon formation should slow or stop if the CO level falls, as predicted by Gibbs et al (1974).

This question can to some extent be resolved by the observation that carbon is formed after breakaway, when the oxide is sufficiently porous for the CO concentration to be essentially the same as the external gas (cf. Section (3.2.3)). Are the same catalysts still active here, for if so, then they should have been active before and during breakaway as well.

The results of Pritchard et al (1974), mentioned in Section (2.4.1), showed that at a fixed time, carbon was present in the oxide mainly near to the metal. This supports the assumption made that carbon is formed

at or near to the metal, but also poses further questions: has the carbon formation rate varied with time to produce this effect, and the carbon then been fixed in the oxide, or has the rate of carbon formation changed less, but the carbon moved by some process, to keep it near to the metal boundary. Such a process should be suggested, if the carbon was susceptible to the reverse Boudouard reaction (2.2.2) to reform CO, because the concentration of CO could be lower further out through the oxide. The CO level would, though, have to be very low to be below the equilibrium of the Boudouard reaction, which is 0.5% (cf. Section (2.2)). This idea could be tested by looking at specimens by the method of Pritchard et al (1974) at different stages of the oxidation process.

Even assuming that the carbon is in fact fixed, the model results can take further the discussion of Gibbs et al (1974), about the induction of breakaway. They suggest that rapid formation of free carbon is taking place in the inner layer, to cause breakaway. The results of the model show that the rate of carbon formation does not need to increase in the inner layer for its proportion of the oxide formed to increase, because of the competition for space, where the space available is falling faster than the carbon formation rate. In this case the use of Equation (3.4.3c) rather than (3.4.3b) is more pessimistic for carbon formation, as it gives faster reductions when the CO falls. This means that it is not necessary to postulate a change in mechanism for breakaway to occur. The existing model predicts that for all cases where the inner oxide is limited by diffusion to form the outer, and carbon formation is occurring, the

carbon proportion will continue to rise until it fills the inner oxide completely. At some point in this process, probably at a critical carbon fraction, the volume control mechanism could cease to function, allowing some extra oxidation, for which the potential will be there, as discussed in Section (5.4.4). This will begin a disruptive process, because increased gas access cannot cause healing of the oxide, because of the carbon present. The assumptions of the present model will have broken down, but the new situation is capable of a simpler model.

6.3 Other variables not considered.

As a part of the process of forming a model simple enough to be soluble, it has been necessary to neglect some of the factors of the real situation. There are several such factors which are known to influence the oxidation process, and the effect of these can now be considered, to see if allowance can be made for their effect on the results. In some cases it might be possible to extend the model to cover these effects.

The main effects which have been neglected are the minor components of the gas, principally water, and alloying elements in the metal, which in experiments has varied from pure iron to mild steels, and low alloy steels. The model has also been considered at a fixed temperature.

Low concentrations of water are known to have a significant effect on the oxidation process, and to increase the oxidation by much more than the mass of water present. This suggests a catalytic role, involving perhaps the shift reactions given in Equations (2.2.9-10). These two reactions cannot both be in equilibrium simultaneously with carbon, CO

and CO_2, because each predicts a different value of the H_2/H_2O ratio. This means that there is the possibility of water reacting to promote mobility of carbon, and thereby changing the way in which carbon interferes with the volume control mechanism.

The role of alloy elements in the metal is difficult to model, and few suggested mechanisms have been advanced. But both here, and in the case of water, mechanisms could be incorporated into the model, and the new set of equations integrated as here. The effect of temperature could only be modelled if the effect of temperature on individual parameters could be quantified, and cases integrated at different temperatures. This could then be tested against the observed activation energies, and the model could then be of use in predicting oxidation behaviour at the lower temperatures of reactor service.

6.4 Final conclusions.

A mathematical model has been constructed of the initial phases of the oxidation of iron and mild steels in carbon dioxide gas containing some carbon monoxide. It demonstrates that it is possible to unify mechanisms suggested for the different processes occurring into a single system of equations, using an overall mass balance; the resulting equations have been integrated numerically. The results of the integration agree in form with experiment, but full quantification is not possible, given the limited information available. Nevertheless, the results show qualitatively effects observed experimentally, such as the relative thickness of the two oxide layers. The oxidation process is best accounted for by a mechanism where the rate control is divided

between different processes at different stages of the oxidation. In the first stage the two oxide layers are separately controlled, but enhanced solid state diffusion controls both in the second stage. The model predicts that for any oxidation process entering the second stage, the proportion of carbon in the inner layer will increase until no oxidation is taking place there. Other work suggests that this is a likely situation for breakaway to occur.

Appendix 1 Manual for Thermodynamic Program

This is a C.E.G.B. internal document
reproduced by permission.

C.E.G.B. INTERNAL USE ONLY

CREATE2L
REF.6352P
20 July 1972
RD/L/P 19/72

CENTRAL ELECTRICITY RESEARCH LABORATORIES

LABORATORY PROGRAM NO. RD/L/P 19/72

(Job No. VF 393)

USERS GUIDE TO A PROGRAM FOR CALCULATING THE EQUILIBRIUM CONSTANTS OF CHEMICAL REACTIONS FROM THERMODYNAMIC DATA FOR INDIVIDUAL COMPOUNDS (CREATE)

- by -

J.P. Fletcher and W.S. Kyte

Approved by: J Inwood.

Head of Division

Date: 20 July 1972

This Document may not be reproduced in whole or in part without the permission of the Director of the Central Electricity Research Laboratories, Leatherhead, Surrey.

SUMMARY

A computer program has been written to evaluate the equilibrium constants and thermodynamic functions for chemical reactions at points over a range of temperatures. The input consists of thermodynamic data for individual compounds or elements, and the desired chemical reactions and temperature ranges. Details are given of the data input.

2.

CONTENTS

1. BRIEF DESCRIPTION OF SCOPE OF PROGRAM

2. DETAILED PROBLEM DESCRIPTION

- 2.1 Description
- 2.2 Major Assumptions and Limitations
- 2.3 Equations Solved
- 2.4 Notation
- 2.5 References in Application Area

3. PROGRAM DETAILS

- 3.1 Restrictions on Problem Size
- 3.2 Data Preparation
  - 3.2.1 Data required
  - 3.2.2 Input
  - 3.2.3 Format of data cards
- 3.3 Description of Output
  - 3.3.1 Output
  - 3.3.2 Accuracy of results
- 3.4 Computer Time Required and Amount of Output
- 3.5 Directly Related Programs

4. PRODUCTION/OPERATING INSTRUCTIONS

- 4.1 Data Assembly
- 4.2 Job Control Language Statements
- 4.3 Job Sheet Details
- 4.4 Error Messages and Common Faults

Appendix 1 Administrative Details

Appendix 2 Sample Data and Sample Output

Appendix 3 Mathematical Analysis

Appendix 4 Programming Details

1. BRIEF DESCRIPTION OF SCOPE OF PROGRAM

The program CREATE evaluates, for each of a series of given reactions and ranges of temperature, the following thermodynamic functions: change in specific heat, heat of reaction, entropy of reaction, free energy of reaction, and the equilibrium constant.

Thermodynamic data must be supplied for each individual compound involved in the reactions, although a standard file is being accumulated.

Details of the reaction to be evaluated are input in free format.

The computation of chemical equilibria and the evaluation of equilibrium constants for a given system are very often required. The computation of chemical equilibria for systems with more than a few species is a very complex problem and must be done numerically. Programs have been presented (e.g. Hughes, 1972) for solving such systems, though in general these programs are too cumbersome and expensive to be economically used on simpler systems.

In a simple system the likely composition can be readily evaluated from a knowledge of the free energies and equilibrium constants of the most probable reactions involved. However, this involves the evaluation of a number of simple but tedious integrals for each temperature and reaction studied. Thus, there is a need for a computer program to evaluate equilibrium constants from basic thermodynamic data. Programs which calculate equilibrium constants exist (Huber, 1968), but are not readily available.

The Program presented here has been written to evaluate simple thermodynamic properties for single reactions. It has been written in a user-orientated manner in order that its use may be as simple and economical as possible.

2. DETAILED PROBLEM DESCRIPTION

2.1 Description

The variation with temperature of thermodynamic functions is related closely to the variation of specific heats with temperature. If an analytic form is assumed for this variation, then the equations can be integrated analytically. The programming problem is to evaluate the thermodynamic functions for the correct stoichiometry, and at the correct temperature.

2.2 Major Assumptions and Limitations

(i) The heat of formation (ΔH_f) of each compound must be known at one temperature (T_H).

(ii) The entropy (S_o) of each compound must be known at one temperature (T_S). T_H and T_S need not be the same, and neither can be OK (Absolute Zero).

(iii) The specific heat at constant pressure (C_p) of each compound must be represented by a formula of the form

4.

$$C_p = A + \frac{BT}{10^3} + \frac{C.10^5}{T^2}$$

which must be valid over the whole range of temperature, from T_H and T_S to the temperature T where the reaction is to be evaluated.

(iv) Separate reference information is therefore needed for the different physical states of a compound.

(v) The reaction stoichiometry must be represented by integers or simple fractions.

2.3 Equations Solved

The equations solved are the following general thermodynamic relationships which may be found in any standard text (e.g. Denbigh, 1966)

$$\Delta C_p = \sum_{i=1}^{n} \nu^i C_p^i \qquad \ldots (1)$$

$$\Delta H = \sum_{i=1}^{n} \nu^i \left[\Delta H_f^i + \int_{T_H^i}^{T} C_p^i \, dT \right] \qquad \ldots (2)$$

$$\Delta S = \sum_{i=1}^{n} \nu^i \left[S_o^i + \int_{T_S^i}^{T} \frac{C_p^i}{T} \, dT \right] \qquad \ldots (3)$$

$$\Delta G = \Delta H - T \, \Delta S \qquad \ldots (4)$$

$$\log K_p = \frac{1}{2.303} \left(- \frac{\Delta G}{RT}\right) \qquad \ldots (5)$$

$$K_p = \exp \left(- \frac{\Delta G}{RT}\right) \qquad \ldots (6)$$

where $C_p = A + \frac{BT}{10^3} + 10^5 \frac{C}{T^2}$ ... (7)

2.4 Notation

A, B, C } Coefficients in polynomial expression for C_p

C_p Specific heat at constant pressure

G Gibbs free energy

H Enthalpy

H_f Enthalpy of formation at temperature T_H

K_p Equilibrium constant

n Number of reactants + products

R Gas constant

S Entropy

S_o Entropy at temperature T_S

T Temperature

ν Stoichiometric coefficient

2.5 References in Application Area

Denbigh, K., 1966, 'The Principles of Chemical Equilibrium' (C.U.P.)

Huber, R.A., 1968, UKAEA Report AERE R5793

Hughes, Miss A., MS/C/P182

3. PROGRAM DETAILS

3.1 Restrictions on Problem Size

Maximum number of compounds on which data can be supplied = 250

Maximum number of compounds in any one reaction = 10

There is no limit to the number of reactions which may be considered, or to the number of temperatures at which each reaction may be evaluated.

3.2 Data Preparation

3.2.1 Data required

For each compound a name must be supplied, together with the values of ΔH_f, T_H, S_o, T_S and A, B & C.

6.

For each reaction, the stoichiometery must be supplied using the names specified in the compound data, and also the first and last temperatures, and the temperature interval, for which evaluation is required.

The units should be as specified in Section 3.2.3.

3.2.2 Input

The data cards are of three types, and the format for each type is given in the next section.

Card A gives the name and reference information for a single compound.

Card B gives the reaction to be evaluated, and can be continued on to more than one card.

Card C gives the temperature range for evaluation. Several can be supplied for a given reaction.

For input, all type A cards should be placed first, followed by a delimiting card with * or & in col. 1. (See Section 3.2.3.) This card must be present even when no type A cards are present.

The first card B should follow, and then one or more cards type C applying to it, then another card B, etc. No end card is needed.

3.2.3 Format of data cards

Card A — Format (10A1, 7G10.0)

Name, ΔH_f, T_H, S_o, T_S, A, B, C

'Name' — The compound name must not exceed 10 characters, and must begin in column one, and contain no blanks. The name must not begin with a numeral, or the characters = + - * &. Otherwise it can take any form e.g. H2O(LIQ), (NH4)2SO4

ΔH_f	Heat of formation	kcal/gmole
T_H	Reference temperature for ΔH_f	K (default 298.15)
S_o	Entropy	kcal/gmole K
T_S	Reference temperature for S_o	K (default 298.15)
A, B, C	Coefficients in the formula $C_p = A + \frac{BT}{10^3} + \frac{10^5 C}{T^2}$ (T in K)	cal/gmole K

Notes Before any type B card is read a delimiting card must be present. There are two types of delimiting card:
If * is punched in col. 1 then the standard file is not read.
If & is punched in col. 1 then further data is provided by the standard file.
If a compound name is inserted more than once, the first is used and the second ignored. Thus, card input can be used to over-ride the standard file.

Card B Format (80A1)

This card contains the chemical reaction in essentially free format, designed so that chemical reactions can be input as they would normally be written, but the following rules must be observed.

(i) Compound names must be exactly the same as the names used on the corresponding cards of type A, and must be preceded and followed by at least one blank.

(ii) The stoichiometric coefficient must be an integer (positive or negative). If it is absent, a default value of + 1 is assumed. Simple fractions are accommodated by multiplying all the coefficients by the lowest integer common denominator and punching this integer at the end. If this is absent, a default value of 1 is assumed.

(iii) The stoichiometric coefficient and its sign may be separated by one or more blanks.

(iv) The following characters have special uses:

* - no further columns of the current card are read, and any comment may be put there.

& - as for *, but the next card is read as a continuation of the current card type B.

Card C Format (I1, F9.0, 2F10.0)

N, T_{start}, T_{stop}, DT

N - 0 or blank if no further cards type C follow

- 1 if further cards type C follow

T_{start} - first temperature to be evaluated - Deg. C

T_{stop} - last " " " " - Deg. C

DT - temperature interval - Deg. C

If this is not greater than 0.01 Deg. C only one evaluation is made, at T_{start}.

8.

3.3 Description of Output

3.3.1 Output

The output from the program is in a simple tabular form. Firstly, the reference data from the compounds are listed in a table, showing which were input from cards, and which from the standard file.

The output from each reaction case consists of the following items: the input reaction card, a message showing the temperature range in both K and Deg. C, and then a table giving the stoichiometric coefficient and name for each name recognised. A message is printed if a lowest common denominator is to divide these values. Finally, there is a table of evaluations at the temperatures requested, and also at 25°C.

The program produces a number of error messages all associated with faulty or inadequate data. The program usually attempts to process the following case.

3.3.2 Accuracy of results

The program is written in double precision arithmetic to minimize the errors which may be caused in thermodynamic calculations by subtraction of nearly equal numbers. Thus, the accuracy will usually be limited by the reliability of input data, rather than by the program.

3.4 Computer Time Required and Amount of Output

Both the computer time used and the amount of output produced are directly related to the number of temperatures at which calculations are required to be carried out.

The total time (CPU 370/165) and lines of output can be estimated from:

$$\text{Time (secs)} = 0.01 + 0.05\,N_C + \sum_{1}^{N_C}\left[1 + \left(\frac{T_{stop} - T_{start}}{DT}\right)\right]$$

$$\text{Lines} = N_A + 25N_C + 1.5\sum_{1}^{N_C}\left[1 + \left(\frac{T_{stop} - T_{start}}{DT}\right)\right]$$

where $N_{A,\ C}$ are the number of card types A and C respectively.

3.5 Directly Related Programs

None.

4. PRODUCTION/OPERATING INSTRUCTIONS

4.1 Data Assembly

The data input consists of any type A cards, and a delimiting card (compulsory), followed by a sequence of cards type B, with one or

more type C after each.

	Cols	Format	Input Parameter	Default
Card A	1 - 10	10A1	Name (left justified)	-
	11 - 20	G10.0	ΔH_f	-
	21 - 30	G10.0	T_H	298.15
	31 - 40	G10.0	S_o	-
	41 - 50	G10.0	T_S	298.15
	51 - 60	G10.0	A	-
	61 - 70	G10.0	B	-
	71 - 80	G10.0	C	-
Delimiting Card	1	A1	* or & (see Section 3.2.3)	
Card B	1 - 80	80A1	Reaction (see Section 3.2.2) (with & continues to next card)	-
Card C	1	I1	N	-
	2 - 10	F9.0	T_{start}	-
	11 - 20	F10.0	T_{stop}	-
	21 - 30	F10.0	DT	-
	Further card type C if N = 1			

4.2 Job Control Statements

(a) Job with card input only. (* in col. 1 on delimiting card)

```
//        JOBCARD
/*SETUP   UNIT=3330,ID=AF
/*MAIN    LINES=2
//STEP1   EXEC STANPROG,VS=AF,PROGRAM=CREATE,N=1A
//DATA    DD *, DCB=(RECFM=FB,BLKSIZE=880)
        Insert data cards for the job
/*
```

10.

(b) Job with input from standard compound file (& in col. 1 on delimiting card)

```
//          JOBCARD
/*SETUP     UNIT=3330,ID=AF
/*SETUP     UNIT=3330,ID=AC
/*MAIN      LINES=2
//CONV      EXEC FUVITC,VS8=AC,NAME8='L2.CERL.LIB23D'
//STEP1     EXEC STANPROG,VS=AF,PROGRAM=CREATE,N=1A
//FT10F001 DD  UNIT=UT,DISP=(SHR,DELETE).
//          DSN=*.CONV.STEPC.FT09F001
//DATA      DD*,DCB=(RECFM=FB,BLKSIZE=880)
          Insert data cards for the job
/*
```

Potential users of any data set referred to in this document should check with the Disk Controller that the data set is held on the volume stated. If necessary, the appropriate manager (as indicated by the section letter) should be consulted.

4.3 Job Sheet Details

Region size required	70 K
CPU time Output	See Section 3.4
Class type B	

4.4 Error Messages and Common Faults

Most of the errors which occur are connected with faulty input, and in the event of an error being detected the program will skip the faulty case and process the next reaction case except when an error is detected in processing the input reactant data.

(i) TOO MANY REACTANT CARDS - FIRST nnnn READ

Explanation Too many reactant cards have been supplied. The excess cards are ignored and the job proceeds but a reaction case may fail later due to lack of reactant data.

Action Reduce number of input reactant cards so that the number of input + records in data file does not exceed nnnn. Ensure that only necessary cards are retained in card input.

(ii) LAST CARD OF FILE WAS A CONTINUATION CARD

Explanation Second reaction card was not supplied.

Action Ensure that continuation card supplied or remove redundant & on card type B.

(iii) MORE THAN TEN REACTANTS IN REACTION-CASE SKIPPED

Explanation The reaction supplied involves too many compounds.

Action Reduce number of compounds or subdivide reaction into two or more reactions.

(iv) CASE SKIPPED AS THIS NAME IS NOT IN THE FILES - aaaa

Explanation A name has been encountered in the reaction which has not been supplied in the data input or in the back-up file.

Action Insert reactant card in input for aaaa and/or check for mispunched data input.

(v) NO & CARD TO END REACTANT CARDS - END OF FILE

Explanation The reactant card input has not been delimited by & or * on the delimiting card.

Action Ensure that reactant card input is delimited by inserting delimiting card with & or * in col. 1.

(vi) INTERVAL TOO SMALL - ONLY ONE EVALUATION MADE

Explanation DT on card type C is $<0.01^{o}C$ and only one evaluation is made at T_{start}. DT has probably not been set.

Action Ensure that DT is specified.

(vii) NO NAME FOUND ON REACTION CARD - CASE SKIPPED

Explanation No reactant name has been detected on reaction card.

Action Ensure that reaction is specified on reaction card or that reactant names do not violate rules given in Section 3.2.3.

(viii) CHARACTER FOLLOWING A 10 CHAR NAME IS NOT A BLANK - ANALYSIS CONTINUES

Explanation No blank has been detected at the end of a ten character name. The program attempts to process the reaction, though a wrong name may be found, and the analysis subsequently fail.

Action If the true name was ten characters long the analysis will probably continue successfully. Otherwise insert blank at end of name.

12.

(ix) MORE THAN ONE = ON REACTION CARD - CASE SKIPPED

Explanation Reaction is improperly specified.

Action Correct reaction.

(x) THE VALUE(S) OF K DENOTED BY + HAS(HAVE) BEEN SET TO ZERO

Explanation The value of ln K exceeds 174.67 and to eliminate machine error messages K is not evaluated but set to zero.

Action If value of K is required re-run the case with a higher divisor of the stoichiometry.

Appendices 1-4 and Drg. No. RL 4.1.1918 attached.

Form API	Abstract No.
	Date :

APPENDIX I

ADMINISTRATIVE DETAILS

1. DOCUMENTATION

Card Indicr.	PROGRAM TITLE:	PROGRAM NAME
1 / 4	Chemical Reaction Evaluation At Thermodynamic Equilibrium	CREATE

Stage Completed	COMPUTING PLAN PROJECT NAME	WORK CODE	COMPUTING PLAN Year	COMPUTING PLAN Ref.
2	MARTO12L	754030	71/72	L2

Project Manager :	F.A.J. Ford	Project Leader :	

Date of final compilation :	April 1972	Language :	FORTRAN IV	Anticipated access to system :	REMOTE
		Compiler Level :	H OPT = 2		

Library Subroutines used	NONE		

2. PRODUCTION REQUIREMENTS

COMPUTER	NAME AND MODEL NO.	REGION SIZE kbytes	APPROX. PERCENTAGE C.P.U. UTILISATION
	IBM 360/85	70	20

	NO. OF TAPE UNITS 9-track	NO. OF TAPE UNITS 7-track	NO. OF TAPES 9-track	NO. OF TAPES 7-track	DISK STORAGE CYLINDERS UTILITY	DISK STORAGE CYLINDERS USER	CALCOMP PLOTTER
PERIPHERALS							

	CARDS IN x 100	LINES OUT x 1000	PAPER TAPE PERIPHERALS Reader	PAPER TAPE PERIPHERALS Punch
REMOTE I/O				

	CARDS x 100 IN	CARDS x 100 OUT	NO. OF PARTS	PRINTER OUTPUT % LINES WITH RESTRICTED CHARS	PRINTER OUTPUT MAX. PRINT LINE LENGTH	LINES x 1000
LOCAL I/O						

PROGRAM NAME: CREATE

PROJECT LEADER / MANAGER SIGNATURE :	DATE :

3. STANDARD ENDORSEMENT

This program conforms to current Bureau Standards as specified in the Standards Manual and all documentation appropriate to the last stage completed, has been submitted.

PROJECT MANAGER SIGNATURE :	DATE :

NOTE : If program exceeds the limits specified in the Bureau Standards, complete sections 5 and 6. Page 2 is not included in the program write-up.

4. PRELIMINARY PRODUCTION ESTIMATES

ESTIMATED NO. OF RUNS PER YEAR :	ESTIMATED AVERAGE COST PER RUN : £	FREQUENCY OF DISK DATA - SET BACK - UP :

APPENDIX 2

SAMPLE INPUT DATA AND PROGRAM OUTPUT

C.E.G.B. COMPUTING BRANCH

PROGRAMMER JPF/WSK.

PROGRAM CREATE

TITLE APPENDIX 2

SAMPLE OF DATA INPUT

SHEET No. 1

DATE 21.4.1972.

DATA. PUNCHING FORM

```
1    5    10   15   20   25   30   35   40   45   50   55   60   65   70   75   80
CŌS                -33.90          55.3          11.33          2.18          -1.83
SŌ2                -70.95          59.3          11.04          1.88          -1.84
H2S                 -4.90          49.15          7.87          2.96          -0.46
CS2                 27.65          57.1          12.45          1.60          -1.80
CH4                -17.89          44.5           5.65         11.44          -0.46
S2                  31.00          54.4           8.72          0.16          -0.90
S8                  30.00         112.5          42.54          1.04          -5.04
C                    0.00           1.361         4.03          1.14          -2.04
O
     2 H2 + Ō2 = 2 H2Ō  2 * NŌTE THAT THE STŌICHIŌMETRY HAS BEEN DIVIDED BY 2.
          300       800       100
     2 CŌ + Ō2 = 2 CŌ2 * 2 TEMPERATURE CASES - CŌ, CŌ2 IN STANDARD FILE
1              0       100       25
          100       1000      100
     16 CŌ2 + S8 = 16 CŌ + 8SŌ2 16 *
          300       800       100
     4 S2 = S8 4 *
          300       800
```

EQUILIBRIUM THERMODYNAMICS OF CHEMICAL REACTIONS

TABLE OF REACTANT DATA SUPPLIED - LIMIT OF 250 COMPOUNDS

NAMES INPUT FROM CARD MARKED ** - REMAINDER ARE FROM STANDARD FILE

	COMPOUND NAME	DELTA H F KCAL/GMOLE	AT DEG.K	S ZERO CAL/DEG.GMOLE	AT DEG.K	CP = A + B*T/(10**3) + C*(10**5)/T**2 A	B	C
1	** CCS	-3.390D 01	298.15	5.530D 01	298.15	1.133D 01	2.180D 00	-1.830D 00
2	** SO2	-7.095D 01	298.15	5.930D 01	298.15	1.104D 01	1.880D 00	-1.840D 00
3	** H2S	-4.900D 00	298.15	4.915D 01	298.15	7.810D 00	2.960D 00	-4.600D-01
4	** CS2	2.765 D 01	298.15	5.710D 01	298.15	1.245D 01	1.600D 00	-1.800D 00
5	** CH4	-1.789D 01	298.15	4.450D 01	298.15	5.650D 00	1.144D 01	-4.600D-01
6	** S2	3.100D 01	298.15	5.440D 01	298.15	8.720D 00	1.600D-01	-9.000D-01
7	** S8	3.000D 01	298.15	1.125D 02	298.15	4.254D 01	1.040D 00	-5.040D 00
8	** C	0.0	298.15	1.361D 00	298.15	4.030D 00	1.140D 00	-2.040D 00
9	CO	-2.640D 01	298.15	4.730D 01	298.15	6.790D 00	9.800D-01	-1.100D-01
10	CO2	-9.405D 01	298.15	5.110D 01	298.15	1.057D 01	2.100D 00	-2.060D 00
11	H2	0.0	298.15	3.121D 01	298.15	6.280D 00	1.240D 00	2.900D-01
12	H2O	-5.780D 01	298.15	4.510D 01	298.15	7.300D 00	2.460D 00	0.0
13	O2	0.0	298.15	4.900D 01	298.15	4.980D 00	0.0	2.400D-01
14	NH3	-1.100D 01	298.15	4.597D 01	298.15	7.110D 00	6.000D 00	-3.700D-01
15	HCN	3.120D 01	298.15	4.821D 01	298.15	9.410D 00	2.700D 00	-1.440D 00
16	NO	2.160D 01	298.15	5.034D 01	298.15	7.030D 00	9.200D-01	-1.400D-01
17	N2	0.0	298.15	4.577D 01	298.15	6.830D 00	9.000D-01	-1.200D-01
18	NO2	8.000D 00	298.15	5.736D 01	298.15	1.007D 01	2.280D 00	-1.670D 00
19	FE	0.0	298.15	6.490D 00	298.15	3.040D 00	7.580D 00	6.000D-01
20	FE3O4	-2.669D 02	298.15	3.620D 01	298.15	2.188D 01	4.820D 01	0.0

EQUILIBRIUM THERMODYNAMICS OF CHEMICAL REACTIONS

CASE NUMBER 1

THE REACTION CONSIDERED IS - 2 H2 + O2 = 2 H2O 2 * NOTE THAT THE STOICHIOMETRY HAS BEEN DIVIDED BY 2

OVER THE TEMPERATURE RANGE 573.2 TO 1073.2 DEG.K. (300.0 TO 800.0 DEG.C.) AT INTERVALS OF 100.0 DEG.

TABLE TO CHECK STOICHIOMETRY

-2 H2
-1 O2
2 H2O

***** THE STOICHIOMETRY OF THE REACTION HAS BEEN DIVIDED BY A FACTOR OF 2

TEMPERATURE		DELTA CP	DELTA H	DELTA S	DELTA G	LOG10(K)	K	
DEG.C	DEG.K	CAL/DEG.GMOLE	KCAL/GMOLE	CAL/DEG.GMOLE	KCAL/GMOLE			
25.0	298.2	-1.567D 00	-5.780D 01	-1.061D 01	-5.464D 01	4.005D 01	1.130D 40	0
300.0	573.2	-8.956D-01	-5.812D 01	-1.140D 01	-5.159D 01	1.967D 01	4.709D 19	1
400.0	673.2	-7.392D-01	-5.821D 01	-1.153D 01	-5.044D 01	1.637D 01	2.387D 16	2
500.0	773.2	-5.953D-01	-5.827D 01	-1.163D 01	-4.928D 01	1.393D 01	8.552D 13	3
600.0	873.2	-4.585D-01	-5.832D 01	-1.169D 01	-4.812D 01	1.204D 01	1.108D 12	4
700.0	973.2	-3.261D-01	-5.836D 01	-1.173D 01	-4.694D 01	1.054D 01	3.497D 10	5
800.0	1073.2	-1.964D-01	-5.839D 01	-1.176D 01	-4.577D 01	9.320D 00	2.099D 09	6

***** THE STOICHIOMETRY OF THE REACTION HAS BEEN DIVIDED BY A FACTOR OF 2

APPENDIX 3

MATHEMATICAL ANALYSIS

(a) Derivation of equations

The equations to be solved are:

$$\Delta C_p = \sum_{i=1}^{n} \nu^i C_p^i \qquad \ldots (1)$$

$$\Delta H = \sum_{i=1}^{n} \nu^i \left[\Delta H_f^i + \int_{T_H^i}^{T} C_p^i \, dT \right] \qquad \ldots (2)$$

$$\Delta S = \sum_{i=1}^{n} \nu^i \left[S_o^i + \int_{T_S^i}^{T} \frac{C_p^i}{T} \, dT \right] \qquad \ldots (3)$$

$$\Delta G = \Delta H - T\Delta S \qquad \ldots (4)$$

$$\log K_p = \frac{1}{2.303} \left(- \frac{\Delta G}{RT} \right) \qquad \ldots (5)$$

$$K_p = \exp \left(- \frac{\Delta G}{RT} \right) \qquad \ldots (6)$$

where

$$C_p = A + \frac{BT}{10^3} + 10^5 \frac{C}{T^2} . \qquad \ldots (7)$$

Since C_p is given by a polynominal the integrals in equations (2) and (3) can be evaluated analytically. Writing

$$B' = \frac{B}{2.10^3} \qquad C' = \frac{10^5 C}{2}$$

then C_p is given by

$$C_p = A + 2B'T + \frac{2C'}{T^2}$$

A7.

and then equation (2) becomes

$$\Delta H = \sum_{i=1}^{n} \nu^i \left[\Delta H_f^i + (T - T_H) \left(A + B' (T + T_H) + \frac{2C'}{TT_H} \right) \right]$$

and (3) becomes

$$\Delta S = \sum_{i=1}^{n} \nu^i \left[S_o^i + A \ln \left(\frac{T}{T_S}\right) + (T - T_S) \left(2B' + C' \frac{(T + T_S)}{T^2 T^2_S} \right) \right]$$

(b) Programming Philisophy

In the first part of the program the names of the chemical reactants are read into an INTEGER*2 array. The back-up file of chemical reactant names is contained in a tape and/or disk file using the program FUVIT (Wickens, 1971). A listing of this file may be obtained from the authors.

The chemical reaction is read into an INTEGER*2 array using an 80A1 FORMAT. This array is then examined character by character and compared with a standard list. If a character is recognized then it must be an integer or one of the special characters used in the program (+ = etc). However, if the character is not recognized it is assumed that the character is the first of a chemical name and the name recognition sequence is started. The name is assembled by adding to the first character the following characters until either a blank is encountered or the name becomes ten characters long. The completed name is then compared with the list of chemical reactants and after successful recognition the reference number of the reactant is stored.

(c) Notation

A, B, C	Coefficients in polynomial expression for C_p
C_p	Specific heat at constant pressure
G	Gibbs free energy
H	Enthalpy
H_f	Enthalpy of formation of temperature T_H
K_p	Equilibrium constant
n	Number of reactants + products
R	Gas constant
S	Entropy

S_o Entropy at temperature T_S

T Temperature

ν Stoichiometric coefficient

(d) References

Wickens, E., 1971, MS/C/P95.

A9.

APPENDIX 4

PROGRAMMING DETAILS

(a) Names and functions of subroutines

None.

(b) Principal variable names

ATH	(250)	R*8	T_H
DHF	(250)	R*8	ΔH_f
ATS	(250)	R*8	T_S
SZR	(250)	R*8	S_o
A	(250)	R*8	A
B	(250)	R*8	B
C	(250)	R*8	C
NSS	(250)	I*4	Card/data bank indication in o/p list
NAME	(10,250)	I*2	Chemical reactant names
NN	(80)	I*2	Chemical reaction storage array
JCOM	(16)	I*2	Data array containing numeric and special character data
K		I*4	Input stream number
NREF		I*4	Reactant reference number } in reaction
NST		I*4	Stoichiometric coefficient } in reaction
NR		I*4	No. of reactants } in reaction

(c) Data Sets

FT10F001 - a data file will be read from tape/disk on encountering an & in col. 1 of delimiting card. This will contain chemical reactant data in input card image (i.e. card type A format).

(d) Outline flow diagram

See overleaf.

(e) Overlay structure

Not applicable.

(f) Core storage requirements

CREATE occupies 64 K of core store (FORTRAN H'OPT=2').

(g) Disk storage requirements for the load module

5 tracks.

(h) Data volumes required

If data from the back-up file is required then volumes AC, AF are required.

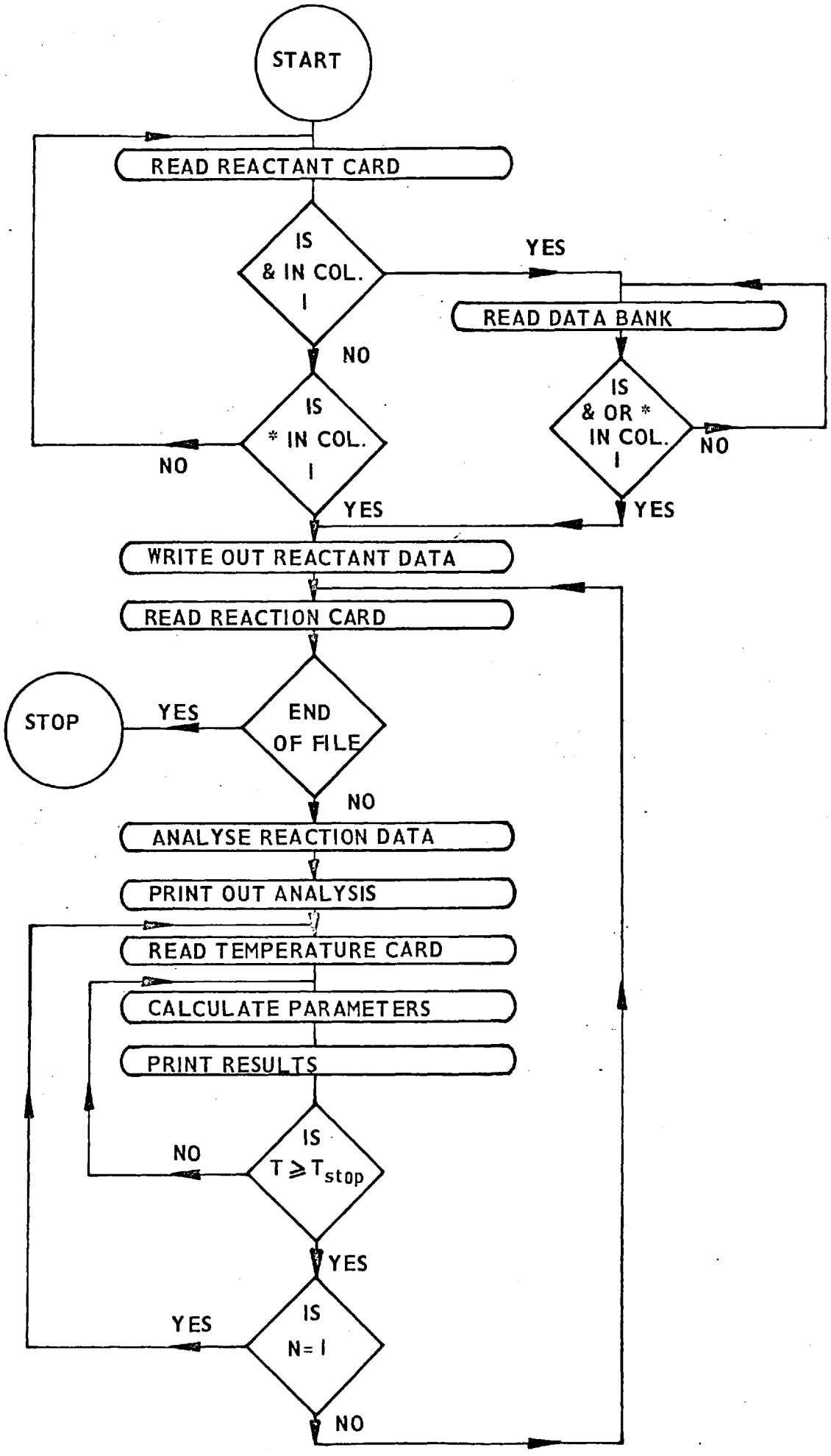

OUTLINE FLOW DIAGRAM

Appendix 2 Program Flowsheet for Mathematical Model

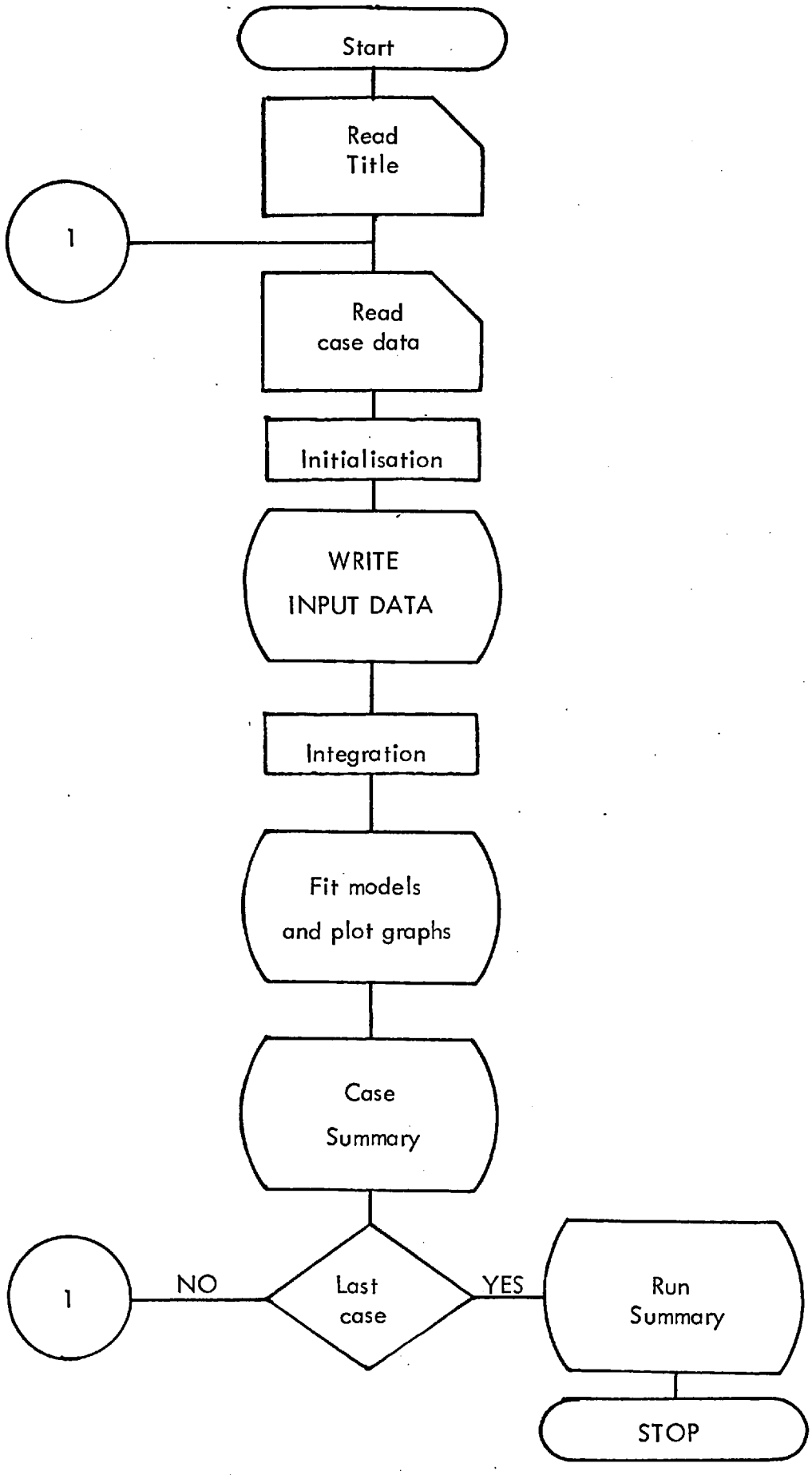

OVERALL DIAGRAM

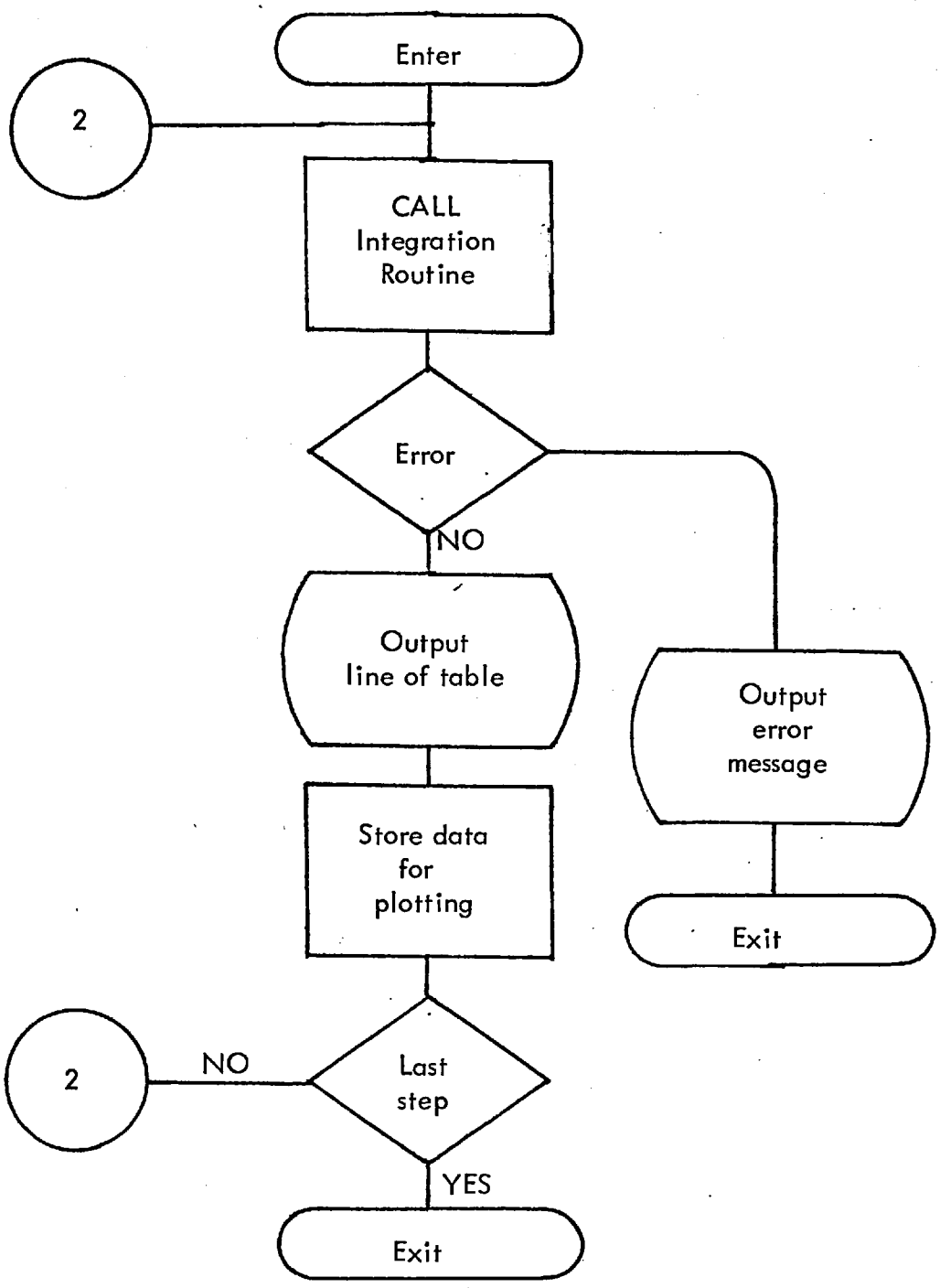

Integration

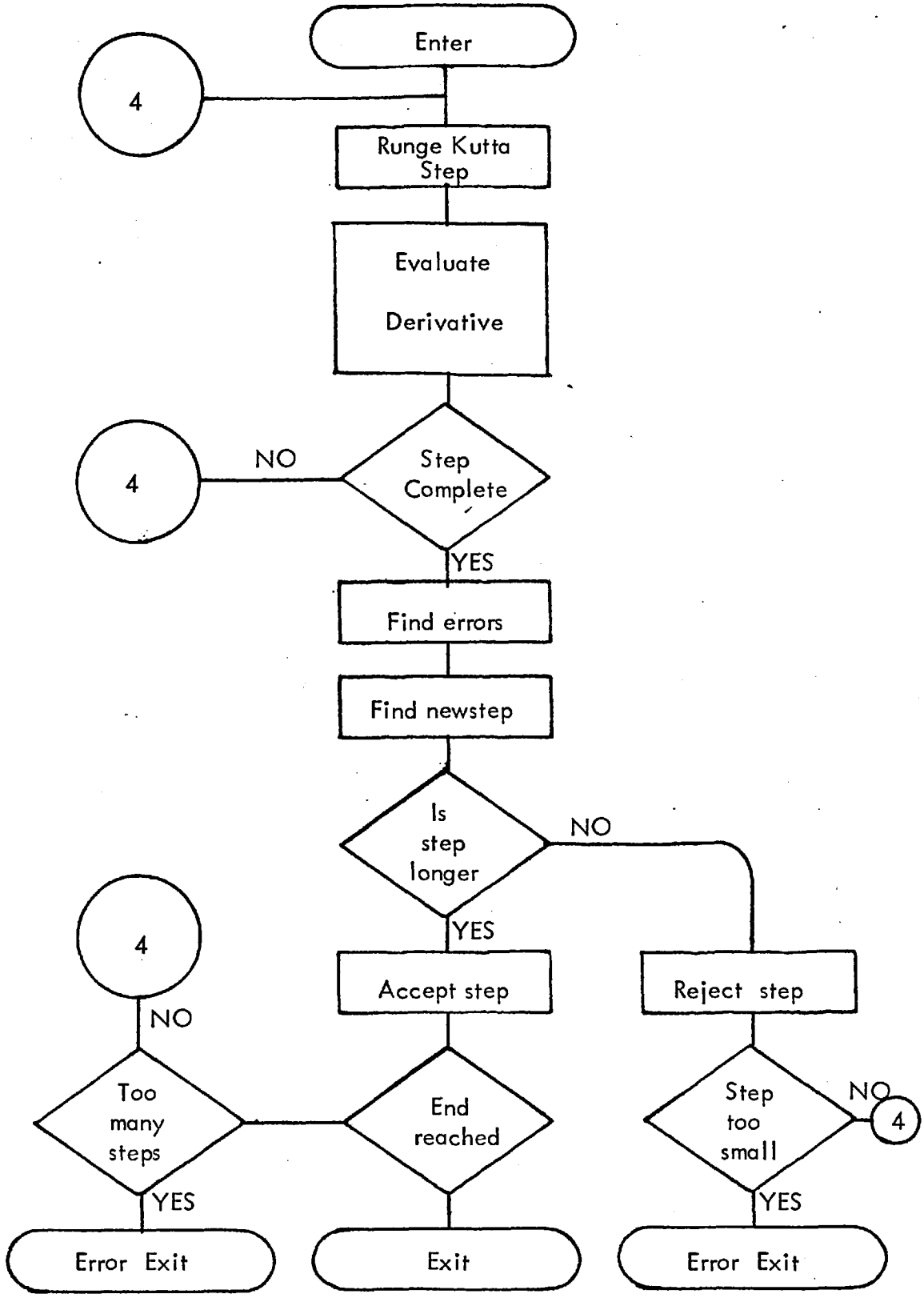

Integration Routine

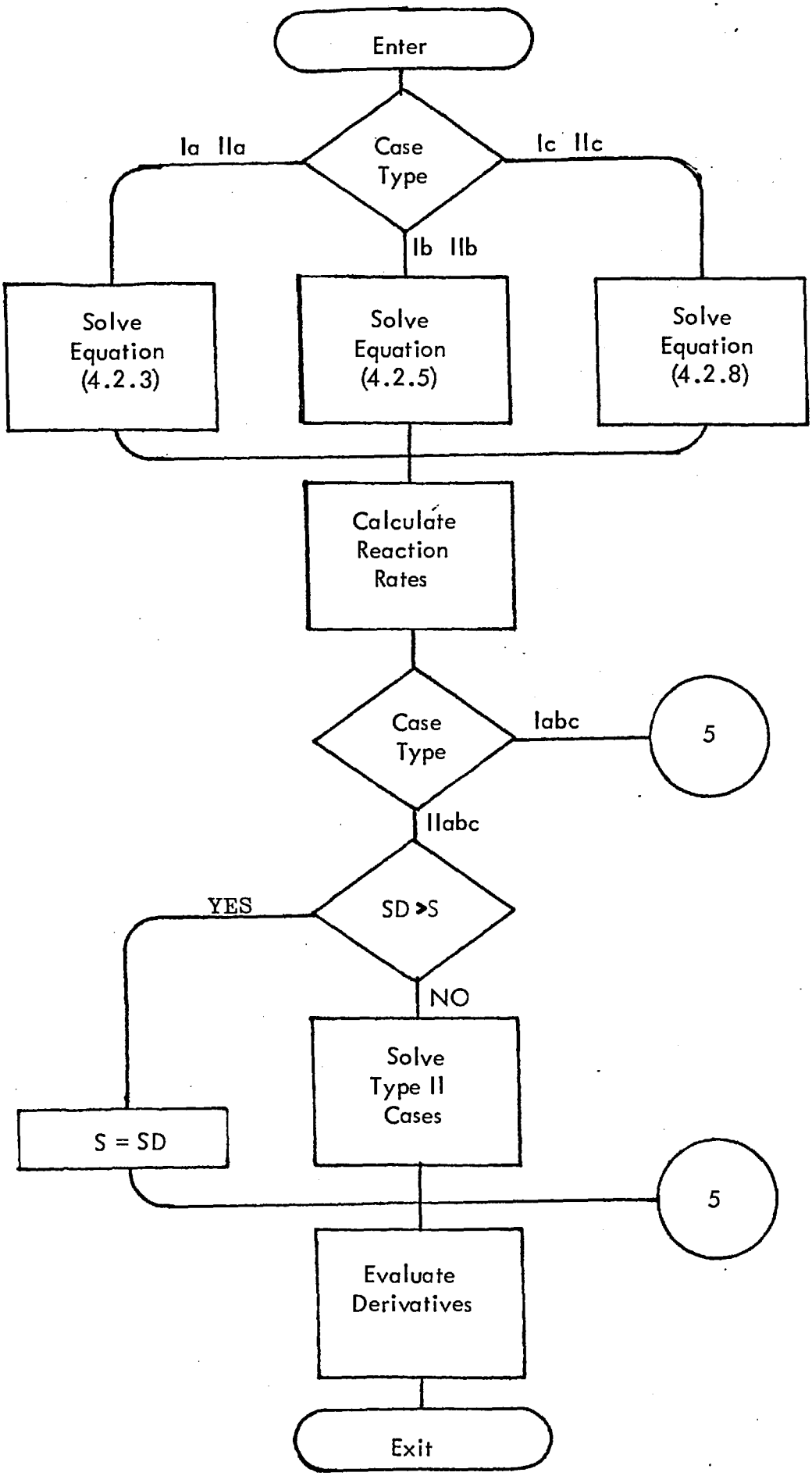

Derivative Evaluation

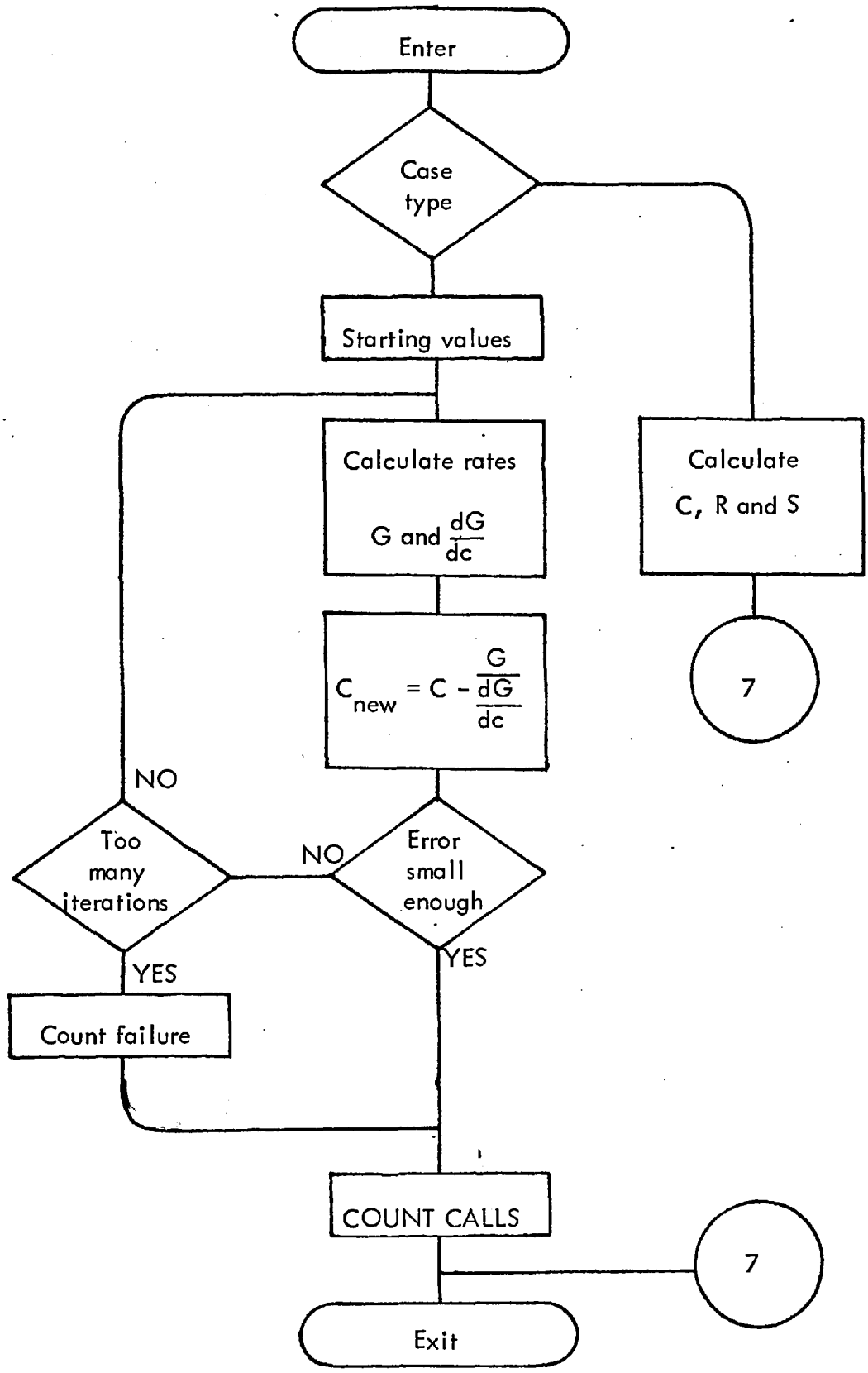

Solution of Type II Cases

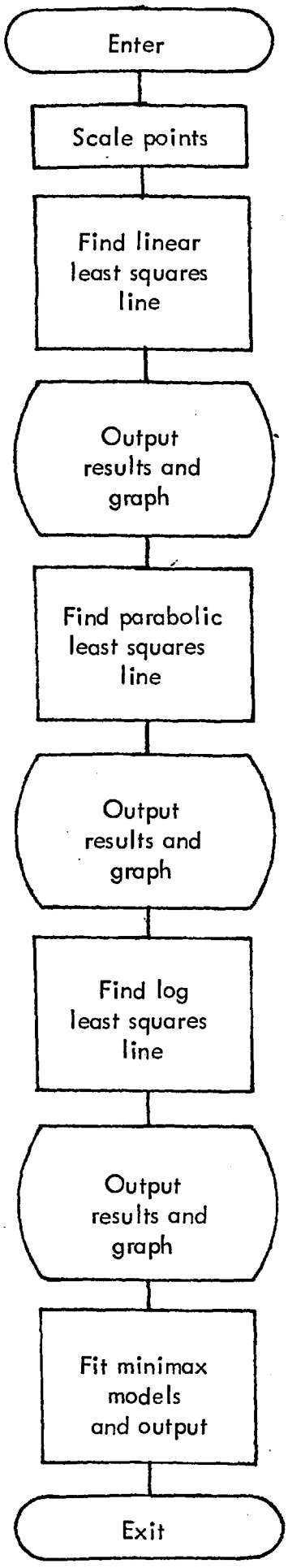

Graph Plot and model fitting

Appendix 3 Manual for Integration Program

This is a C.E.G.B. internal document
reproduced by permission.

CENTRAL ELECTRICITY RESEARCH LABORATORIES

LABORATORY PROGRAM NO. RD/L/P 25/72

(Job No. VF 393)

ORKM - USERS GUIDE TO AN OPTIMIZED RUNGE-KUTTA-MERSON INTEGRATION ROUTINE FOR SYSTEMS OF ORDINARY DIFFERENTIAL EQUATIONS

- by -

J.P. Fletcher* and W.S. Kyte

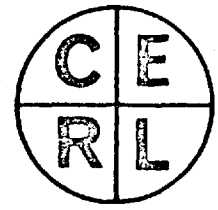

* Dept. of Chem. Engineering,
University of Aston, Birmingham

Approved by:

Head of Division

Date: 22 November 1972

This Document may not be reproduced in whole or in part without the permission of the Director of the Central Electricity Research Laboratories, Leatherhead, Surrey.

SUMMARY

A subroutine ORKM is presented for integrating systems of ordinary differential equations by the Runge-Kutta-Merson method. This routine which uses an improved method of step-length control is suitable for use on both the IBM 1130 and IBM 370. A double precision version DORKM is also available for use on the IBM 370.

2.

CONTENTS

1. BRIEF DESCRIPTION OF SCOPE OF PROGRAM

2. DETAILED PROBLEM DESCRIPTION

- 2.1 Description
- 2.2 Major Assumptions and Limitations
- 2.3 Equations Solved
- 2.4 Notation
- 2.5 References in Application Area

3. PROGRAM DETAILS

- 3.1 Restrictions on Problem Size
- 3.2 Data Preparation
- 3.3 Description of Output
  - 3.3.1 Output
  - 3.3.2 Accuracy of results
- 3.4 Computer Time Required
- 3.5 References to Related Programs

4. PRODUCTION/OPERATING INSTRUCTIONS

- 4.1 Data Assembly
- 4.2 Job Control Statements
- 4.3 Job Sheet Details
- 4.4 Error Messages and Common Faults

APPENDIX I ADMINISTRATIVE DETAILS

APPENDIX II SAMPLE DATA AND SAMPLE OUTPUT

APPENDIX III MATHEMATICAL ANALYSIS

APPENDIX IV PROGRAMMING DETAILS

1. BRIEF DESCRIPTION OF SCOPE OF PROGRAM

The Runge-Kutta method for the integration of ordinary differential equations is often the most convenient to use, as it is self-starting, has good stability and high-order accuracy. Moreover the method is readily extended to systems of first order equations and thus equations of higher order may be integrated.

As is the case for other methods, its efficiency and accuracy are critically dependent on the choice of step-length and various methods of selection of the step-length have been described (Lapidus, 1962; Christiansen, 1970). The usual procedure used is to halve the step-length when the error falls below some lower bound and double the step-length when the error exceeds an upper bound. This procedure generally results in the step-length being on average a factor $\sqrt{2}$ from its optimum value.

The C.E.G.B. library subroutines RUNKUS and RUNKUD and the IBM Scientific Subroutine Package routines RKGS and DRKGS all use this method of monitoring the step-length. Recently, a more sophisticated error monitoring method has been described by Kinsey (1972), which offers at least a thirty per cent improvement on other methods, and also allows some anticipation of step-length changes, with a corresponding reduction in the number of function evaluations. The routine described in this note (ORKM) has been written using this method.

2. DETAILED PROBLEM DESCRIPTION

2.1 Description

The fourth-order Runge-Kutta method due to Merson (Fox, 1962) gives a measure of the local error in a given step and hence allows automatic step-length monitoring to keep the local error at a predetermined level. This method uses five function evaluations; thus for the equation

$$\frac{dy}{dx} = f(x,y)$$

the following evaluations must be made

$$k_1 = h.f(x,y)$$

$$k_2 = h.f\left[x + \frac{h}{3}, y + \frac{k_1}{3}\right]$$

$$k_3 = h.f\left[x + \frac{h}{3}, y + \frac{k_1 + k_2}{6}\right]$$

$$k_4 = h.f\left[x + \frac{h}{2}, y + \frac{k_1 + 3k_3}{8}\right]$$

$$k_5 = h.f\left[x + h, y + \frac{k_1 - 3k_3}{2} + 2k_4\right]$$

4.

Then the new value of y at x + h is given by

$$y_{x+h} = y_x + \frac{1}{6}(k_1 + 4k_4 + k_5)$$

and the estimated local error ε is given by

$$\varepsilon = \frac{1}{30}(2k_1 - 9k_3 + 8k_4 - k_5)$$

Given a preassigned error limit E an automatic step-length adjustment can be made by multiplying h by a factor ω after each step with ω given by

$$\omega = \alpha \left(\frac{E}{\varepsilon}\right)^{1/5}$$

where $0 \leq \alpha \leq 1$.

Then ω is tested and the step is repeated if $\omega < \alpha$. Using this procedure the optimum step-length is rapidly reached whatever its initial (non-zero) value is.

The method is readily applicable to systems of first order differential equations and thus to higher order equations since any n-order ordinary differential equation can be expressed as n simultaneous first order equations.

Thus, the second order equation

$$y'' = f(x,y,y')$$

may be replaced by

$$y' = p$$

$$p' = f(x,y,p)$$

2.2 Major Assumptions and Limitations

Not applicable.

2.3 Equations Solved

See Section 2.1.

2.4 Notation

E - error limit

h - step-length

x - independent variable

y - dependent variable

α - error bias

ϵ - local step error

ω - step-length adjustment factor

2.5 References in Application Area

Christiansen, J., 1970, Num. Math. 14, 317

Fox, L., 1962, "Numerical Solution of Ordinary and Partial Differential Equations", Pergamon Press (Oxford)

Kinsey, D.V., 1972, Dragon Project Technical Note DPTN/270

Lapidus, L., 1962, "Digital Computation for Chemical Engineers", McGraw-Hill (NY)

3. PROGRAM DETAILS

3.1 Restrictions on Problem Size

There is no limit on the number of simultaneous first order ordinary differential equations to be evaluated. Since equations of higher order can be reduced to simultaneous first order equations there is also no limit on the order of the equations.

3.2 Data Preparation

Before using ORKM the differential equations must be put into the form

$$\frac{dy_i}{dx} = f_i\ (y_1, y_2 \ \ldots\ y_n, x) \quad \text{for } i = 1, \ \ldots\ n$$

These equations are then set up in the calling program and in an user-supplied subroutine DYBDX. The CALL statement for the integration routine is of the form:-

```
CALL ŌRKM (Y,ŌY,A,B,C,D,E,N,XS,XF,DX,DXAV,NMAX,CRIT,LERR,NERR,DYBDX,
          TEST,K,NS,NR)
```

where

Y(N) - R*4 Vector of dependent variables - contains the updated values on return to the calling program.

ŌY(N) - R*4 Work space for Y vector containing the values of Y for the last successful step taken.

A(N), B(N), C(N), D(N), E(N) - R*4 Work space arrays which must be reserved by the user.

N - I*4 Number of first order differential equations.

6.

XS - R*4 Starting value of independent variable - unchanged on return.

XF - R*4 Desired finishing value of independent variable - on return it contains the final value of the independent variable actually reached. XF may be greater or less than XS.

DX - R*4 Estimated step length - on return it contains the optimum step length of the last full step taken. The correct sign will be automatically given to DX by the routine. If DX is set to zero then ORKM puts DX = (XF-XS)/NMAX.

DXAV -R*4 On return contains the average step size, or zero if no steps were made successfully.

NMAX - I*4 Limit for the number of integration steps.

CRIT - R*4 Criterion for local error - this is satisfied by the maximum error in the Y vector for all successful steps.

LERR - I*4 Type of error criterion to be considered

-1 errors are not considered and constant DX (as specified) is used

0 for relative errors

1 for absolute errors

NERR - I*4 On entry any non-zero value will suppress the printing of error messages

On return contains indication of error and user conditions detected

<0 Error detected and integration terminated

-1 DX has been reduced by a factor of 10^{-6}

-2 NMAX has been exceeded

-3 No successful steps were taken

0 No error or user-set conditions detected

>0 User condition set by user's subroutine TEST detected and integration terminated

DYBDX - Name of user supplied subroutine to calculate right-hand sides of differential equations. DYBDX must be specified in an EXTERNAL statement in the calling program.

TEST - User supplied subroutine to test values of variables. TEST must be specified in an EXTERNAL statement.

K - I*4 Data set reference number of error messages ($1 \leq K \leq 99$). If a value of K other than 6 is used a DD card will be required for data set K on the IBM 370. On the IBM 1130 K should normally be set to 5.

NS - I*4 Number of successful steps

NR - I*4 Number of repeated steps

A double-precision version (DORKM) of this routine exists which has an identical calling sequence, though all the REAL variables must now be made R*8 in the calling program. This double-precision version is not compatible with the IBM 1130. For greater precision with the 1130 ORKM should be used with the EXTENDED PRECISION facility.

The facility for using an error criterion based on relative error should be used with caution if the dependent variable is likely to become zero, in which case use could be made of the TEST facility and ORKM re-entered using absolute errors until the dependent variable had passed through zero. Care must also be exercised in setting the error criterion CRIT as the use of too tight an error criterion will lead to a large number of integration steps or even to an infinite number of steps when CRIT is less than the machine round-off error. If a low error criterion is required then it is recommended that the double-precision version DORKM be used.

If the routine is re-entered to continue the integration then only XS, XF and NERR need to be reset.

Two user subroutines must be supplied by the user and must be of the following form:

```
      SUBROUTINE DYBDX (Y, F, N, X)
     [IMPLICIT REAL*8 (A-H, O-Z)]
      DIMENSION Y(1), F(1)

      SUBROUTINE TEST (Y, OY, N, X, DX, NERR, K)
     [IMPLICIT REAL*8 (A-H, O-Z)]
      DIMENSION Y(1), OY(1)
```

where:

Y vector of values of dependent variables at the current value of the independent variable X

$\bar{O}Y$ vector of values of dependent variables at the previous value of the independent variable (X-DX)

F vector of right-hand sides of differential equations to be calculated by DYBDX from the current values of Y and X

N number of first order differential equations to be integrated

X current value of the independent variable

DX last value of steplength used

NERR zero on entry - may be set to any positive integer by TEST.

8.

A non-zero value of NERR will cause ORKM to return control to the calling program

K Data set reference number for any output required in TEST. This will be the same number as set in the call to ORKM. The standard output data set may also be used.

The subroutine TEST allows the user to monitor the course of the integration and to modify or stop the integration by using the parameter NERR and the facility to re-enter ORKM. Even if the facility is not required a dummy subroutine must be provided to return control to ORKM.

The routines (D)ORKM call subroutines (D)RKM for each integration step, thus the user can obtain single step integration by calling RKM directly. This routine has the following calling statement:

```
CALL RKM  (Y,A,B,C,D,E,N,X,DX,DYBDX)
```

and on return Y(N) will contain the new values at X (which has been updated) and E(N) will contain the absolute error estimates. A user subroutine DYBDX must be supplied to calculate the derivatives.

3.3 Description of Output

3.3.1 Output

ORKM produces no output except for error messages which are specified in Section 4.4. These messages may be suppressed by giving NERR a non-zero value on entry to the routine.

3.3.2 Accuracy of results

The specified criterion (CRIT) for local error is met for all successful steps. This criterion is applied to the maximum estimated error in the dependent variable vector Y at each step.

3.4 Computer Time Required

The computer time required is directly proportional to the number of equations being integrated and the total number of steps taken. Hence the time required is influenced by the error criterion set. However, due to the optimization of the step-length the amount of computer time used is minimized.

3.5 References to Related Programs

Not applicable.

4. PRODUCTION/OPERATING INSTRUCTIONS

4.1 Data Assembly

Data would normally be assembled in the correct form by the calling program as described in Section 3.2.

4.2 Job Control Statements

ORKM and DORKM are contained within a CERL private library. Therefore the following additional JCL is required:-

```
/*SETUP UNIT=3330,ID=AC
//          DD UNIT=3330,DISP=SHR,VOL=SER=AC,DSN=L2.CERL.LIB23
//G.FTOkF001 DD UNIT=(CTC,,DEFER),LABEL=(,NL),
//          DCB=(RECFM=VBA,LRECL=137,BLKSIZE=911)
```

The second JCL statement must be concatenated with the //L.SYSLIB DD card. The third JCL statement must be included unless K=6 when it may be omitted.

Potential users of any data set referred to in this note should check with the Disk Controller that the data set is held on the volume stated. If necessary the appropriate manager (as indicated by the section letter) should be consulted.

ORKM is also stored on the stand-alone disk (2003) on the C.E.R.L. 1130. Potential users from other departments should contact the C.E.R.L. Computing Liaison Officer.

4.3 Job Sheet Details

These will, in general, be determined by the calling program.

4.4 Error Messages and Common Faults

If on entry to the routine NERR is set to zero the following error messages are produced. The value of NERR returned to the calling program is given after the message. These values are returned whatever the value of NERR on entry and enable the user to take his own corrective actions.

(i) MAXIMUM NUMBER OF STEPS (NMAX) HAS BEEN SET TO 100 BY (D)ORKM (NERR=0)

Explanation NMAX on entry was < 1. The routine sets NMAX to 100 and execution continues normally.

Action Re-set NMAX to maximum number of steps required.

(ii) (D)ORKM INITIAL STEP LENGTH HAS BEEN REDUCED BY A FACTOR OF 1.0E-6 (NERR= -1)

Explanation During the course of integration the step-length has been reduced by a factor of 10^{-6} from the original DX set on entry.

Action Examine the differential equations to determine whether a singularity exists within the range of integration. If a relative error criterion is being used, near-zero values of the independent variable may cause excessively small steps to be taken. In this case absolute errors should be

10.

used. Also the error criterion being used may be too stringent. Otherwise, restart the integration with the last DX generated as input.

(iii) MAXIMUM NUMBER OF STEPS EXCEEDED IN (D)ORKM
(NERR= -2)

Explanation The number of steps taken has exceeded NMAX.

Action Examine the error criterion to see if it is too stringent. This may also be caused by the reasons given in (ii). Otherwise, reduce the range of integration or increase NMAX.

(iv) NO SUCCESSFUL STEPS TAKEN

Explanation As (ii) but occurring on the first step

Action As (ii)

If DX is set to zero on entering the routine, then ORKM estimates DX from

$$DX = (XF - XS)/NMAX$$

If XF = XS then the routine immediately returns control to the calling program. In neither of these cases is a message given to the user.

Appendices 1-1V and Drg. No. RL 4.1.2039 attached.

APPENDIX I

ADMINISTRATIVE DETAILS

Form API	Abstract No.
	Date :

1. DOCUMENTATION

Card Indicr.	PROGRAM TITLE :	PROGRAM NAME
1 4	Optimized Runge-Kutta-Merson Integration Routine for Systems of Ordinary Differential Equations	(D)ORKM

Stage Completed	COMPUTING PLAN PROJECT NAME	WORK CODE	COMPUTING PLAN Year	COMPUTING PLAN Ref.
2	MART012L	754030	72/73	L2

Project Manager :	F.A.J. FORD	Project Leader :	

Date of final Compilation :	Oct. 1972	Language : FIV (1130 version)	Anticipated access to system :	REMOTE XXXXXX
		Compiler Level : H 'OPT=2'		

Library Subroutines used	NONE		

2. PRODUCTION REQUIREMENTS

COMPUTER	NAME AND MODEL NO.	REGION SIZE kbytes	APPROX. PERCENTAGE C.P.U. UTILISATION
	370/165J		

PERIPHERALS	NO. OF TAPE UNITS 9-track	NO. OF TAPE UNITS 7-track	NO. OF TAPES 9-track	NO. OF TAPES 7-track	DISK STORAGE CYLINDERS UTILITY	DISK STORAGE CYLINDERS USER	CALCOMP PLOTTER

REMOTE I/O	CARDS IN x 100	LINES OUT x 1000	PAPER TAPE PERIPHERALS Reader	PAPER TAPE PERIPHERALS Punch

LOCAL I/O	CARDS x 100 IN	CARDS x 100 OUT	NO. OF PARTS	PRINTER OUTPUT % LINES WITH RESTRICTED CHARS.	PRINTER OUTPUT MAX. PRINT LINE LENGTH	PRINTER OUTPUT LINES x 1000

PROGRAM NAME : ORKM

PROJECT LEADER/MANAGER SIGNATURE :	DATE :

3. STANDARD ENDORSEMENT

This program conforms to current Bureau Standards as specified in the Standards Manual and all documentation appropriate to the last stage completed, has been submitted.

PROJECT MANAGER SIGNATURE :	DATE :

NOTE : If program exceeds the limits specified in the Bureau Standards, complete sections 5 and 6. Page 2 is not included in the program write-up.

4. PRELIMINARY PRODUCTION ESTIMATES

ESTIMATED NO OF RUNS PER YEAR :	ESTIMATED AVERAGE COST PER RUN : £	FREQUENCY OF DISK DATA - SET BACK - UP :

A2.

APPENDIX II

SAMPLE DATA AND SAMPLE OUTPUT

ORKM contains no input or output other than error messages.

APPENDIX III

MATHEMATICAL ANALYSIS

(a) Derivation of Equations

The fourth-order Runge-Kutta-Merson integration formula (Fox, 1962) gives a measure of the errors involved in a given step. This method uses five stages - for an equation $\frac{dy}{dx} = f(x,y)$ five function evaluations are made as follows:-

$$k_1 = h.f(x,y)$$

$$k_2 = h.f\left[x + \frac{h}{3}, y + \frac{k_1}{3}\right]$$

$$k_3 = h.f\left[x + \frac{h}{3}, y + \frac{k_1 + k_2}{6}\right]$$

$$k_4 = h.f\left[x + \frac{h}{2}, y + \frac{k_1 + 3k_3}{8}\right]$$

$$k_5 = h.f\left[x + h, y + \frac{k_1 - 3k_3}{2} + 2k_4\right]$$

Then the new value of y at x+h is given by

$$y_{x+h} = y_x + \frac{1}{6}(k_1 + 4k_4 + k_5)$$

and the estimated local error ε is given by

$$\varepsilon = \frac{1}{30}(2k_1 - 9k_3 + 8k_4 - k_5)$$

A considerable improvement in the procedure is achieved by continuous step-length adjustment. In a method due to Kinsey (1972) the step-length is adjusted by multiplying h by a factor ω after each step with ω given by

$$\omega = \alpha \left(\frac{E}{\varepsilon}\right)^{1/5}$$

where $0 < \alpha \leq 1$

A4.

Then ω is tested and the step is repeated if $\omega < \alpha$. The 'bias' α, which is normally chosen to be close to, but less than 1 (ORKM uses 0.99) to avoid oscillations which are possible when $\alpha=1$. It has been found useful to set the limits

$$0.25 \leq \omega \leq 4.0$$

to avoid excessively large changes in h at one step.

In using this procedure the (biased) optimum value of h is rapidly reached whatever its initial (non-zero) value; then as the integration proceeds h is continuously adjusted keeping the error per step almost constant. After the first successful step, too frequent repetitions of steps are avoided by changing the bias α, multiplying α by a factor 0.995 whenever a step has to be repeated.

(b) Programming Philosophy

ORKM has been written using the IBM 1130 FORTRAN IV language so that ORKM can be used on both the 1130 and 370.

(c) Notation

E Error limit

h Step-length

x Independent variable

y Dependent variable

α Error bias

ε Local step error

ω Step-length adjustment factor

(d) References

Fox, L., 1962, 'Numerical Solution of Ordinary and Partial Differential Equations', Pergamon Press (Oxford)

Kinsey, D.V., 1972, Dragon Project Technical Note DPTN/270

APPENDIX IV

PROGRAMMING DETAILS

(a) Names and functions of subroutines

(D)RKM performs Runge-Kutta-Merson numerical integration for one step

DYBDX user supplied subroutine to calculate vector of right-hand sides of the first order differential equations

TEST user supplied subroutine to monitor the course of the integration

(b) Principal variable names

See Section 3.2

(c) Data sets

See Section 3.2

(d) Outline flow diagram

Given on following sheet

(e) Overlay structure

Not applicable

(f) Core storage requirements

ORKM 5K bytes (On 1130 1.5K bytes)

DORKM 5K bytes

(g) Disk storage requirements

ORKM)
) 1 track
DORKM)

(h) Data volumes required

Volume AC is required.

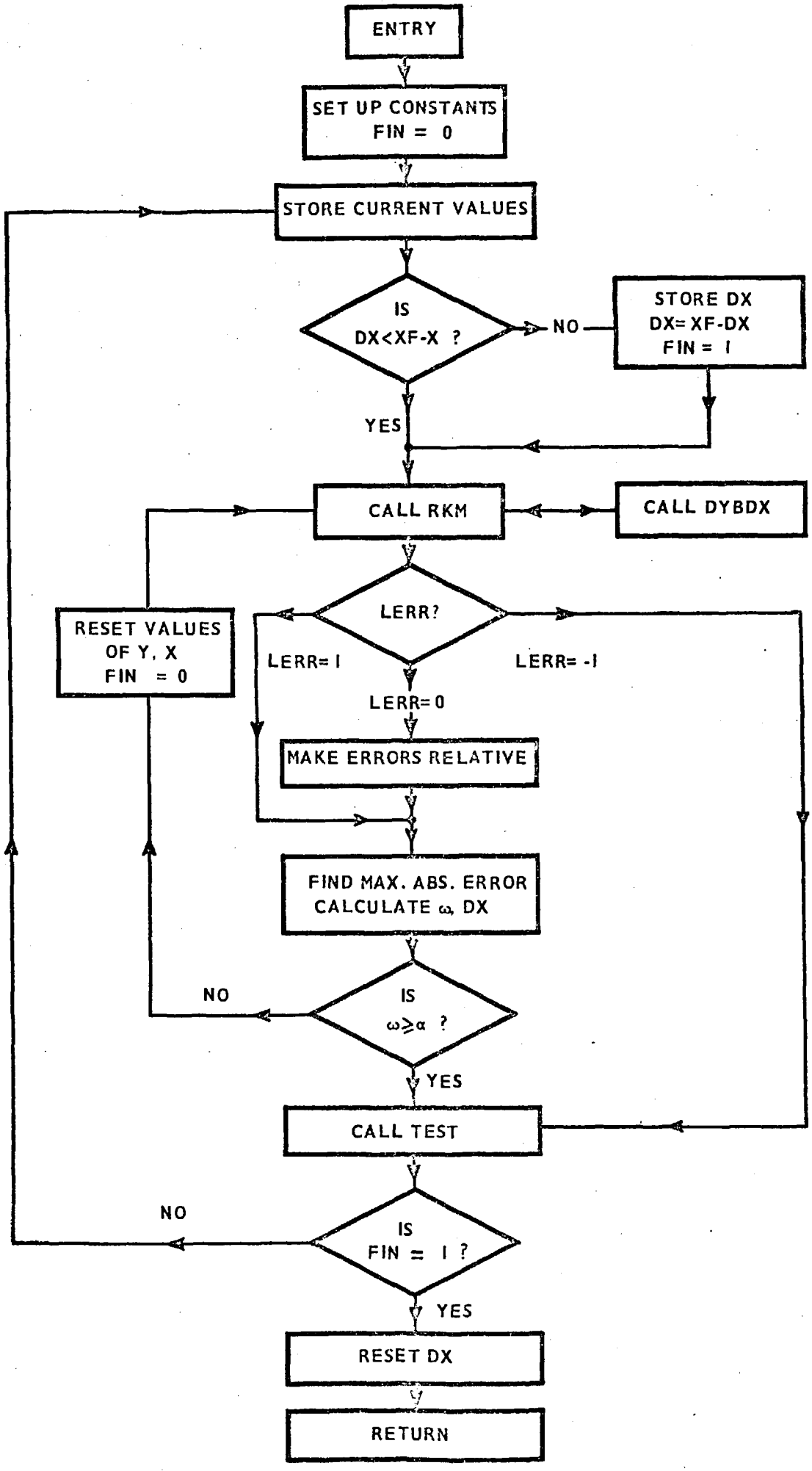

OUTLINE FLOW DIAGRAM

Appendix 4 Specimen Output

ONE POINT MODEL OF PREBREAKAWAY OXIDATION
==========

YW5622JETAPE P=20 MANY VALUES OF CO AND OFE

CASE NO 5

CONSTANTS FOR SIMULATION OF OXIDATION

OXIDE PROPERTIES

VOIDAGE OF OUTER LAYER = 1.000-04
VOIDAGE OF INNER LAYER = 1.000-04

REACTION INFORMATION

TEMPERATURE OF SYSTEM = 427.0 DEG C (700.15 DEG K)
TOTAL PRESSURE = 20.00 ATMOSPHERES
RATE CONSTANT FOR OXIDATION = 1.000-06 MM/S
EFFECTIVE DIFFUSION COEFFICIENT = 1.000-07 MM 2/S
EQUILIBRIUM MOLE FRACTION OF CO = 50.00 PER CENT
EXTERNAL MOLE FRACTION OF CO = 0.62 PER CENT
CRITICAL MOLE FRACTION OF CO = 30.00 PER CENT
TOTAL GAS CONCENTRATION = 3.480-07 GMOL/MM 3

INTEGRATION DATA

TOTAL TIME = 5.000 02 HRS (SECS IF STATED BELOW)
INITIAL TIME STEP = 1.440 03 SECS, MAXIMUM NUMBER OF STEPS PER PRINT INTERVAL = 100
NUMBER OF PRINT INTERVALS = 50

*** IRON DIFFUSION COEFFICIENT IS 1.000-11 MM 2/S, WITH CONCENTRATION FUNCTION (CO2/CO)** 0.333

OXIDE CONCENTRATION OF IRON 6.710-05 GATOM/MM 3, NUMBER FOR FE FLUX 8.520-09 GATOM/MM

AND RELATIVE CONVERGENCE TEST (IF NEEDED) OF 1.000-04

*** SECOND ORDER RATE CONSTANT FOR CARBON DEPOSITION = 1.000 01 MM 4/GMOL S

***** 4 EQUATIONS USED IN THIS RUN

TIME	CO	CARBON	WEIGHT GAIN AND RATE			OXIDE DEPTH AND RATE		REACTION 1	R3/R1	X1/X2	STEPS	
HRS	PRCNT	G/MM 2	G/MM 2	G/MM 2 S		MM	MM/S	MM/S				
0.0	0.62	0.0	0.0			1.000D-05						
10.00	4.20	5.094D-10	2.795D-06	4.246D-11		1.943D-03	2.966D-08	4.580D-07	1.339D-02	6.439	36	10
20.00	5.66	1.814D-09	4.102D-06	3.192D-11		2.976D-03	2.231D-08	4.434D-07	2.516D-02	4.558	3	0
30.00	6.76	3.852D-09	5.157D-06	2.720D-11		3.614D-03	1.902D-08	4.324D-07	3.679D-02	3.726	2	0
40.00	7.67	6.588D-09	6.082D-06	2.436D-11		4.260D-03	1.704D-08	4.233D-07	4.831D-02	3.231	1	0

130.0	9.82	4.970D-08	1.202D-05	1.411D-11	9.419D-03	9.876D-09	2.807D-07	1.158D-01	1.910	1 0
140.0	9.76	5.473D-08	1.252D-05	1.354D-11	8.767D-03	9.473D-09	2.776D-07	1.199D-01	1.868	1 0
150.0	9.74	5.971D-08	1.300D-05	1.303D-11	9.192D-03	9.123D-09	2.669D-07	1.238D-01	1.831	1 0
160.0	9.71	6.466D-08	1.346D-05	1.258D-11	8.424D-03	8.805D-09	2.573D-07	1.275D-01	1.799	1 0
170.0	9.67	6.958D-08	1.390D-05	1.217D-11	8.736D-03	8.517D-09	2.487D-07	1.310D-01	1.771	1 0
180.0	9.64	7.446D-08	1.433D-05	1.180D-11	1.004D-02	8.256D-09	2.408D-07	1.344D-01	1.746	1 0
190.0	9.61	7.931D-08	1.475D-05	1.146D-11	1.033D-02	8.017D-09	2.336D-07	1.377D-01	1.724	1 0
200.0	9.58	8.414D-08	1.516D-05	1.115D-11	1.062D-02	7.797D-09	2.270D-07	1.409D-01	1.703	1 0

TIME	CO	CARBON	WEIGHT GAIN AND RATE		OXIDE DEPTH AND RATE		REACTION 1	R3/R1	X1/X2	STEPS
210.0	9.56	8.893D-08	1.556D-05	1.086D-11	1.089D-02	7.594D-09	2.209D-07	1.439D-01	1.685	1 0
220.0	9.53	9.370D-08	1.594D-05	1.059D-11	1.116D-02	7.406D-09	2.152D-07	1.469D-01	1.668	1 0
230.0	9.50	9.844D-08	1.632D-05	1.035D-11	1.143D-02	7.231D-09	2.100D-07	1.497D-01	1.652	1 0
240.0	9.48	1.032D-07	1.669D-05	1.011D-11	1.168D-02	7.068D-09	2.051D-07	1.525D-01	1.638	1 0
250.0	9.45	1.078D-07	1.705D-05	9.897D-12	1.193D-02	6.915D-09	2.005D-07	1.552D-01	1.625	1 0
260.0	9.43	1.125D-07	1.740D-05	9.693D-12	1.218D-02	6.772D-09	1.962D-07	1.578D-01	1.612	1 0
270.0	9.41	1.172D-07	1.774D-05	9.503D-12	1.242D-02	6.637D-09	1.922D-07	1.603D-01	1.601	1 0
280.0	9.39	1.218D-07	1.808D-05	9.321D-12	1.266D-02	6.509D-09	1.884D-07	1.628D-01	1.590	1 0
290.0	9.36	1.264D-07	1.842D-05	9.150D-12	1.289D-02	6.389D-09	1.848D-07	1.652D-01	1.580	1 0
300.0	9.34	1.310D-07	1.874D-05	8.988D-12	1.312D-02	6.275D-09	1.813D-07	1.676D-01	1.571	1 0
310.0	9.32	1.355D-07	1.906D-05	8.835D-12	1.334D-02	6.167D-09	1.781D-07	1.699D-01	1.562	1 0
320.0	9.30	1.401D-07	1.938D-05	8.689D-12	1.356D-02	6.064D-09	1.750D-07	1.721D-01	1.553	1 0
330.0	9.28	1.446D-07	1.969D-05	8.550D-12	1.378D-02	5.966D-09	1.721D-07	1.743D-01	1.545	1 0
340.0	9.27	1.491D-07	1.999D-05	8.417D-12	1.399D-02	5.873D-09	1.693D-07	1.765D-01	1.538	1 0
350.0	9.25	1.536D-07	2.029D-05	8.290D-12	1.420D-02	5.783D-09	1.666D-07	1.786D-01	1.530	1 0
360.0	9.23	1.580D-07	2.059D-05	8.169D-12	1.441D-02	5.698D-09	1.641D-07	1.807D-01	1.524	1 0
370.0	9.21	1.625D-07	2.088D-05	8.053D-12	1.461D-02	5.617D-09	1.617D-07	1.827D-01	1.517	1 0
380.0	9.19	1.669D-07	2.117D-05	7.942D-12	1.481D-02	5.538D-09	1.593D-07	1.847D-01	1.511	1 0
390.0	9.18	1.713D-07	2.145D-05	7.835D-12	1.501D-02	5.463D-09	1.571D-07	1.866D-01	1.505	1 0
400.0	9.16	1.758D-07	2.173D-05	7.733D-12	1.521D-02	5.390D-09	1.549D-07	1.885D-01	1.499	1 0

TIME	CO	CARBON	WEIGHT GAIN AND RATE		OXIDE DEPTH AND RATE		REACTION 1	R3/R1	X1/X2	STEPS
410.0	9.14	1.801D-07	2.201D-05	7.634D-12	1.540D-02	5.321D-09	1.528D-07	1.904D-01	1.494	1 0
420.0	9.13	1.845D-07	2.229D-05	7.539D-12	1.559D-02	5.254D-09	1.508D-07	1.923D-01	1.489	1 0
430.0	9.11	1.889D-07	2.256D-05	7.447D-12	1.578D-02	5.189D-09	1.489D-07	1.941D-01	1.484	1 0
440.0	9.10	1.932D-07	2.282D-05	7.359D-12	1.596D-02	5.127D-09	1.471D-07	1.959D-01	1.479	1 0
450.0	9.08	1.976D-07	2.308D-05	7.274D-12	1.615D-02	5.067D-09	1.453D-07	1.976D-01	1.474	1 0
460.0	9.07	2.018D-07	2.334D-05	7.191D-12	1.633D-02	5.009D-09	1.436D-07	1.993D-01	1.470	1 0
470.0	9.05	2.061D-07	2.360D-05	7.112D-12	1.651D-02	4.953D-09	1.419D-07	2.010D-01	1.465	1 0
480.0	9.04	2.104D-07	2.386D-05	7.034D-12	1.669D-02	4.898D-09	1.403D-07	2.027D-01	1.461	1 0
490.0	9.02	2.147D-07	2.411D-05	6.960D-12	1.686D-02	4.846D-09	1.387D-07	2.044D-01	1.457	1 0
500.0	9.01	2.189D-07	2.436D-05	6.887D-12	1.703D-02	4.795D-09	1.372D-07	2.060D-01	1.453	1 0

TIME	CO	CARBON	WEIGHT GAIN AND RATE		OXIDE DEPTH AND RATE		REACTION 1	R3/R1	X1/X2	STEPS
HRS	PRCNT	G/MM 2	G/MM 2	G/MM 2 S	MM	MM/S	MM/S			

***** CRITICAL CO LEVEL NEVER ATTAINED *****

CASE NO 5

*** NUMBER OF ITERATIVE CALLS TO DY80X = 268, AVERAGE NUMBER OF ITERATIONS = 1.9 AND CONVERGENCE FAILED 0 TIMES

GRAPH OF PREBREAKAWAY OXIDATION SIMULATION FROM 0.0 TO 500.00 HRS (FOR PARAMETERS SEE TABLE ABOVE)

CASE NO 5

SCALE FACTORS FOR THE GRAPHS ARE –

SYMBOL	NAME	FACTOR	UNITS
*	CO (AT INSIDE)	0.250 *10** -1	MOLE FRACTION
+	WEIGHT GAIN	0.500 *10** -5	GM / MM 2
0	OXIDE THICKNESS	0.250 *10** -2	MM
X	WT GAIN SQUARED	1.000 *10**-10	GM 2 / MM 4

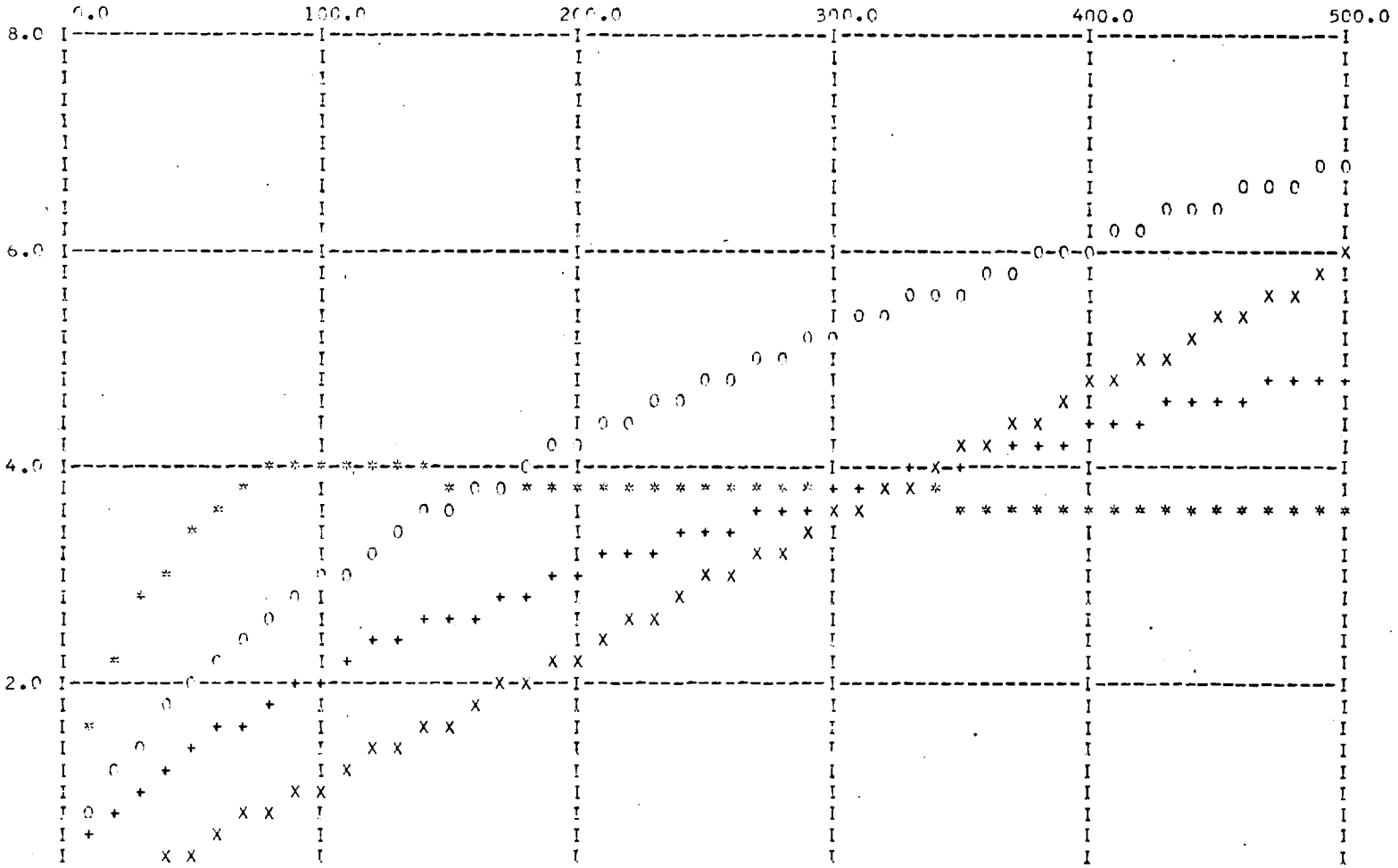

PARABOLIC RATE CONSTANT FROM WEIGHT VS T/W PLOT

CASE NO 5

PARABOLIC RATE CONSTANT = 3.6130D-16 G 2/MM 4 S (1.2996D-02 MG 2/CM 4 HR)
CORRELATION COEFFICIENT = 0.9997 DURBIN-W 0.2099
COORDINATES OF PARABOLA ORIGIN ARE 1.C702D-06 G/MM 2, AND 8.8127D-01 HRS

THE SCALE FACTORS ARE - WEIGHT GAIN 10** -5 G/MM 2
TIME/WEIGHT 10** 10 MM 2 S/G

DATA POINTS ARE '+', REGRESSION LINE '*',' MEAN POINT 'O'

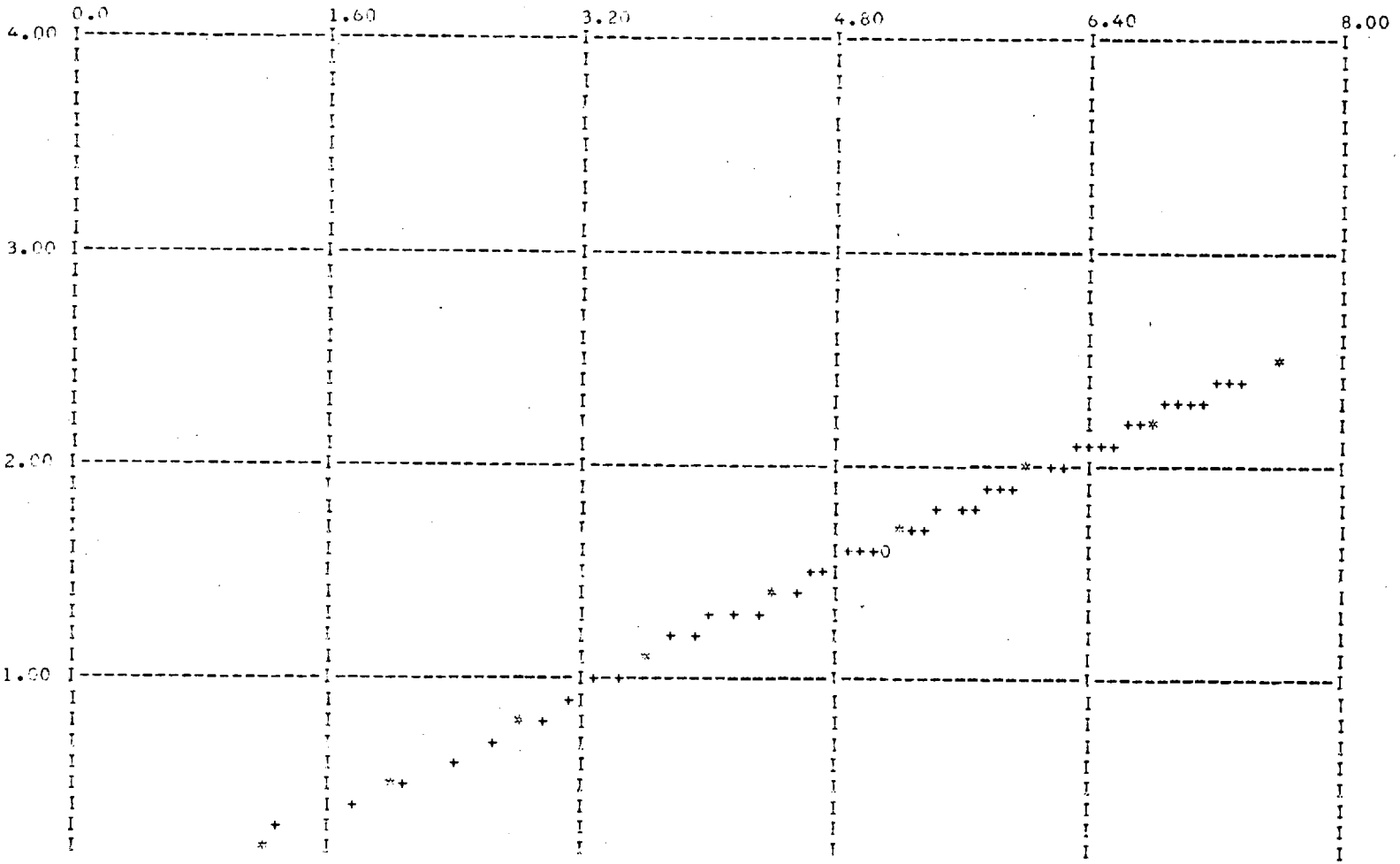

GENERALISED ORDER FROM PLOT OF LOG10(W) AGAINST LOG10(T)

LINEAR REGRESSION TO FIND K AND N IN W = K * T ** N

CASE NO 5

N = 0.5509, AND K = 8.8755D-09 (LOG10(K) = -8.0518)

CORRELATION COEFFICIENT = 0.9997 AND DURBIN-WATSON NO 0.0343

DATA POINTS ARE '+', REGRESSION LINE '*',' MEAN POINT 'O'

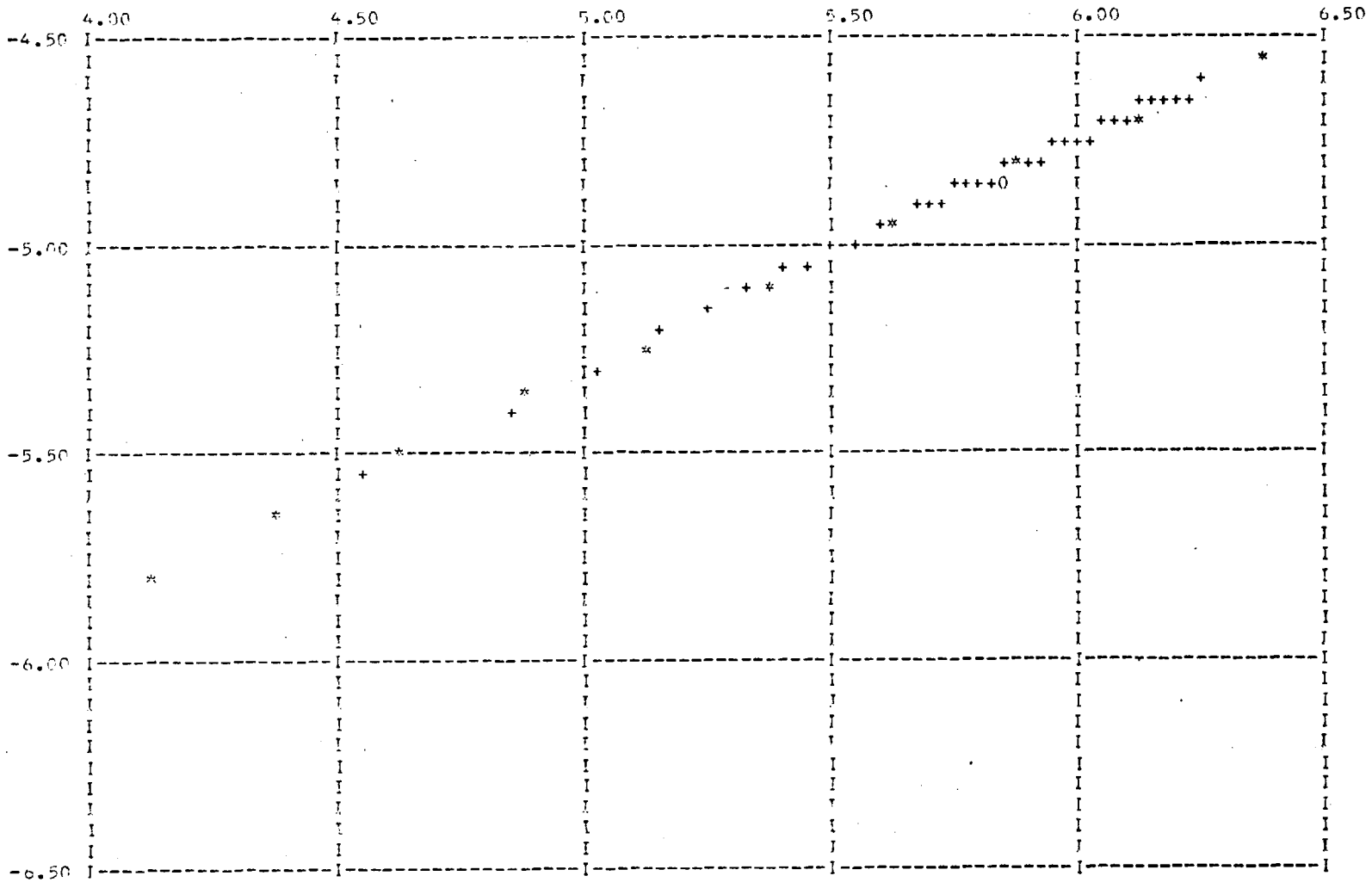

MINIMAX POLYNOMIAL ANALYSIS OF WEIGHT GAIN DATA
==========

A POLYNOMIAL IN w (NORMALISED) IS FITTED TO THE TIME (ALSO NORMALISED)
THIS IS USED TO CALCULATE OXIDATION RATE CONSTANTS

CASE NO 5

POLYNOMIAL OF ORDER 1 FITTED
==========

DELTA = 9.23911270-02

CHEBYCHEV POLYNOMIAL $P_M^*(X)=A_M X^M+\ldots+A_0$

P	A_P
0	-1.99429947D-01
1	1.10703872D 00

LINEAR RATE ESTIMATE
==========

LINEAR RATE CONSTANT 1.2223D-11 GM/MM 2 S, WEIGHT AT ZERO TIME 4.3879D-06 G/MM 2

MAXIMUM ERROR 2.0328D-06 G/MM 2

POLYNOMIAL OF ORDER 2 FITTED
==========

DELTA = -3.31323820-03

CHEBYCHEV POLYNOMIAL $P_M^*(X)=A_M X^M+\ldots+A_0$

P	A_P
0	3.8640844450-03
1	5.2752328340-02
2	9.3706974850-01

PARABOLIC RATE ESTIMATE
==========

PARABOLIC RATE CONSTANT 3.5438D-16 G 2/MM 4 S (1.2758D-02 MG 2/CM 4 HR)

COORDINATES OF PARABOLA ORIGIN ARE 8.2170D-07 G/MM 2 AND -1.2398D-05 HRS

MINIMAX POLYNOMIAL ANALYSIS OF WEIGHT GAIN DATA
==========

A FUNCTION OF T (NORMALISED) IS FITTED TO w (NORMALISED)
THIS IS USED TO CALCULATE OXIDATION RATE CONSTANTS

CASE NO 5

POLYNOMIAL OF ORDER 1 FITTED
==========

DELTA = -8.3457901D-02

CHEBYCHEV POLYNOMIAL $P_M^*(X) = A_M X^M + \ldots + A_0$

P	A_P
0	1.6014712910-01
1	9.0231077150-01

LINEAR RATE ESTIMATE FROM w = A + B * T
==========

LINEAR RATE CONSTANT 1.2223D-11 GM/MM 2 S, WEIGHT AT ZERO TIME 4.3879D-06 G/MM 2

MAXIMUM ERROR -2.0329D-06 G/MM 2

POLYNOMIAL OF ORDER 1 FITTED
==========

DELTA = 5.6821C28D-03

CHEBYCHEV POLYNOMIAL $P_M^*(X) = A_M X^M + \ldots + A_0$

P	A_P
0	-3.7193675510-02
1	1.0342654080 00

PARABOLIC RATE ESTIMATE FROM w = A + B * (T**1/2)
==========

PARABOLIC RATE CONSTANT 3.5257D-16 G 2/MM 4 S (1.2593D-02 MG 2/CM 4 HR)

MAXIMUM ERROR 1.3840D-07 G/MM 2, AND MISMATCH AT THE ORIGIN IS -9.0590D-07 G/MM 2

YQ5A22JF
========

CASE 5

TAPE P=20 MANY VALUES OF CO AND DEP

TOTAL TIME	500.0 HRS
WEIGHT GAIN	2.4360-05 G/MM 2
EXTERNAL CO	0.62 PER CENT
PRESSURE	20.00 ATMOSPHERES
FINAL CO	9.01 PER CENT
CARBON DEPOSIT	1.06 PER CENT

RATE CONSTANTS
==============

	MINIMAX	LEAST-SQ
LINEAR	+	
G/MM2 S	1.2220-11	1.1040-11
PARABOLIC	+	
G2 /MM4 S	3.5440-16	3.6140-16
(MG2/CM4)2	1.2760-02	1.3040-02)

AGREEMENT 10% + , 1% ++ , 0.1% +++

TAPE RECORD 5 WRITTEN FOR CASE NO 5

SUMMARY TABLE OF CASES RUN YQ5622JF TAPE P=20 MANY VALUES OF CC AND DFE
========== ********

ITEM	PRES	CRTCON	RATE CONST	D EFF	C EXT	TIME	MOL FRAC	WEIGHT	OXIDE	PARA CONS	CASE
1	20.	1.00E 01	1.00E-06	1.00E-07	6.25E-03	5.000E 02	6.259E-03	2.340E-07	1.743E-04	1.218E-06	1
2	20.	1.00E 01	1.00E-06	1.00E-07	6.25E-03	5.000E 02	6.350E-03	7.733E-07	5.510E-04	1.236E-05	2
3	20.	1.00E 01	1.00E-06	1.00E-07	6.25E-03	5.000E 02	7.270E-03	2.479E-06	1.742E-03	1.242E-04	3
4	20.	1.00E 01	1.00E-06	1.00E-07	6.25E-03	5.000E 02	1.638E-02	7.862E-06	5.497E-03	1.242E-03	4
5	20.	1.00E 01	1.00E-06	1.00E-07	6.25E-03	5.000E 02	9.009E-02	2.436E-05	1.703E-02	1.276E-02	5
6	20.	1.00E 01	1.00E-06	1.00E-07	6.25E-03	5.000E 02	2.537E-01	6.542E-05	4.609E-02	1.007E-01	6
7	20.	1.00E 01	1.00E-06	1.00E-07	1.25E-02	5.000E 02	1.250E-02	1.951E-07	1.500E-04	8.336E-07	7
8	20.	1.00E 01	1.00E-06	1.00E-07	1.25E-02	5.000E 02	1.257E-02	6.605E-07	4.749E-04	8.978E-06	8
9	20.	1.00E 01	1.00E-06	1.00E-07	1.25E-02	5.000E 02	1.323E-02	2.132E-06	1.503E-03	9.175E-05	9
10	20.	1.00E 01	1.00E-06	1.00E-07	1.25E-02	5.000E 02	1.993E-02	6.778E-06	4.745E-03	9.220E-04	10
11	20.	1.00E 01	1.00E-06	1.00E-07	1.25E-02	5.000E 02	7.710E-02	2.114E-05	1.477E-02	9.382E-03	11
12	20.	1.00E 01	1.00E-06	1.00E-07	1.25E-02	5.000E 02	2.482E-01	5.780E-05	4.074E-02	8.074E-02	12
13	20.	1.00E 01	1.00E-06	1.00E-07	2.50E-02	5.000E 02	2.499E-02	1.415E-07	1.342E-04	3.633E-07	13
14	20.	1.00E 01	1.00E-06	1.00E-07	2.50E-02	5.000E 02	2.502E-02	5.404E-07	4.030E-04	5.746E-06	14
15	20.	1.00E 01	1.00E-06	1.00E-07	2.50E-02	5.000E 02	2.544E-02	1.795E-06	1.278E-03	6.415E-05	15
16	20.	1.00E 01	1.00E-06	1.00E-07	2.50E-02	5.000E 02	3.008E-02	5.755E-06	4.042E-03	6.610E-04	16
17	20.	1.00E 01	1.00E-06	1.00E-07	2.50E-02	5.000E 02	7.177E-02	1.805E-05	1.263E-02	6.710E-03	17
18	20.	1.00E 01	1.00E-06	1.00E-07	2.50E-02	5.000E 02	2.437E-01	5.070E-05	3.577E-02	6.424E-02	18
19	20.	1.00E 01	1.00E-06	1.00E-07	5.00E-02	4.472E 01	4.999E-02	2.501E-08	4.376E-05	2.396E-07	19
20	20.	1.00E 01	1.00E-06	1.00E-07	5.00E-02	4.474E 02	4.992E-02	3.531E-07	4.387E-04	2.259E-06	20
21	20.	1.00E 01	1.00E-06	1.00E-07	5.00E-02	5.000E 02	5.002E-02	1.414E-06	1.064E-03	3.669E-05	21
22	20.	1.00E 01	1.00E-06	1.00E-07	5.00E-02	5.000E 02	5.259E-02	4.724E-06	3.364E-03	4.348E-04	22
23	20.	1.00E 01	1.00E-06	1.00E-07	5.00E-02	5.000E 02	7.560E-02	1.502E-05	1.055E-02	4.546E-03	23
24	20.	1.00E 01	1.00E-06	1.00E-07	5.00E-02	5.000E 02	2.233E-01	4.370E-05	3.087E-02	4.886E-02	24
25	20.	1.00E 01	1.00E-06	1.00E-07	1.00E-01	1.259E 01	1.000E-01	1.281E-08	7.081E-06	0.0	25
26	20.	1.00E 01	1.00E-06	1.00E-07	1.00E-01	2.087E 01	9.995E-02	5.117E-08	7.085E-05	0.0	26
27	20.	1.00E 01	1.00E-06	1.00E-07	1.00E-01	1.961E 02	9.951E-02	6.062E-07	7.150E-04	1.427E-05	27
28	20.	1.00E 01	1.00E-06	1.00E-07	1.00E-01	5.000E 02	9.878E-02	3.464E-06	2.723E-03	2.032E-04	28
29	20.	1.00E 01	1.00E-06	1.00E-07	1.00E-01	5.000E 02	1.107E-01	1.181E-05	8.451E-03	2.688E-03	29
30	20.	1.00E 01	1.00E-06	1.00E-07	1.00E-01	5.000E 02	2.039E-01	3.587E-05	2.539E-02	3.195E-02	30
31	20.	1.00E 01	1.00E-06	1.00E-07	2.00E-01	5.000E 02	1.972E-01	1.038E-06	1.051E-03	9.924E-04	31
32	20.	1.00E 01	1.00E-06	1.00E-07	2.00E-01	5.367E-01	2.000E-01	2.585E-09	9.627E-06	0.0	32
33	20.	1.00E 01	1.00E-06	1.00E-07	2.00E-01	7.312E 00	1.997E-01	7.578E-08	9.650E-05	0.0	33
34	20.	1.00E 01	1.00E-06	1.00E-07	2.00E-01	6.924E 01	1.973E-01	8.485E-07	9.887E-04	7.541E-05	34
35	20.	1.00E 01	1.00E-06	1.00E-07	2.00E-01	5.000E 02	1.842E-01	7.496E-06	6.712E-03	8.619E-04	35
36	20.	1.00E 01	1.00E-06	1.00E-07	2.00E-01	5.000E 02	2.146E-01	2.626E-05	1.890E-02	1.516E-02	36

END OF FILE 55 LINES OF OUTPUT.

Appendix 5. Methods used to analyse weight gain data.

A5.1 Least squares linear fit.

For the general linear Equation (A5.1), the standard formulae given

$$y = A + B\,x \tag{A5.1}$$

by Himmelblau (1970) are stated in Equations (A5.2-4).

$$\bar{x} = \Sigma\, x_i/n \;;\; \bar{y} = \Sigma\, y_i/n \tag{A5.2}$$

$$B = \frac{\Sigma (y_i - \bar{y})(x_i - \bar{x})}{\Sigma (x_i - \bar{x})^2} \tag{A5.3}$$

$$A = \bar{y} - B\,\bar{x} \tag{A5.4}$$

The residual sum of squares, R, and correlation coefficient, C, are given by Equations (A5.5-6). All summations are over the n data points.

$$R = \Sigma (y_i - A - Bx_i)^2 \tag{A5.5}$$

$$C^2 = \frac{(\Sigma\, (y_i - \bar{y})(x_i - \bar{x}))^2}{\Sigma\, (y_i - \bar{y})^2\;\; (x_i - \bar{x})^2} \tag{A5.6}$$

A5.2 The Durbin-Watson test.

The test, due to Durbin and Watson (1951), is described by Himmelblau (1970). It provides a measure of the degree of correlation of the residual errors, E_i, at each of the points fitted by a model. In the case of Equation (A5.1), the residuals are given by Equation (A5.7), and the test number, D, by Equation (A5.8).

$$E_i = y_i - A - Bx_i \qquad (A5.7)$$

$$D = \frac{\sum_{i=2}^{n} (E_i - E_{i-1})^2}{R} \qquad (A5.8)$$

The test number is between 0 and 4, with high correlation indicated by numbers less than 1, and negative correlation by numbers greater than 3. Uncorrelated residuals are indicated by results near 2. Tables of confidence limits are given by Himmelblau (1970).

A5.3 Minimax Method.

The method of Curtis and Frank (1959) is used to find the polynomial P(x) which minimises the largest residual, E_{max}.

$$E_{max} = \max_{i=1,n} (ABS(y_i - P(x_i))) \qquad (A5.9)$$

The program used follows the algorithm described by them, with the addition of a test to prevent the search continuing when the relative error is of the same order as the precision of the computer.

As explained in Section (5.2.1), the polynomials are fitted to normalised weight gain time data, and the coefficients are in terms of the normalised data. The following expressions are used to calculate the unnormalised rate constants established using Equations (5.2.8-11), in terms of the maximum weight, W_m, and time, t_m.

For Equation (5.2.8) the linear rate constant, k_1 and error at the origin, W_{OR}, are given by Equations (A5.10-11)

$$k_1 = \frac{B_{21} W_m}{t_m} \tag{A5.10}$$

$$W_{OR} = A_{21} W_m \tag{A5.11}$$

The same quantities for Equation (5.2.9) are:

$$k_1 = \frac{W_m}{B'_{21} t_m} \tag{A5.12}$$

$$W_{OR} = - k_1 A'_{21} t_m \tag{A5.13}$$

In the case of the parabolic models, Equations (5.2.10-11), the rate constant, k_2, and error at the origin, W_{OR}, are given by corresponding equations. For Equation (5.2.10) these are

$$k_2 = \frac{(B_{22} W_m)^2}{t_m} \tag{A5.14}$$

$$W_{OR} = A_{22} W_m \tag{A5.15}$$

The expression for Equation (5.2.11) are

$$k_2 = \frac{W_m^2}{C'_{22} t_m} \tag{A5.16}$$

$$W_{OR} = - \frac{A'_{22} W_m}{B'_{22}} \tag{A5.17}$$

In this case the origin of the parabola can also be determined, as in the case of Equation (5.2.6). The co-ordinates of the origin are given by W_0 and t_0 in Equations (A5.18-19).

$$W_0 = \frac{B'_{22} W_m}{2\, C'_{22}} \qquad \text{(A5.18)}$$

$$t_0 = \frac{W_0^2}{k_2} - A'_{22} t_m \qquad \text{(A5.19)}$$

These formulae provide the necessary guide to the interpretation of the Specimen Output in Appendix 4.

A5.4 Factorial Analysis of Variance.

Factorial analysis has been used to assess the relative effect of variation of the different parameters of the model. The method used is that of Ralston and Wilf (1962). This uses the results of a Run in which all possible combinations of 2 or 3 values of each parameter to be tested have been used for a simulation, and the results of each case stored for further computation. The analysis calculates the contribution which each parameter makes to the sum of squares, S, of deviations from the overall mean; this is also computed for interactions among the parameters. Associated with each term is a number of degrees of freedom, N. The number computed to compare the sizes of the effects is the mean square deviation, as a percentage of the total sum of squares, T, and given by M in Equation (A5.20).

$$M = \frac{100S}{T\,N} \qquad \text{(A5.20)}$$

The analysis is performed separately for each dependent variable, for the same combinations, to form the tables of results in Section (5.3.1). Values of 0.1 or less are neglected.

This analysis cannot be regarded as fully statistical, as in the situation where repeat experiments are used to assess the residual error. The method amounts to attempting to fit an overall linear model to the variations, and thus either succeeds, indicating that there are only a few large effects, or else produces a complex pattern of interactions, indicating that an overall model is not applicable. In this case, more detailed examination of the actual results is necessary.

LIST OF SYMBOLS

A	Pre-exponential factor in Equation (2.3.1)	
A B C	boundary positions in Figure (3.1)	
$(A)^x$	Molar concentration of species A at x cf. Section (3.1.1)	gmol mm^{-3}
A_{ij}, A'_{ij} B_{ij}, B'_{ij}	Coefficients in Equations (5.2.6-11)	
C	gas phase mole fraction of CO	
C^x	gas phase mole fraction of CO at x	
C_{ext}	external gas phase mole fraction of CO	
C_{eq}	equilibrium gas phase mole fraction of CO	
C^o_{Fe}	iron vacancy concentration in solid Fe_3O_4	gatom mm^{-3}
C_n	mass fraction of carbon in solid	
C_{tot}	molar gas concentration	gmol mm^{-3}
D	appropriate diffusion coefficient in Equation (3.2.13)	$mm^2\ s^{-1}$
D_{12}	bulk gas diffusion coefficient in Equation (3.2.7)	$mm^2\ s^{-1}$ $cm^2\ s^{-1}$
D_{eff}	effective diffusion coefficient in Equation (3.2.13)	$mm^2\ s^{-1}$
D_{Fe}	iron solid-phase diffusion coefficient	$mm^2\ s^{-1}$
D_k	Knudsen diffusion coefficient in Equation (3.2.11)	$mm^2\ s^{-1}$ $cm^2\ s^{-1}$
E_1 E_4 E_C	effectivenss factors defined by Equations (3.5.9-11)	
E	desired error in Runge-Kutta algorithm Equation (4.3.3)	

e	actual error vector in Runge-Kutta algorithm Equation (4.3.2)	
F	Oxide thickness growth rate	mm s^{-1}
f	iron vacancy fraction in solid Fe_3O_4	
f	vector of functions in Runge-Kutta algorithm Equation (4.3.2)	
G_A		
G_C	dimensionless volume factors defined by Equations (3.5.18-20)	
G_{OX}		
G	Number to be made zero in Equation (4.2.18)	
h	Step length in Runge-Kutta algorithm in Equation (4.3.2)	
K_1		
K_2	factors related to specific volumes of solids, Equation (3.3.51)	mm^3 $gmol^{-1}$
K_3		
K_C		
k_j	local volume factors in Equations (3.1.1-6)	mm^3 $gmol^{-1}$
k	weight gain rate constant, Equation (1.1)	
k	vector of factors in Runge-Kutta algorithm Equation (4.3.2)	
k	constant in Equation (3.2.26)	
M	Molecular weight	
N_A^x	inward molar flux of species A at x defined in Section (3.1.1)	gmol mm^{-2} s^{-1}
n	Exponent of weight gain Equation (1.1)	
P	pressure	bar
Q	ratio of oxide growth rates defined by Equation (3.3.60)	
Q	activation energy in Equation (2.3.1)	kcal $mole^{-1}$

R	gas constant in Equation (2.3.1)	kcal $mole^{-1}$ k^{-1}
R_i	reaction rates per unit area of oxide defined in Equations (3.3.31-4)	gmol mm^{-2} s^{-1}
r	distance in Equation (3.2.10)	
r_i	reaction rates per unit volume of oxide defined in Section (3.1.1)	gmol mm^{-3} s^{-1}
r_1		
r_{31}	reaction rate constants defined in Equations (3.4.1,3b-c)	
r_{32}		
r_e	equivalent pore radius, Equation (3.2.22)	µm
S	ratio of reaction rates R_4/R_1 defined by Equation (3.3.59)	
S_D	temporary value of S in Equation (4.2.12)	
Sg	Specific surface area in Equation (3.2.11)	cm^2 g^{-1} m^2 g^{-1}
T	temperature	K
t	time	h,s
t_o	parabola origin in Equation (5.2.3)	h
V	specific volume of Fe_3O_4, Equation (3.3.51)	mm^3 $gmol^{-1}$
V_{Fe}	specific volume of iron, Equation (3.3.57)	mm^3 $gmol^{-1}$
V_P		
V_A	volumes available and taken up during oxidation per unit area of oxide, defined by Equations (3.5.14-17)	mm s^{-1}
V_C		
V_{OX}		
W	weight gain per unit area of oxide	g mm^{-2}
$\dot{W}$	weight gain rate per unit area of oxide	g mm^{-2} s^{-1}
W_O	parabola origin in Equation (5.2.3)	g mm^{-2}

w	step length factor in Runge-Kutta algorithm, Equation (4.3.3)	
X	oxide thickness	mm
$X1$	outer oxide thickness	mm
$X2$	inner oxide thickness	mm
x	independent variable in Runge-Kutta algorithm, Equation (4.3.2)	
y	dependent vector in Runge-Kutta algorithm, Equation (4.3.2)	
Z	ratio of reaction rates R_3/R_1	
α	factor in Runge-Kutta algorithm, Equation (4.3.3)	
δ	gas boundary film in Equation (3.2.14)	mm
ε	voidage of oxide layer	
ε_C	volume fraction of carbon in oxide	
ε^*	effective voidage for solid state diffusion	
ε_{ij}	parameter in Leonard-Jones Equation (3.2.10)	
ρ	density	g mm^{-3}
σ	parameter in Leonard-Jones Equation (3.2.10)	
ζ	tortuosity factor in Equation (3.2.13)	
Φ	function in Leonard-Jones Equation (3.2.10)	
Ω_D	parameter in Leonard-Jones Equation (3.2.7)	

LIST OF REFERENCES

Antill J. E., Campbell C. S., Goodison D., Jepson W. B. and Stevens C. G., 1964, Proc. 3rd Geneva Conf. Peaceful Uses of Atomic Energy, 9, 523

Antill J. E., Peakall K. A. and Warburton J. B., 1968, Corrosion Science, 8, 689

Birchenall C. E., 1968, National Bureau of Standards Special Publication No. 296

Brown A. M., 1975, Private Communication

Cameron D. I., 1958, J. Iron and Steel Institute, 189, 251

Castle J. E., Emsley A. M. and Surman P. L., 1971, Nature, 231, 86

Castle J. E. and Mann G. M. W., 1966, Corrosion Science, 6, 253

Castle J. E. and Surman P. L., 1969, J. Physical Chemistry, 73, 632

Channing D. A. and Graham M. J., 1972, Corrosion Science, 12, 271

Cowen H. C. and Tyzack C., 1968, Br. Corros. J., 3, 220

Crane P. C. and Fox P., 1969, Numer. Math. Program Library Proj., Computing Sci. Res. Center, Bell Telephone Labs Inc., Murray Hill, N. J.

Curtis P. C. and Frank W. L., 1959, J. Assoc. Comp. Mach.,395

Donovan A. J. and Willbe C. M., 1974, Management Services Department, Computing Bureau, Report MS/C/N637, C.E.G.B.

Durbin J. and Watson G. S., 1951, Biometrica, 38, 159

Fox P., 1972, Comm. Assoc. Comp. Mach., 15, 941

Fox L. and Mayers D. F., 1968, Computing Methods for Scientists and Engineers, O.U.P., Oxford.

Gibbs G. B., 1973, Oxidation of Metals, 7, 173

Gibbs G. B., Pendlebury R. E. and Wootton M. R., 1974, British Nuclear Energy Society Materials Conference (to be published)

Gibbs G. B., Wootton M. R., Price W. R. and Hodgson K. E., 1973, Oxidation of Metals, 7, 185

Godfrey W. R. and Phennah P. J., 1968abc, J. British Nuclear Energy Society, 7, Part I, 151, Part II, 217, Part III, 224

Goodison D., Harris R. J. and Goldenbaum P., 1969, Br. Corros.J., 4, 293

Himmelblau D. M., 1970, Process Analysis by Statistical Methods, Wiley

Hinton, Sir C., 1958, The A.B.C. of Atomic Energy, The British Broadcasting Corporation

Hirschfelder J. O., Curtiss C. F. and Bird R. B., 1954, Molecular Theory of Gases and Liquids, Wiley

Hodgman C. D., ed., 1960, Handbook of Chemistry and Physics, The Chemical Rubber Publishing Co., Cleveland, Ohio

Jenson V. G. and Jeffreys G. V., 1963, Mathematical Methods in Chemical Engineering, Academic Press, London

Kelley K. K., 1960, Contributions to the data on theoretical metallurgy, XIII, U.S.G.P.O. Bulletin 584

Kinsey D. V., 1972, Dragon Project Technical Note DPTN/270

Leach J. S., 1974, British Nuclear Energy Society Materials Conference (to be published)

Merson R. H., 1957, Proceedings Symposium on Data Processing, Weapons Research Establishment, Sailisbury, South Australia

Moore C. and Raine T., 1961, Steels for Reactor Pressure Circuits, Iron and Steel Institute, Special Rep. No. 69, 136

Price W. R. and Whittle I., 1967, Journal Iron and Steel Inst., 205, 668

Pritchard A. M., Antill J. E., Cottell K. R. J., Peakall K. A. and Truswell A. E., 1974, British Nuclear Energy Society Materials Conference (to be published)

Ralston A. and Wilf H., 1962, Mathematical Methods for Digital Computers, Wiley

Satterfield C. N., 1970, Mass Transfer in Heterogeneous Catalysts, Cambridge (Mass.)

Surman P. L., 1972, Private Communication

Surman P. L., 1973, Corrosion Science, 13, 825

Surman P. L. and Brown A. M., 1974, British Nuclear Energy Society Materials Conference (to be published)

Surman P. L. and Castle J. E., 1969, Corrosion Science, 9, 771

Tomashov N. D., 1966, Theory of Corrosion and Protection of Metals, Macmillan

Tyzack C., Campbell C. S. and Trowse F. W., 1963, J. British Nuclear Energy Society, 2, 246